ION-MOLECULE INTERACTIONS IN THE GAS PHASE

By

RICHARD D. BURTON

A DISSERTATION PRESENTED TO THE GRADUATE SCHOOL
OF THE UNIVERSITY OF FLORIDA IN PARTIAL FULFILLMENT
OF THE REQUIREMENTS FOR THE DEGREE OF
DOCTOR OF PHILOSOPHY

UNIVERSITY OF FLORIDA

1997

ACKNOWLEDGMENTS

Over the course of my studies at the University of Florida, several individuals have contributed greatly to my educational experience and I wish to thank them. First, I wish to thank Dr. Kirk Schanze for acting as my mentor for the first two years of my graduate study. It was from Kirk that I learned never to accept mediocrity from myself or my work. Also, I wish to thank Dr. Alan Katritzky for providing a great deal of direction in my research projects. In getting the opportunity to work with the Katritzky group, I was able to greatly enhance my chemical background in a wonderfully diverse cultural setting.

I especially wish to thank my advisor, Dr. John Eyler for all of his patience and guidance during my time here. Despite his very busy schedule, he was always there when I needed his wisdom, his knowledge, or his friendship. Finally, I give all my love and thanks to my family who have always believed in and supported me.

TABLE OF CONTENTS

LIST OF TABLES

LIST OF FIGURES

Abstract of Dissertation Presented to the Graduate School
of the University of Florida in Partial Fulfillment of the
Requirements for the Degree of Doctor of Philosophy

ION-MOLECULE INTERACTIONS IN THE GAS PHASE

By

Richard D. Burton

May, 1997

Chairman: Dr. John R. Eyler
Major Department: Chemistry

For years Fourier transform ion cyclotron resonance mass spectrometry (FTICR MS) has been used in the study of gas phase ion-molecule reactions. In this study, a wide range of gas phase ion-molecule interactions have been examined using this "gas phase chemical laboratory." Furthermore, various mechanistic aspects have been probed in four different chemical reaction systems. First, effects of solvation have been examined for two ruthenium(II) ammine complexes through microsolvation using electrospray ionization. These solvated adducts have been successfully trapped and isolated in the FTICR analyzer cell. In addition, the relative stability of these species has been studied in attempts to measure the corresponding binding energies of solvation.

In another system, FTICR has been utilized in the measurement of appearance energies for the fragmentation of a series of acylpyridinium cations. These energies were found to range from less than 23 kcal/mol to 80 kcal/mol. This fragmentation was found to occur via two alternate pathways. In one process, dissociation results in the formation of an

acylium ion, while in the other, a protonated pyridinium cation is observed. Attempts to generate an S_N2 reaction between these acylpyridinium cations and several neutral nucleophilic species produced several unexpected adducts but no definitive evidence for this process.

In a similar chemical system, attempts were made to generate both intermolecular and intramolecular gas phase S_N2 reactions with several N-substituted pyridinium and acridinium cations. Several of these compounds were found to undergo intramolecular S_N2 reactions via cyclization. Again, two different mechanistic pathways were found to occur. In the first, direct nucleophilic attack was observed resulting in the formation of a heterocyclic cation. In the second process, a protonated acridinium cation was produced via cyclization of the heteroatomic sidechain followed by fast proton transfer from an ion-induced dipole complex. Finally, several attempts to generate intermolecular S_N2 reactions were unsuccessful.

In the final study, FTICR was used to measure the proton affinities of several commonly used MALDI (matrix assisted laser desorption ionization) matrices. This proton transfer process represents another gas phase process which is effectively studied using this powerful "gas phase chemical laboratory."

CHAPTER 1
INTRODUCTION

Fourier Transform Ion Cyclotron Resonance Mass Spectrometry: A Gas Phase Chemical Laboratory

FTICR MS: A Brief History

Ion Cyclotron Resonance Mass Spectrometry (ICR MS) is an analytical technique which has existed since the mid-1960s and was first developed in its modern form via collaboration between John D. Baldeschwieler (Stanford) and Peter Llewellyn, who headed a group at Varian Associates. Almost immediately, ICR MS was considered a useful technique in the study of gas phase ion-molecule chemistry. Many early researchers, including Anders, Beauchamp, Buttrill, Blair, Brauman, Comisarow, Djerrasi, Eyler, Huntress, Marshall, McIver, Smyth, and Riveros effectively utilized the technique in this area. Several advances over the past few decades have enabled ICR MS to advance from a promising mass spectrometric technique to one of great versatility.

The first serious ion-molecule reaction studies were conducted in the late 1960s by Beauchamp et al.[1] In this study, reactions involving chloroethylene were examined using ICR. Since that time, ICR has been often used as an extremely viable tool in studies of ion-molecule reactions. Furthermore, with the advent of trapped-ion pulsed ICR[2,3] and the effective implementation of Fourier transform techniques (FTICR MS)[4-5] in the early 1970's, ICR has benefited from increased mass

resolution as well as faster and more effective computer data processing capabilities. In addition, through the use of high-field superconducting magnets, mass resolution capability has increased even further,[6] often exceeding 1 million in modern systems.[7,8] Still another advance involved the use of MS/MS (tandem mass spectrometry) in collision-induced dissociation studies.[9] Application of MS/MS has enhanced the capabilities of FTICR MS in studies involving both structural determination of ions and the chemical reactivity of various ion-molecule systems. This technique will be discussed in greater detail later in this chapter.

The continuing evolution of FTICR MS has enabled it to compete with other mass spectral techniques in an increasingly effective manner. Currently recognized advantages of FTICR MS include, but are not limited to, high resolution/mass accuracy, high trapping efficiency of ions, effective data processing, and the multiplex advantage (ability to detect ions over a large mass range simultaneously). Each of these advantages contributes to make FTICR MS an ideal technique for examining various ion-molecule interactions in the gas phase.

The FTICR MS Technique

In order to understand the dynamics of this mass spectrometric technique, one first needs to understand ion motion in a magnetic field.[10-11] In a magnetic field **B**, an ion travels in a circular (cyclotron) orbit in a plane perpendicular to the magnetic field axis. While on this course the ion of mass m and charge z experiences two counterbalanced forces which enable it to remain in a stable orbit. The first force is an outward, centrifugal force on the ion equal to mv^2/r,

where v = velocity and r = orbital radius. The second force acts in the opposite direction (inward), and is equal to $z\mathbf{B}v$. Thus, since the two forces are equal ($z\mathbf{B}v = mv^2/r$), and the cyclotron frequency, f_c, of the orbiting ion is given by $v/r = \omega_c = 2\pi f_c$, the following fundamental cyclotron equation may be derived. Eq. 1 relates the frequency of ion motion to the magnetic field strength and the ion's mass to charge, m/z.

$$f_c = z\mathbf{B}/2\pi m \qquad \text{(Eq. 1)}$$

This equation demonstrates that a group of ions of the same m/z will orbit with the same frequency, f_c. Finally, the aforementioned relationship, $v/r = \omega c$, when combined with Eq. 1, indicates that larger ions exhibit orbits with smaller radii than smaller ions with higher momentum.

The fact that ions travel in a consistent and predictable manner in a magnetic field allows for effective trapping in an analyzer cell. However, in addition to their cyclotron motion, the ions also undergo motion along the magnetic field axis (conventionally assigned as the z-axis). Because of this, a force must be present to trap the ions along this axis as well. Thus, a cubic cell may be utilized where two trapping plates are positioned at each end of the cell (perpendicular to the z-axis) in order to trap the ions (Figure 1). The plates are normally charged to ± 1.0V (depending on the charge of the ions, mass, pressure, etc.) in order to trap the ions in the z-direction. Finally, the ions undergo a third type of motion (magnetronic) which is circular about a guiding center that follows a path of constant electric potential.

In order to detect the ions of mass-to-charge m/z, an RF excite pulse is applied to the two opposing transmit plates in the cell (Figure

1) as an alternating electric field. When the applied frequency is equal to the cyclotron frequency, f_c, of an ion, a resonance condition

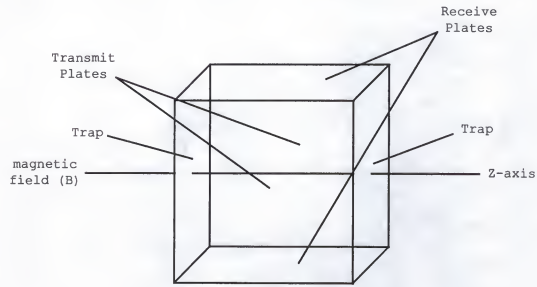

Figure 1. Diagram of a cubic ICR cell

is achieved and the ion is excited translationally (thus increasing its velocity). In order to maintain its cyclotron frequency it travels outward to an orbit of larger radius (closer to the plates) where it induces an alternating 'image' current in the two receive plates as depicted in Figure 2. The RF signal which is produced is extremely weak and must then be amplified as soon as possible after the cell (via a preamplifier) before being filtered and digitized (via a analog to digital converter, ADC). Following digitization, the signal (transient data) is processed via the CPU (central processing unit). The ion signal is represented by a combination of overlapping sine waves with each exhibiting the cyclotron frequency of a given ion. In order to disentangle this raw data, Fourier transformation techniques are utilized to separate the various frequency components from each other as

well as from the inherent noise. From this process, a plot of ion abundance (intensity) versus frequency is generated which is immediately converted into a mass spectrum via the aforementioned cyclotron equation (Eq. 1).

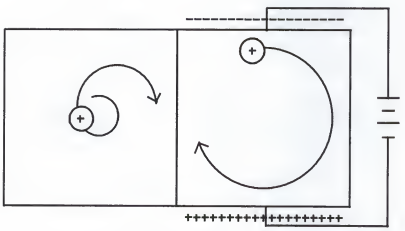

Figure 2. RF excitation of the ion packet increases its translational energy, exciting it to a cyclotron orbit with a greater radius, where it induces an "image" current in the detect plates of the analyzer cell.

In examining gas phase ion-molecule reactions (MS/MS), FTICR is utilized in a manner analogous to that observed in a chemical laboratory for solution phase reactions.[10] In this process, FTICR is used as both the synthetic and analytical means for the reaction process. Complete control of the reaction conditions can be exercised in a time-resolved manner in order to obtain structural information as well as probing reactivity. The overall FTICR laboratory experiment is depicted in Figure 3.

FTICR as a Gas Phase Chemical Laboratory

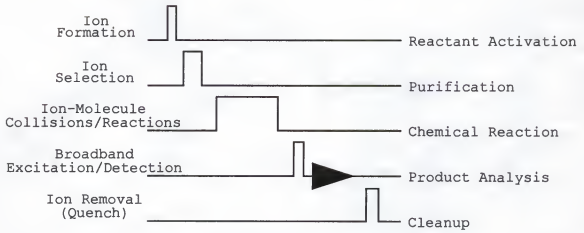

Figure 3. Examination of a basic FTICR ion-molecule (MS/MS) experiment reveals the similarities to a solution phase chemical reaction process.

Ion Formation

In the first step, ions must be formed and transported to the analyzer cell (if they were not formed there initially), where they are trapped. The ions may be generated in an external source region and then transported to the cell, or they may be formed in the cell from a neutral analogue. In MS/MS experiments, the ionization step may be considered analogous to a catalytic step in a solution phase reaction, where a reactant is activated (e.g. acid or base-catalysis). Of course, the ionization is also a necessity in FTICR in order to generate ions, as only charged species can be trapped and detected. A variety of ionization methods are currently available in conjunction with FTICR mass spectrometry. Neutral species may be ionized either internally or externally via electron impact (EI), chemical ionization (CI),[12,13] laser desorption (LD),[14] fast atom bombardment (FAB),[15] secondary ion mass spectrometry (SIMS),[16-20] plasma desorption (PD),[21-24] multi-photon

ionization (MPI),[25-26] electrospray ionization (ESI),[27] and matrix-assisted laser desorption ionization (MALDI),[28,29] to name the most popular methods.

In EI, a neutral species is introduced into either the source or analyzer region of the instrument, usually via precision leak valves or a heated solids probe. For the work described in this thesis, a Bruker Bioapex system (Figure 4) was used in conjunction with a 4.7 Tesla superconducting magnet (Magnex). Following introduction of a neutral species, a high energy electron beam is then passed through the gas producing ions. In the aforementioned setup involving the Bruker system, ions were formed in the external source and then transported (via a series of electrostatic optics) to the cell, where they were trapped.

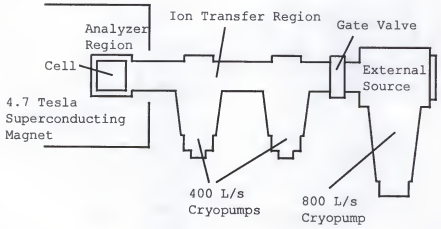

Figure 4. Bruker BioApex FTICR mass spectrometer system equipped with 4.7 T Magnex superconducting magnet

In chemical ionization, a second reagent gas is utilized in addition to the analyte gas. In this method, the reagent gas is first ionized and then undergoes either electron or proton transfer with the

analyte to produce ions of the analyte. The reagent gas should ideally have an ionization potential only slightly higher than the analyte in order to allow for mildly exothermic charge transfer. This technique is less energetic than basic EI and produces less fragmentation of the analyte. Chemical ionization (CI) will be discussed further in chapter 5.

In laser desorption, the analyte is coated on a solids probe target. A UV (ultraviolet) or CO_2 (carbon dioxide) laser is then utilized to heat the analyte, thus desorbing it from the probe surface with concurrent formation of analyte ions. Laser desorption has proven to be a useful means for introducing solid samples of lower volatility. Unfortunately, this technique (like EI) is highly energetic and often produces a great deal of fragmentation (especially in larger organic species). Only recently, a new form of laser desorption has been developed which produces much cooler ions. This method is especially effective with larger organic molecules which had been difficult to ionize previously without the occurrence of substantial fragmentation.

In matrix-assisted laser desorption ionization (MALDI), a chemical matrix is utilized to absorb the majority of the electronic (or vibrational) energy imparted by the laser. In this technique, a chemical system is chosen where only the matrix absorbs the energy of the laser. Thus, the ionizing energy is indirectly imparted to the analyte resulting in less fragmentation. In some cases, the matrix is utilized as a proton donor to the analyte while in others a sodium adduct is formed (in situations where protonation is not favored). The mechanism for proton transfer has been the subject of much discussion in the literature and will be examined in chapter five. Since the analyte

is not directly excited, the result is a much 'softer' ionization process (than with basic laser desorption) where much larger organic (especially for biological systems and polymers) ions may be formed and studied. While MALDI has been used successfully with ICR in producing large singly charged organic ions, trapping difficulties have limited the upper mass range to around m/z 15,000.[30] Another newly developed 'soft' ionization technique, electrospray ionization, has been successful in introducing ions greater than 6,000,000 amu with higher charge states.[31]

In the early 1980's, electrospray ionization (ESI) was developed by Yamashita and Fenn.[32] In ESI, the analyte is first dissolved in a suitable solvent which has a sufficiently high dielectric constant (50/50 H_2O-methanol is commonly used). The solution is sprayed from a needle tip which is at a high positive potential (ca. +3000 to 4000 V for positive ions) relative to a stainless steel capillary (effectively ground) positioned opposite it at a distance of ca. 1 cm as in Figure 5. (Note: For negative ions, the polarity of the needle is reversed.) The needle is placed slightly off-axis with respect to the capillary due to the dynamics of the spray. The spray (microdroplets) which leaves the tip of the needle is conical in shape and is commonly referred to as a "Taylor cone". These microdroplets undergo desolvation before exiting the capillary (which is normally heated to aid in desolvation of the analyte) into the low pressure region of the external source (see Figure 5).

The entire process results in singly as well as multiply-charged (especially for larger molecules) ions being formed in a process which imparts relatively little energy to the ions. Like MALDI, ESI has been

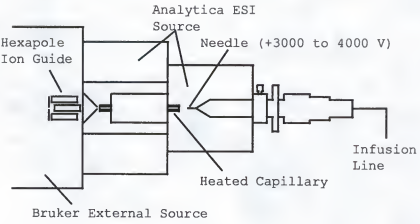

Figure 5. Analytica external ESI setup used for the work to be presented in this publication

utilized very effectively as a low energy ionization alternative for both inorganic and organic systems. However, since ESI readily produces highly-charged states, ions of very high mass may be formed and trapped in the ICR analyzer cell. In fact, molecular masses as high as 6,000,000 amu have been ionized and studied using FTICR.[31] In addition to high molecular mass organic systems though, ESI has proven to be extremely useful in introducing smaller organic and inorganic ions from solutions of their salts, as will be demonstrated in this work.

Ion Selection

Several different ions are often formed in the analyzer cell by the various formation processes. Before reaction of the intended ion may be initiated, it must first be isolated by removal of the other species. This step may be equated with purification of a reagent prior to a solution phase synthetic process. FTICR has several methods of ion ejection for single m/z frequencies or frequency ranges. In all of these techniques, RF-ejection of the desired ions is effected using a frequency generator. The most basic form of ejection is via chirp

excitation. Furthermore, low and high mass RF frequency sweeps may be utilized to isolate an ion of a given m/z. Often, single frequency chirps are used along with the sweeps to eject specific ions which are close in frequency to the ion which is to be isolated. Ideally, the amplitude for this type of excitation would be constant over the desired frequency range; however, this is not the case. In fact, the resulting RF response contains a certain amount of inconsistency and "bleed-off" outside the set range. The amount of bleed-off is especially dependent on the length of the chirp. Longer chirps result in a more highly resolved RF response with less bleed-off. Nevertheless, unwanted excitation of the ion to be isolated is common and difficult to avoid if interfering ions to be ejected are close in m/z to the precursor ion. In order to better control the excitation, the SWIFT approach (stored waveform inverse Fourier transform) was developed by Marshall et al.[33] In SWIFT, the waveform necessary for ejection of a particular m/z range is first generated and then converted to a frequency response following inverse Fourier transformation. The resulting isolation is "cleaner" with much less excitation of the precursor ion. In this work, a similar shaped-pulse method, developed by Bruker, was utilized for isolating single isotopic peaks of several solvated species, as will be discussed in chapter 2.

Ion-Molecule Collisions/Reactions

Following isolation of the ion of interest, a neutral species is usually introduced via a precision leak valve, heated solids probe, or pulsed valve. Typically, the neutral gas is introduced to a background pressure between 10^{-6} and 10^{-8} Torr. At this pressure, the total number of neutral molecules greatly outnumbers the ion population. Because of

this statistical arrangement, ion-molecule encounters predominate while ion-ion collisions are quite rare. Ion-molecule collisions may result in either fragmentation or chemical reactions depending on the system. As in the solution-phase reaction, the difference in the energies of the products and reactants determines whether or not a reaction is energetically favored. In addition, sufficient energy must be present in both solution-phase and gas phase reactions in order to surmount the transition-state barrier. In solution phase reactions, thermal or light energy is used to provide the necessary activation energy. The same is true of gas phase reactions; however, in the case of thermal reactions, the vibrational energy is often introduced by other means.

In the gas phase, reactants may be excited either vibrationally or electronically via laser irradiation as in solution; however, direct thermal heating of the reactants is somewhat inefficient because of the low pressures which are often used. In ICR, internal heating of the ions is usually accomplished indirectly by RF chirp excitation at the cyclotron frequency of the ions. This type of excitation results in increased translational energy in the ions; however, upon collision with a neutral molecule, this energy is converted (to some extent) to vibrational and/or electronic energy. Nevertheless, this RF irradiation is somewhat cumbersome in that continued excitation may result in ejection of some ions from the analyzer cell as discussed previously. A short burst of RF energy must therefore be used (typically 1-10 ms) in order to avoid ejection. With careful tuning of the excitation parameters, this type of excitation can be used very effectively as will be seen in later chapters. However, obvious difficulties exist in maintaining a thermally "hot" ion population for any extended period

(e.g. seconds) of time. Furthermore, at the low reaction pressures inherent in FTICR, relatively few collisions occur on a low millisecond timescale.

In order to circumvent this problem, sustained off-resonance irradiation (SORI) may be used.[34] In SORI, single-frequency excitation is applied 1 to 1.5 kHz off-resonance from the cyclotron frequency of the ion of interest. Thus, a condition of irradiation is achieved where the ion is constantly being excited and relaxed during alternating in-phase and out-of-phase segments. This phenomenon allows for a longer reaction period (milliseconds - seconds) and often an enhanced reaction yield.

Broadband Excitation/Detection

In solution-phase chemistry, the reaction's progress is followed by various analytical techniques such as chromatography, NMR (nuclear magnetic resonance spectroscopy), IR (infrared spectroscopy), and mass spectrometry. In FTICR, mass spectrometric detection is nearly instantaneous and is well resolved in the time domain. Unlike other mass spectrometric techniques, FTICR benefits from multiplex detection of the ions. That is to say, all of the ions are detected virtually simultaneously, with no scanning time being necessary. In order to detect the ion population following the reaction period, RF chirp excitation is applied across the entire mass spectral region to be examined. The ions are subsequently excited to a higher cyclotron orbit, as discussed previously, where they induce an alternating 'image' current in the two receive plates.

Ion Removal (Quench)

Following detection of the reaction products, the analyzer cell must be cleared of all ions before initiation of the next reaction cycle. This is again analogous to solution-phase work, where the reaction vessel must be cleaned before another reaction may be run. In the case of FTICR ion removal is generated by a "quench" where the potential on one (or both) of the trapping plates is dropped to clear the cell of any remaining ions. This is done after each experimental sequence and even between co-added acquisitions to avoid ion buildup and the resulting space-charge effects which may occur when too many ions are trapped in the cell.

Gas Phase Studies of Unimolecular and Bimolecular Reactions

As discussed in the preceding paragraphs, FTICR lends itself to the effective study of ion-molecule reactions. Furthermore, both unimolecular and bimolecular ion-molecule reactions have been examined in the work to be presented. In using FTICR for the study of gas phase reactions, one is able to follow the formation of products from reactants in a time-resolved manner with the observation of reaction intermediates in some cases. For these data, a great deal of mechanistic information for the reactions may be obtained through physical measurements of reaction kinetics. Furthermore, the aforementioned RF ejection capability is also useful in the elucidation of reaction pathways. For instance, a potential reaction intermediate may be continuously excluded from the analyzer cell during the reaction period to examine its effect. From this, its role in the observed reaction process may be ascertained.

Another major advantage of FTICR is the ability to do studies of multi-step reactions. Unlike most other mass spectrometric techniques capable of performing MS/MS experiments, FTICR theoretically has no limit to the number of MS stages since the detection process is nondestructive; i.e. no ions need be removed from the cell for detection. Furthermore, recent advances in ion remeasurement involving quadrupolar axialization[35] have provided efficiencies of ion loss less than 1 percent; therefore, many stages of MS may be implemented. In addition, with the exact mass accuracy of FTICR (typically less than 3 ppm error for higher field systems), invaluable information may be gained concerning the atomic composition of the product as well as the parent ions. The smaller the fragments produced via MS^n, the higher the certainty for the atomic composition.

Besides providing an excellent platform for studying the mechanistic details of a gas phase ion-molecule reaction, FTICR may be used to examine the energetics involved. The RF excitation or laser irradiation used for ion activation may be controlled over a known range of energies and times. Thus, the overall energy imparted to the system may be calculated and used to determine energies of activation (e.g. bond dissociation energies, heats of reaction, etc.) for reaction processes. The most basic ion-molecule reactions studied are the unimolecular processes.

Unimolecular Reactions in the Gas Phase

In the FTICR analyzer cell, unimolecular reactions are the most easily studied since no background pressure of a reactant gas is required. Instead, an inert collision gas such as argon may be used in order to induce the reaction (usually fragmentation). In this type of

reaction, the ion is excited translationally (in the presence of the neutral gas) until a collision with the inert neutral molecule occurs. In the collision, the translational energy is converted to vibrational and/or electronic energy, which is then distributed throughout the molecule into the various vibrational modes. If sufficient energy is present in a given bond to surmount the transition state barrier, the ion may fragment to a product ion(s) (successor ion) and a neutral molecule, which is immediately lost from the cell. This collisionally-induced dissociation (CID)[36] provides a great deal of physical information. The known translational energy imparted to the ion may be varied over a range of values to give a profile of percent fragmentation vs. excitation energy. It is from these data that the appearance energy for the product ion(s) may be determined.

Bimolecular Reactions in the Gas Phase

In addition to unimolecular reactions, FTICR provides an excellent laboratory setting for studying bimolecular reactions. In the gas phase, ion-molecule interaction is often energetically favored with the frequent formation of transient ion-induced dipole adducts. These adducts exhibit some characteristics of microsolvation and have been observed to play a role in some reactions. As in unimolecular reactions, energy may be imparted through excitation of the ionic reactants by the aforementioned means (RF or hν) and ionic products detected. In this case, however, the neutral gas plays a reactive role in the reaction process. As mentioned earlier, a sufficiently volatile reactant gas may be introduced in the presence of the trapped ions in a time-resolved manner. Following a variable reaction delay period of ca. 30 ms to hours, detection of the ion population may occur. By varying

the reaction delay period, one is able to gain a very good understanding of reaction dynamics during the entire synthetic process. Various fundamental reactions which can be examined in this way include proton transfer, substitution and elimination reactions, etc..

Gas Phase Reactions to be Examined

Gas Phase S_N2 Reactions

One of the most studied organic reactions over the years has been the S_N2 reaction. A great deal of work has been conducted in this area in both solution and the gas phase; thus, much is known mechanistically for many chemical systems.[37,38] Nevertheless, considerable interest remains in this area because of the importance of this reaction chemistry. It is well known that in an aliphatic S_N2 reaction, an electron-rich nucleophile attacks an electron-poor substrate with the backside loss of a relatively stable leaving group. This is in sharp contrast to the S_N1 reaction, where loss of the leaving group precedes nucleophilic attack (Figure 6).[37]

In reality, it is believed that many reaction processes fall somewhere between these two extreme cases. Furthermore, the transition state may have varying degrees of bond breaking and bond making over a continuous range. It is also known that solvent plays an important role in deciding the mechanistic pathway a reaction will follow. These solvent effects are quite complex, with many factors being involved. In general, for solution phase reactions, polar solvents are known to stabilize ionic species better than nonpolar solvents and thus favor S_N1 chemistry. Also, solvents may serve as a directing influence while guiding the nucleophile into the correct orientation for backside attack

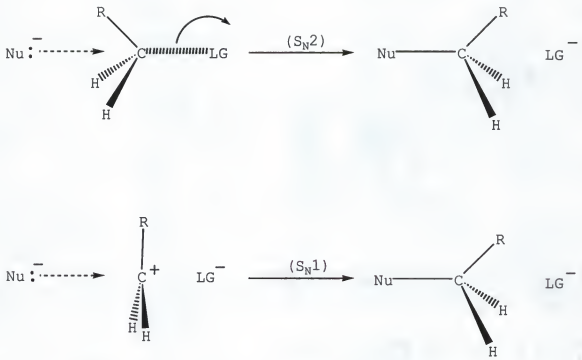

Figure 6. Mechanisms for S_N2 and S_N1 Reactions

in an S_N2 reaction. In other reactions, the solvent may stabilize the activated complex (relative to the reactants), effectively lowering the barrier to activation. Because of the profound influence of solvent, it is difficult to gain insight into the fundamental reaction dynamics of an S_N2 reaction in solution. It is primarily for this reason that S_N2 reactions have been so heavily studied in the gas phase.

In the gas phase none of the aforementioned solvent effects are present; thus it is possible to probe the extent of bond breaking and making as a function of a reactant's structure and energy. The currently accepted model for gas phase ion/molecule reactions was originally proposed by Brauman and Pellerite.[39,40] In studying several halide displacement (S_n2) reactions, they found that very few ion-induced dipole species proceeded to form products. This was attributed to the presence of a transition state barrier (see Figure 7) separating

two minima corresponding to ion-induced dipoles. This type of S_N2 chemistry involving an anionic nucleophile with a neutral substrate has been well studied in the gas phase since Brauman's initial work. However, surprisingly few studies have examined the gas phase S_N2 reaction chemistry of neutral nucleophiles with cationic substrates. One of the main goals of this work was to examine this type of reaction chemistry for a series of pyridinium ions in order to ascertain the mechanistic extent of bond breaking and making in the transition state. These attempts will be discussed in detail in chapter 4.

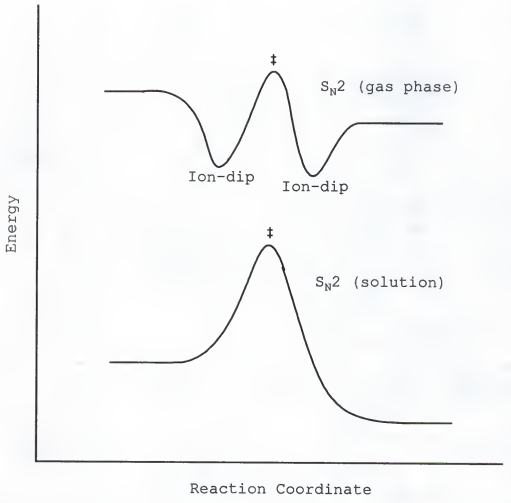

Figure 7. Energy Diagram of S_N2 reactions in the gas phase and solution

Gas Phase Acyl Transfer Reactions

As in nucleophilic substitution reactions, acyl transfer reactions involve the attack of an electron rich nucleophile upon a electron deficient carbonyl system with the loss of a leaving group. Again, these reactions have been studied heavily in solution and a great deal has been learned concerning the mechanistic details.[37] Unlike most aliphatic S_N2 reactions, the nucleophile may attack prior to loss of the leaving group (addition-elimination) with the production of a semi-stable tetrahedral intermediate (Figure 8). Subsequent loss of the leaving group yields the final product.

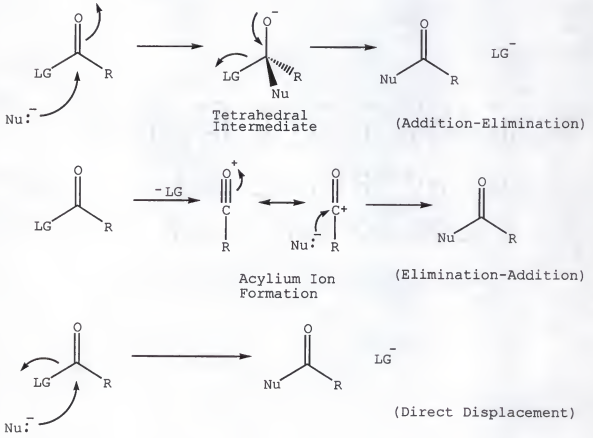

Figure 8. Proposed mechanisms for acyl transfer reactions in solution

In contrast, the leaving group may be lost prior to nucleophilic attack (elimination-addition), thus producing an unusually stable cationic intermediate known as an "acylium ion". This acylium ion benefits from resonance stabilization, as depicted in Figure 8. Following attack of the nucleophile, the final product is formed. The obvious compromise of these two opposing mechanisms is the potential direct displacement reaction where bond making (nucleophilic attack) and bond breaking (loss of the leaving group) occur simultaneously.

This type of mechanism may be considered analogous to the aforementioned S_N2 process. As in the case of the S_N2 reaction, many degrees of bond making and bond breaking may present in the transition state. Again, solvent may profoundly affect the mechanistic route of the reaction. In addition, the R-group on the acyl substrate may have an effect on the energetics of acylium ion formation and thus "steer" the reaction in one direction or another. Another goal of the work presented here was thus to measure the effect of the R-group in acylium ion formation for a series of acylpyridiniums in the gas phase. In order to do this, the R-group was varied widely in a series of CID (collisionally-induced dissociation) experiments where the appearance energies were measured for acylium ion formation. These data may be used as a factor in predicting whether a given carbonyl substrate will likely undergo elimination-addition. Furthermore, future work in this area may demonstrate a correlation between these energies and mechanistic tendencies of substrates containing a given R-group. This work will be discussed in detail in chapter 3.

Gas Phase Measurement of Proton Affinities for MALDI Matrix Molecules

In addition to substitution reactions, another bimolecular process which is effectively studied via FTICR is proton transfer. Since the reaction chemistry in the analyzer cell is thermodynamically controlled (in an equilibrium), proton affinities may be accurately measured for many systems. In matrix-assisted laser desorption ionization (MALDI), proton transfer is important in ionizing the analyte in a reaction which preferably has low exothermicity. As mentioned earlier, MALDI has only recently provided mass spectrometrists with a low energy method for introducing ions of larger organic species (especially biomolecular species). In MALDI, proton transfer occurs from a matrix (usually a carboxylic acid) molecule to the analyte in the desorption plume. However, there has been a great deal of debate into the mechanistic details of this ionization process. Furthermore, it is well known that certain matrices tend to produce greater amounts of fragmentation in the analyte, presumably from a higher energy process. It has been suggested that the amount of energy transferred to the analyte may be dependent on the proton affinity of the matrix. Unfortunately, data on the proton affinities of most MALDI matrices are sparse.

Again, FTICR provides an excellent approach to the measurement of these proton affinities. In work presented in chapter 5, the proton affinities of several common MALDI matrix molecules were measured by bracketing experiments using reference compounds with known proton affinities. Indeed, the numbers do show some correlation between the proton affinities and the degree of fragmentation caused by several matrices.

Microsolvation in the Gas Phase

Comparing gas phase chemistry to that observed in solution is not without its difficulties. Favored solution-phase reactions often are found to be energetically impossible in the absence of solvation, as will be demonstrated repeatedly in the coming chapters. Conversely, many known gas phase reactions are not observed in solution. The advantage of gas phase studies is that they provide a more unperturbed view into the energetics of chemical reactions without the influence of solvent. In certain instances, gas phase chemistry actually provides some understanding of solvent effects by providing a reference point (zero solvent effects).

The effects of solvent can be divided into two main groups, including primary effects and bulk properties of the solvent.[37] The primary effects are caused mainly by the first solvation sphere. In solution, the differential solvation of the products, reactants, and activated complex serves to control the energetics of a reaction. In addition, solvation often controls positional relationships between potential reactants by 'directing' the reactive functional groups into the necessary stereochemistry for a reaction to occur. In solvated environments, the reactants may collide several times in the solvent cage thus enhancing the statistical likelihood of a reaction. In the gas phase, the reactants meet in isolated (often inelastic) collisions.

It stands to reason that the controlled formation of microsolvates in the gas phase could be particularly useful in studying primary solvent effects. In particular, reaction chemistry as well as photochemistry could be examined for many inorganic and organic systems as a function of solvation. The recent advent of electrospray

ionization has provided an excellent means for the production of solvated species. As discussed previously, the process actually relies on the production of solvated species which are subsequently desolvated in order to produce analyte ions. This procees has been studied extensively by Kebarle and Tang.[41] In the spray coming from the needle, microdroplets are formed with many ions being present. As the droplets traverse the heated capillary (sometimes a heated drying gas such as N_2 is used), desolvation occurs with smaller and smaller droplets being formed with a greater density of charge per droplet. Eventually, the microdroplets reach such a high density of charge that solvated ions "sputter" off the droplet and are finally desolvated to form individual ions of the analyte. It is therefore apparent that milder desolvation conditions should result in some microsolvated species being produced. Work conducted by Burns et al.[42] has utilized this general approach for the controlled generation of various microsolvates.

This work[42] has produced an excellent method for the controlled formation of several solvated species using an external ESI source. This technique, which was developed using a quadrupole mass spectrometer, appeared to be viable for use in conjunction with the aforementioned Bruker Bioapex FTICR. Nevertheless, differences in the Analytica source design coupled with an extensive network of ion transfer optics made developmental changes a necessity. Past research in the Eyler research group using an internal ESI system produced various H_2O-methanol solvates of several organometallic ammine complexes.[43] However, little work was done in regard to developing a reliable methodology for solvate production.

It was thus a goal of this project to develop such a routine means for the reliable production of solvated organometallic species. From this technique several solvates of ruthenium tetra- and pentaammine complexes were formed and studied. In examining the solvates produced for these complexes, a great deal of information was obtained concerning their relative stability.

The ability to trap and isolate these solvates using FTICR should provide an excellent platform for their continued study by the Eyler-Richardson group in the future. One of the primary goals of this work will be to examine the electron-transfer process in these ruthenium donor-acceptor complexes as a function of solvation. Initial attempts to examine this chemistry were conducted and will be discussed in the next chapter.

Ion-molecule Interactions in the Gas Phase

The gas phase work discussed in the coming chapters is bound by the underlying premise of ion-molecule interactions in the gas phase. Both unimolecular and bimolecular reaction processes have been studied via the multi-dimensional FTICR "gas phase chemical laboratory". In examining the gas phase chemistry of acylium ion formation, nucleophilic substitution chemistry, proton transfer, and gas phase microsolvates, this laboratory has proven to be an invaluable resource in studying an impressively wide range of ion-molecule interactions in the gas phase.

CHAPTER 2
SPECIFIC SOLVATION OF RUTHENIUM-AMMINE COMPLEXES IN THE GAS PHASE

Introduction

Importance of Studying Gas Phase Solvates

As mentioned in the previous chapter, gas phase studies are very useful for examining solvent effects in chemical systems in that they provide an extreme reference point (no solvent) for corresponding solution-phase work. Much of this gas phase work has involved thermal reactions, photochemical reactions, and photophysical studies. However, most of these studies provide little insight into the effects of solvation on a molecular level. Furthermore, it is difficult to ascertain whether these effects are due to bulk properties of the solvent or specific solvation.

Recent mass spectrometric studies involving the successful formation and detection of gas phase solvates via electrospray ionization suggest exciting new possibilities for the study of microsolvation.[42] In examining these microsolvates, primary solvent effects may be probed on a molecular level. In these types of studies, FTICR should prove to be very useful with its trapping abilities and non-destructive detection capability. Studies of this kind should provide a great deal of information regarding the structural nature and stability of these solvates.

Using an Analytica external ESI source, and the process developed by Burns et al.[42] for generating solvates (in conjunction with a quadrupole mass spectrometer), it was the goal of this project to extend this technology to FTICR. In doing so, we hoped not only to form these solvates but to trap and isolate them for more detailed studies involving solvate stability, chemical reactivity, and photophysical properties.

Electrospray Ionization: Mechanism for Desolvation

Over the past decade electrospray ionization (ESI) has proven to be a very useful method for introducing ions into the gas phase directly from solution. As mentioned in the previous chapter, this ion desolvation is energetically unobtrusive relative to most other ionization methods. The mechanism for this desolvation process has been well-studied, but the process is still not understood with any certainty. This mechanism has been examined[41] and explained via two similar mechanisms, which will be discussed here.

The ESI process may be divided into four distinct stages. The first (ion separation) involves the formation of charged droplets from the end of the electrospray needle tip (Figure 9). A high positive potential (for positive ions) of +3000 to 5000 V is applied to the needle while the heated capillary entrance is kept at ground. The necessary needle potential is dependent on the solvent and will be discussed below. Typically the analyte is dissolved in a relatively polar solvent (e.g. 50/50 methanol-H_2O) and the solution is infused through the needle at a rate of 1-5 µl/min. The analyte concentration

which is used usually ranges from 1 x 10^{-3}M to 1 x 10^{-6}M depending on the nature of the analyte.

As the solution approaches the needle tip, the electric field strength increases and the negatively-charged ions begin to migrate toward the stainless steel needle which is at a high positive potential. In addition, there is a corresponding buildup of positive charge at the surface of the solution as it leaves the needle (Figure 9). This redistribution of charge results in a drop in the imposed field inside the liquid. This buildup of positive charge results in destabilization of the liquid surface because the ions are drawn downfield, but are unable to escape the liquid. Thus, the liquid is drawn outward as a cone toward the capillary, which is at ground (Figure 9). When the electric field strength is sufficiently high, the cone becomes unstable and a filament of solution (a few μm in diameter) is emitted from the cone tip. This liquid filament has a surface which is greatly enriched in positive ions. The length of this liquid filament may be controlled somewhat by increasing or decreasing the field strength. As the field

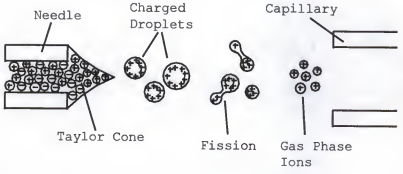

Figure 9. Electrospray mechanism for the production of gas phase ions

strength is increased, the length of the filament decreases. Decreasing the field strength can prove useful in generating solvated gas phase ions as will be shown later.

Eventually, the filament breaks down to form charged droplets having an excess of positive charge (positive ions) on the surface. In other words, the positively-charged analyte ions migrate primarily to the outer region of the droplets. The size of these droplets depends on several experimental parameters such as concentration, solvent, nature of the analyte, flow rate, etc.. This ion separation mechanism is commonly referred to as the electrophoretic process.

For the aforementioned electrospray process to occur, a minimum onset voltage must be applied to the needle tip. This potential is dependent on several factors including the needle radius and the distance between the needle and the capillary. However, the most important factor involved is the surface tension of the solvent used. The atmospheric pressure environment of the interface between the needle and capillary actually proves useful in preventing electrical breakdown during the spray. This is due to the relatively high electrical breakdown potential of oxygen. Finally, the ion current produced may be measured on the capillary ground to provide a useful quantitative estimate of ion formation.

Following the droplet formation, the next stage of the ionization process involves shrinkage of the charged droplets. During this period, evaporation of solvent molecules from the droplets occurs with the formation of droplets having a higher charge density and less stability at their surface (where much of the charge is localized). As the droplets shrink to the point where they approach the Rayleigh limit,

they become unstable and undergo fission. The nature of this fission has been examined and found to be uneven. That is to say that the parent droplets and their offspring are neither identical in size nor charge. Prior to fission, the parent droplets undergo inelastic vibrations which result in the formation of a 'tail' which emits smaller, more highly charged droplets (higher charge to mass ratio). This process may occur several times during this stage of the ionization until very small, highly charged droplets are formed. Eventually, gas phase ions are produced; however, two possible mechanisms for their formation have been suggested.

The first possible mechanism was advanced by Dole et al.[44] and involves the formation of solvated single ions from the small, highly-charged droplets. These single ion solvates would then undergo desolvation to form the gas phase ion. This mechanism is known as the "single ion in droplet theory (SIDT). The second mechanism was suggested by Iribarne and Thomson[45] and involves the emission of gas phase ions from the surface of the very small, highly charged droplet. These droplets are believed to typically have a radius ca. 8 nm with 70 charges. Still, there is no degree of certainty in the literature regarding the mechanism for this third stage.

The fourth and final event in ESI involves secondary processes where gas phase ions may be modified in either the atmospheric or ion sampling regions of the mass spectrometer. These processes vary not only with the nature of the analyte, but also with the electrospray conditions used. These processes often result from unstable ions which may have been thermally or translationally excited either during ion formation or transfer to the detection region of the mass spectrometer.

These unstable ions may undergo collisionally-induced dissociation or other thermal reactions. Nevertheless, these secondary processes are quite common and often difficult to avoid, as will be seen later in this chapter.

Physical Properties of Ruthenium Ammine Complex Solvates

The role of specific solvation in the chemistry and spectroscopy of transition-metal ammine complexes has been investigated for a variety of systems. Some examples include the solvent dependence of reaction kinetics,[46] electronic transitions,[47] properties of mixed-valence compounds,[48] photochemistry,[49] and electrochemistry.[50] Generally, the significant interaction is considered to be hydrogen bonding between a donor solvent and the N-H acceptor of the metal-bound ammonia. It is expected that the N-H bond of a metal cation-bound ammonia is a relatively strong H-bond acceptor due to the transfer of electron density from N to the metal in the coordinate covalent bond. However, relatively little is known about the structures and energetics of these specific interactions.

Recently, Zerner and coworkers reported semiempirical molecular orbital calculations on $[Ru(NH_3)_5(pyridine)](H_2O)_n^{2+}$ with n=0-15.[51] Their results suggested that hydrogen bonding by water to ruthenium(II)-bound ammonia leads to a large red shift in the metal-to-ligand charge transfer (MLCT) transition energy and that the MLCT energy would be approximately that observed in solution with ca. 15 waters clustered on the dicationic complex. Other investigators have correlated solvent shifts for MLCT and metal-to-metal CT transitions with donor numbers (DN),[52] suggesting that the shifts are associated with the strength of

the hydrogen bond between solvent and bound ammonia. Drago, et al.,[53] have used a unified solvation model[54] to separate the roles of specific acid-base and nonspecific solvent interactions in solvent dependencies of electrochemical potentials and various electronic transitions for mononuclear and binuclear ruthenium ammine complexes.

Structural details of specific solvation for these types of complexes remain unknown. Theoretical approaches have limited applicability in the absence of experimental data since the computational problems are severe for doing global minimizations of solvent interactions when many binding sites and solvent molecules are involved.

To provide further experimental evidence for specific solvation, we have been investigating gas-phase multi-charged metal complex ions that can be produced by using electrospray ionization (ESI)[55] coupled to Fourier Transform Ion Cyclotron Resonance (FTICR) mass spectrometry.[56] It is well known that under appropriate source conditions, ESI produces solvated complex ions, and the early publications on the application of ESI to metal complexes describe the formation of such solvates.[57] It has typically been reported that up to several solvent molecules can be bound to the complex ion when the source conditions are sufficiently gentle so that the weakly bound solvent molecules are not stripped away via collisionally induced dissociation in the source. Generally, all possible solvates $[ML_x]S_n^{q+}$ with n=1-N are seen in a distribution, where N is the maximum observed number of bound solvent molecules. In some solvent clusters detected by mass spectrometry, certain cluster compositions are more prevalent and are described as having "magic numbers" of solvent molecules.

Experimental

Instrumental Parameters Used for Ru(II) Complexes

These studies were conducted on a Bruker BioApex Fourier Transform Ion Cyclotron Resonance (FTICR) mass spectrometer equipped with an external ion source and a 4.7T Magnex superconducting magnet. An Analytica external electrospray ionization (ESI) source was used to generate the ions. For this work, the commercially-sold glass capillary which utilizes heated N_2 for desolvation was removed in favor of a heated metal capillary which produces a more stable ion current. This stainless steel capillary, embedded in a brass body containing a cartridge heater, was heated to 120^0C (under normal conditions) in order to generate desolvated gas phase ions.

For the ionization process, the electrospray needle was kept at a +3500 V potential while the capillary was effectively at ground. Following desolvation prior to and or within the capillary (capillary exit potential = 65 V), the ions were focused through a skimmer (skimmer potential = 18 V) and hexapole ion guide (no ion accumulation period) into the Bruker external ion source. The dc offset of the hexapole was set to ca. -38 V while the exit voltage was maintained at 80 V.

The electrospray source was evacuated by two mechanical pumps and a turbo drag pump while the external ion source is pumped down to a pressure of $2x10^{-6}$ Torr via an 800 L/s cryopump (Edwards). A subsequent 20ms ionization pulse was next utilized to direct the ions through various electrostatic optics en route to the analyzer region of the instrument. The pressure in the analyzer region was maintained at $2x10^{-9}$ Torr via pumping from two 400 L/s cryopumps (Edwards). Before

entering the analyzer cell, the ions were given an off axis "kick" in order to minimize z-axis loss of ions.[58] Finally, the ions were trapped in the analyzer cell utilizing trapping plates with +1.0 and 1.4 V potentials.

Detection of the ions was effected via RF chirp excitation with frequencies corresponding to a mass range of 100 to 2500 m/z. For each of the mass spectra obtained, 20 to 50 transients were generated and co-added to insure good signal to noise. All of the spectra generated contained 8k data points. Small data sets were used in order to minimize acquisition times for reasons which will be discussed below. It was thus necessary to zero-fill the data three times along with apodization using a Blackman-Harris function in order to improve spectral resolution.

Instrumental Parameters Used for Solvate Production

Solvated species of $BpyRu(NH_3)_4$ (Bpy = 2,2'-bipyridyl) and $IsnRu(NH_3)_5^{2+}$ (Isn = isonicotinamide) were formed in the needle-capillary region of the electrospray source by passing a bath gas of the intended solvent through this area. The solvent gas was generated by bubbling $N_{2(g)}$ through the solvent into the ionization region of the electrospray source (Figure 10). In addition, in order to generate these solvates, the temperature of the heated capillary was lowered to 90^0C and the needle voltage was lowered to +2800V. Furthermore, the exit voltage on the capillary exit was reduced to 15 V while the skimmer voltage was dropped to 10 V in order to minimize capillary-skimmer CID.

The ion transfer parameters were also optimized for solvate transmission to the analyzer cell. Although the potentials on the ion

optics varied from experiment to experiment, they were considerably different than those utilized for conventional gas phase ion transfer.

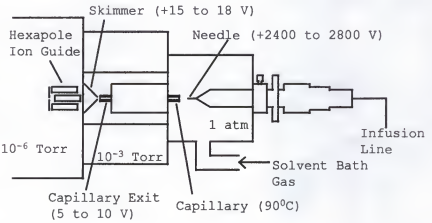

Figure 10. ESI setup and parameters utilized for solvate production

Solvate Decomposition Experimental Parameters

For all of the solvate stability experiments, the individual solvates were isolated in the analyzer cell via a shaped excitation pulse. For this isolation, a gaussian waveform was utilized with a 20 ms duration. Only the major isotope (^{102}Ru) was isolated in order to provide a "cleaner", more easily interpreted spectrum. In order to follow solvate decomposition, a variable reaction delay period was used ranging from 1 to 20 seconds depending on the relative stability of the solvates. Because of the instability of these solvates, excitation (detection) conditions were optimized in order to limit CID of the parent solvates during detection. To that end, the acquisition period was minimized with some resulting loss in resolution.

Results

Solvate Formation from Ru(II) Ammine Complexes

For these studies, two similar L-$Ru(NH_3)_x^{2+}(PF_6^-)_2$ complexes were used for reasons discussed previously. Under normal electrospray conditions, the counterions are expelled in forming the doubly-charged species depicted in Figure 11. The solvation of $BpyRu(NH_3)_4^{2+}$ (m/z 163.1; Bpy = 2,2'- bipyridyl) and $IsnRu(NH_3)_5^{2+}$ (m/z 154.6; isn = 1-isonicotinamide) was effected via electrospray ionization as described in the experimental section and these species were isolated in the FTICR analyzer cell. Under these conditions, solvation occured with the preferential formation of adducts containing 1-4 solvent molecules with some displacement of the ammine ligands by solvent molecules in some of them (Table 1). In the case of $BpyRu(NH_3)_4^{2+}$, several solvates of the parent ion have been observed with acetonitrile, acetone, and butyronitrile.

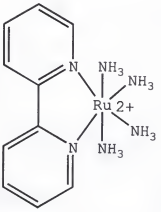

$BpyRu(NH_3)_4^{2+}$

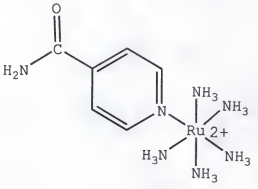

$IsnRu(NH_3)_5^{2+}$

Figure 11. Ruthenium-ammine complexes utilized for these studies

Solvation of $BpyRu(NH_3)_4^{2+}$ using acetonitrile(AcCN) resulted in the formation of one, two, and three solvate adducts (Figure 12) which were observed at m/z 183.6 (n=1) and 204.1 (n=2). In addition, several solvates were formed where one or more NH_3 groups had been replaced by an acetonitrile ($BpyRu(NH_3)_xAcCN_x$, where x = 1,2,3). These adducts were observed at m/z 175.1, 190.6, and 195.6. Each of the tetraammine acetonitrile solvates was isolated (major isotope peak only) in the analyzer cell, and subjected to a variable storage period of 1 to 20 seconds. All of these solvates were found to be metastable and to decompose over several seconds to form the parent ion and species which had lost 1,2,3, or all 4 NH_3 groups. Loss of the ammine ligands probably occured in thermally "hot" ions which were excited either during ion transfer through the electrostatic optics or from bleed-off from the isolation excitation.

In the case of the acetone (Ace) solvates of $BpyRu(NH_3)_4^{2+}$, one and two solvate analogs of the parent ion were observed. Again, several species were formed where 1 or 2 NH_3 groups had been displaced in favor of solvent ($BpyRu(NH_3)_3AcCN_{1,2}$, $BpyRu(NH_3)_2\,Ace_{1,2}$) coordination. Following isolation of the major isotope, each of the solvates of the parent ion were again found to be unstable and decomposed to form the parent ion. Loss of NH_3 groups from thermally "hot" parent ions was again observed.

Finally, when butyronitrile (BuCN) was used as the solvent vapor, one and two molecule solvates of the parent ion were observed as well as displacement species ($BpyRu^{2+}(NH_3)_3BuCN_{1,2}$), as in the cases of acetonitrile and acetone. However, in addition, two species were observed where the Ru had apparently undergone oxidation to the 3+ state

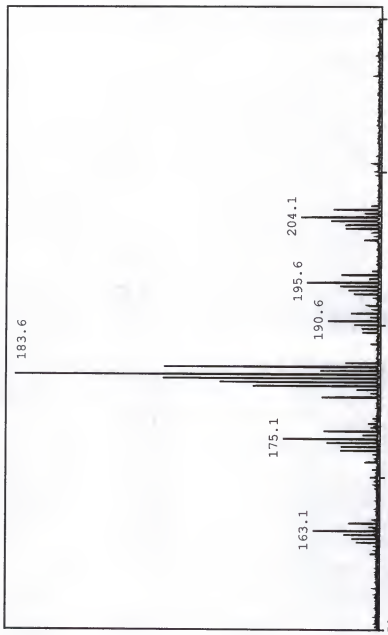

Figure 12. $BpyRu(NH_3)_4^{2+}$ acetonitrile solvates

and a methoxide, MeO^-, ligand had become attached. It is likely that this adduct was formed either in the high voltage electrospray ionization source or in the hexapole ion guide (source region), where the ions are stored for a brief period of time before being introduced into the analyzer region of the instrument. Isolation of the individual solvates followed by the aforementioned reaction delay resulted in the formation of decomposition products similar to those seen for the acetonitrile and acetone solvates.

Table 1. Solvated Ru(II) complexes produced (solv : solvent molecules- e.g. acetonitrile (AcCN), butyronitrile (BuCN))

Solvated Complexes	AcCN Solvates		BuCN Solvates		Acetone Solvates	
	y	x	y	x	y	x
$BpyRu(NH_3)_x(Solv)_y^{2+}$	1	4	1	4	1	4
	2	4	2	4	2	4
Bpy:	3	4	1	3	1	3
2,2'-bipyridyl	1	3	2	3	2	3
	2	3			1	2
(see Figure 11)	3	3			2	2
	y	x	y	x	y	x
$IsnRu(NH_3)_x(Solv)_y^{2+}$	1	5	1	5	1	5
	2	5	2	5	2	5
Isn:	3	5	1	4	3	5
Isonicotinamide	4	5	2	4	1	4
	2	4	2	3	2	4
(see Figure 11)	3	4	3	3	3	4
					2	3
					3	3

The formation of solvates of $IsnRu(NH_3)_5^{2+}$ followed similar trends as observed for the $BpyRu(NH_3)_4^{2+}$. When acetonitrile was used as the solvent vapor, solvates of the parent ion formed where one (m/z 175.0), two (m/z 195.6), three (m/z 216.1), and four (m/z 236.5) solvent groups were attached (Figure 13). In addition to these adducts, several species were observed where an NH_3 had been displaced in favor of an acetonitrile ($IsnRu^{2+}(NH_3)_4AcCN_{2,3}$). These adducts were observed at m/z

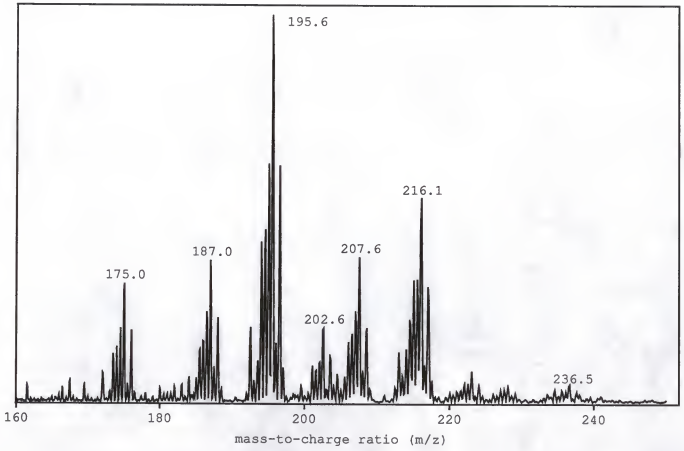

Figure 13. $IsnRu(NH_3)_5^{2+}$ acetonitrile solvates

187.0, 202.6, and 207.6. Furthermore, two other adducts were formed which contain an oxidized Ru^{3+} and a methoxide ligand ($IsnRu^{3+}(NH_3)_4(OMe^-)AcCN_{2,3}$) as discussed before. When the solvated parent ions ($IsnRu^{2+}(NH_3)_5AcCN_{1-4}$) were isolated and allowed to react for 1 to 20 seconds, loss of all solvent groups was observed as was the case with $BpyRu(NH_3)_4$.

Attempts to create acetone solvates of $IsnRu(NH_3)_5^{2+}$ resulted in 1, 2, and 3-molecule solvates of the parent ion $(IsnRu(NH_3)_5acetone_{1-3})^{2+}$. Again, several adducts were formed where 1 or 2 NH_3 groups had been displaced and 1, 2, or 3 acetones had attached (see table 1). Isolation of the solvated parent ion containing 2 acetone solvent molecules followed by a 10 second reaction delay resulted in formation of the parent ions which suffered loss of 1-3 NH_3 groups from "hot" ions.

Isotopically-labeled Solvates

In order to verify the aforementioned assignment of the solvated Ru(II) complexes, isotopic studies of solvate formation were conducted with the $IsnRu(NH_3)^{2+}$ using acetonitrile as the bath gas. In these studies, deuteriated electrospray solvents and bath gas solvents were substituted for the protiated analogs as described previously. Initially, an experiment was conducted where acetonitrile-d_3 was used in place of the protiated species for the bath gas, while the compound was sprayed from protiated acetonitrile. The observed mass spectrum indicates the presence of three primary solvates (all doubly-charged) at m/z 176.5, 198.5, and 220.5. These peaks correspond (in m/z) to the previously assigned solvates taking into account the expected shifts in mass due to the deuterium substitution (Figure 14). Thus, the solvates

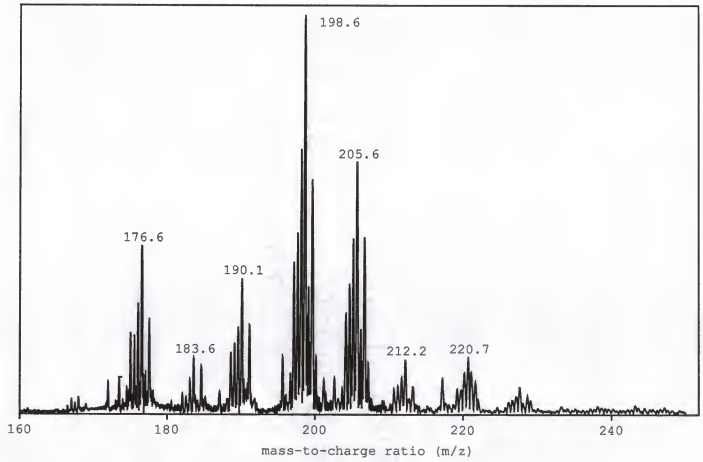

Figure 14. $IsnRu(NH_3)_5^{2+}$ solvates using acetonitrile-d_3 bath gas

have shifted by +1.5 (1 CD_3CN), 3 (2 CD_3CN), and 4.5 (3 CD_3CN) m/z units due to the presence of the deuteriums. There was no evidence of any deuteriation of the parent complex. Furthermore, other solvates observed at m/z 190.1, 205.6 and 212.1 could be attributed to the loss of (NH_3) ligands from thermally energized parent ions as discussed above.

The situation was altered when methanol-d_1 was used as the electrospray solvent in place of acetonitrile while, protiated acetonitrile was used as the bath gas. In this case, complete deuterium exchange was observed between the methanol-d_1 and $IsnRu(NH_3)_5^{2+}$. Again, solvation by the protiated AcCN resulted in the same three primary solvates being formed, now at m/z 183.6, 204.1, and 224.6. As expected, the only shift in mass could be attributed to the perdeuteriated ruthenium complex (Figure 15). In other words, each of the solvates were shifted 8.5 m/z units via deuteriation of the parent ions (with protiated solvent molecules). Additional solvates observed at m/z 194.1, 209.7, and 215.1 were attributed to loss of (NH_3) ligands.

Finally, the $IsnRu(NH_3)_5^{2+}$ was sprayed from methanol-d_4 in the presence of a bath gas of acetonitrile-d_3. As expected, the observed major solvates at m/z 185.1, 207.1, and 229.3 could be attributed to complete deuteriation of the species produced. Both the parent complex and solvent molecules were deuteriated with no evidence of protiated analogs of any kind. Again, several less intense solvates observed were found to be the result of a loss of (NH_3) ligand(s). In all of the deuteriated solvates produced, there was little or no deuterium-proton scrambling observed. The ramifications of these results are very interesting and will be discussed later.

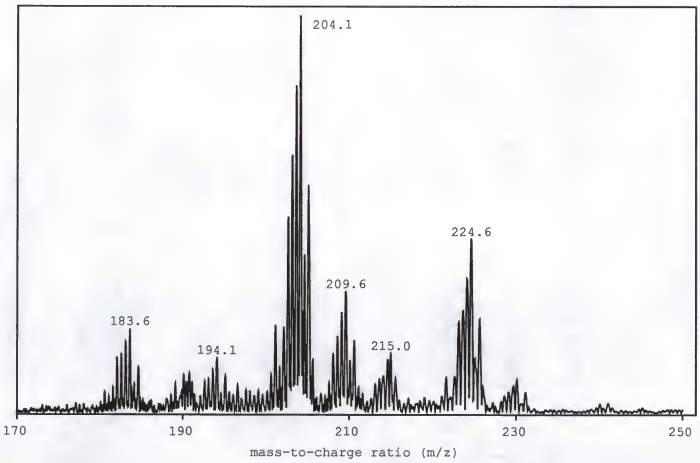

Figure 15. Perdeuteriated $IsnRu(ND_3)_5^{2+}$ with protiated acetonitrile bath gas

Solvate Fragmentation via Photoexcitation

As discussed in the introduction to this work, one goal of this project was the study of metal-to-ligand charge transfer in organometallic Ru(II) compounds as a function of specific solvation. Attempts were made to fragment the isolated Ru(II) solvates via photoexcitation of the metal-to-ligand charge transfer (MLCT) band. For these experiments, a Nd-YAG dye laser was aligned so that the collimated beam passed through the middle of the analyzer cell. Irradiation was generated between 525 and 680 nm with the laser power being varied from 50 mJ to 200 mJ. At laser power greater than 200 mJ, ions were no longer detected in the cell. The aforementioned excitation resulted in no apparent formation of smaller solvates or parent complex. At this time, it is unclear why no fragmentation was observed; however, considerable blue-shifting of the MLCT band (relative to that observed in bulk solution) may occur in this microsolvate environment. Thus, excitation at lower wavelengths (<500 nm) may be necessary for photoexcitation. Also, a brief increase in pressure was observed in the analyzer region following the laser shot. It is possible that the laser desorbed large clouds of neutrals from the cell walls which collisionally removes the solvates from the cell.

Discussion

Relative Stablity of Ru(II) Ammine Solvates

Several trends were observed for the $BpyRu(NH_3)_4$ and $IsnRu(NH_3)_5$ solvates with regard to decomposition. First of all, all of the acetonitrile, acetone, and butyronitrile solvates were found to undergo

loss of all of the solvent groups to form the doubly-charged parent ion which underwent decomposition with the loss of NH_3 groups. It appeared that acetone was expelled slightly faster than acetonitrile and butyronitrile which were found to be a little more stable (Figure 16). This was not unexpected since acetonitrile and butyronitrile are known to be better π-acids than acetone and can readily undergo π back-bonding. Also, it appeared that solvates of $IsnRu(NH_3)_5^{2+}$ were more stable than solvates of $BpyRu(NH_3)_4$ (Figure 16). This may have been due to the presence of one additional NH_3 ligand with $IsnRu(NH_3)_5^{2+}$ and thus, more hydrogen bonding interaction. This effect may also arise from greater steric hindrance with the presence of the bidentate 2,2'-bipyridyl ligand as opposed to the monodentate isonicotinamide moiety.

Finally, single solvates appeared to have greater stability than their double-solvate counterparts, which decayed more rapidly. The effect was not large, but appeared to be consistent. Attempts to cool the solvates in the cell via collisional cooling with argon produced no noticeable effect on the decomposition rate.

In an effort to obtain reaction rate constants for these decomposition processes, first order (decay) plots (ln(Ion Intensity) vs. Time) were constructed (Figure 17). However, these plots were also found to be non-linear with a faster component and a slower component. The faster component was probably due to 'hot' ions, which fragmented faster than the thermalized ions. Furthermore, an insufficient number of data points prevented a more detailed analysis at this time.

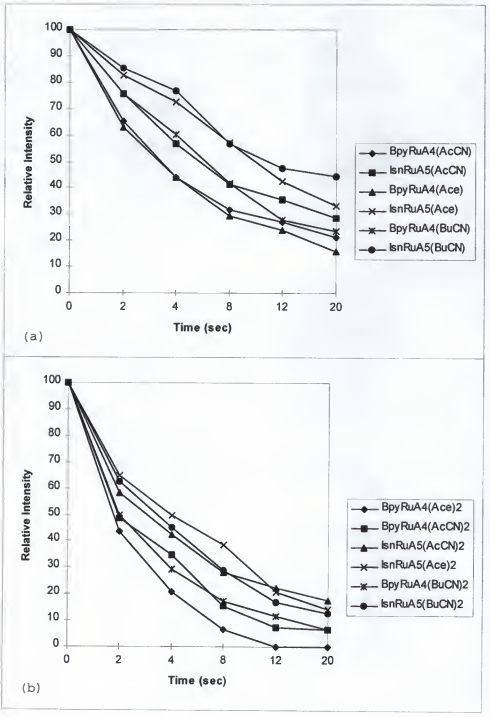

Figure 16. Plot of Ion Intensity vs. Time (sec) for both singly (a) and doubly (b) solvated ru(II) complexes

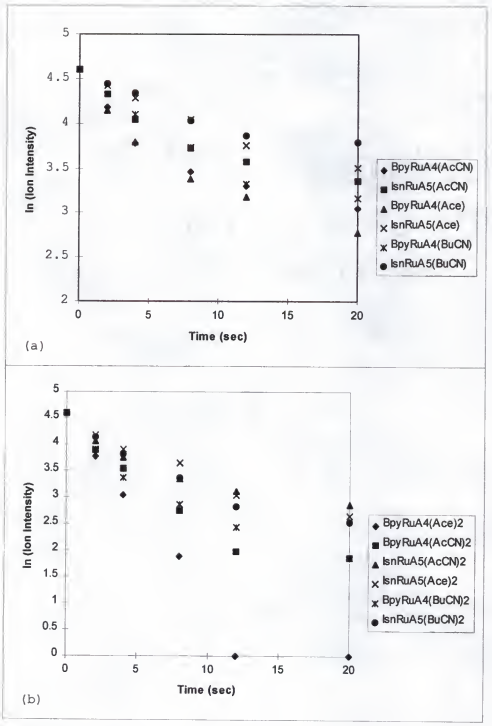

Figure 17. Plot of ln(Ion Intensity) vs. Time (sec) for both singly (a) and doubly (b) solvated ru(II) complexes

Attempts to Generate other Solvated Species

Another solvent utilized in attempts to generate solvates with $IsnRu(NH_3)_5^{2+}$ and $BpyRu(NH_3)_4^{2+}$ was isopropylamine. Unfortunately, the only resulting ion observed was protonated isonicotinamide (m/z 123). Other attempts to generate solvates of the ruthenium complex ions using MeOH, isopropanol, pyridine, dimethyl sulfoxide, and ethanol failed. In these cases, various products were observed with apparent loss of ammine ligands and some corresponding coordination of water. It is somewhat surprising that no solvates of methanol, ethanol, or dimethylsulfoxide were observed since all of these were observed by Posey.[41] However, the work by Posey was conducted using a quadrupole mass spectrometer where less ion transfer is required and detection is faster (several milliseconds). Furthermore, as discussed above, the trapped solvates observed were found to be unstable and decayed over several seconds. It is possible that other less stable solvates are produced, but don't survive the transfer process through the electrostatic optics.

Importance of Isotopic Labeling Studies

From the isotopic labeling experiments, a great deal of insight was gained concerning the solvation process and ultimately, the electrospray ionization process for these Ru(II) hexammine complexes. As mentioned above, when deuteriated acetonitrile was used as the bath gas in place of the protiated analog, deuteriated solvates were produced, as expected. While this certainly supports the conclusion that these species are the assigned solvates, of greater interest is the total lack of corresponding protiated analogs. This indicates several things about the process for gas phase solvate formation.

First of all, solvation of the complexes must be coming exclusively from the bath gas and not from insufficient drying (evaporation) of the electrospray solvent. Otherwise, some protiated analog should be observed. Also, this indicates that complete desolvation must precede resolvation from the bath gas. It is possible that these observations could also be explained by a dominating background pressure of bath gas relative to the electrospray solvent. However, this seems unlikely since such a high pressure of deuteriated gas would likely result in additional deuterium exchange with the complex, and this was not observed. Finally, these observations suggest the possibility that desolvation is occurring very early after leaving the needle, and certainly before entering the capillary. The fact that variation in the capillary temperature results in relatively little change in the solvate composition supports this conclusion. Early desolvation is somewhat surprising since current theory suggests that solvation occurs later.

Conclusions

It is evident from the aforementioned results that metastable solvates of $BpyRu(NH_3)_4^{2+}$ and $IsnRu(NH_3)_5^{2+}$ were produced using the technique described earlier. The reason for this instability was not determined; however, several reasons seem possible. First of all, the binding energies of these solvates are minimal (presumably less than 20 kcal/mol) and thus, little energy is required to dissociate them. This energy might be coming from the ionization process itself; however, electrospray ionization is generally regarded as a non-energetic method for ionization. Furthermore, the dissociation energy may be acquired

during the ion transfer process since many sets of ion electrostatic optics are utilized. Finally, the solvates may simply be unstable in the gas phase. Despite the apparent instability of these solvates, it has been demonstrated that they may be trapped and isolated with lifetimes of several seconds. This should present an adequate opportunity for studies of chemical reactivity and photophysical properties (especially electron transfer spectroscopy) as a function of microsolvation. Solvates of acetonitrile, acetone, and butyronitrile were formed with both parent ions. All of these solvents are non-aromatic, non-conjugated π solvents which may explain the observed trend.

CHAPTER 3
COLLISIONALLY ACTIVATED DISSOCIATION OF N-ACYLPYRIDINIUM CATIONS

Introduction

Acyl cations are important reaction intermediates well recognized in both solution and gas phase chemistry. Salts of simple acyl cations with non-nucleophilic anions, RCO^+X^-, have been prepared in solution[59,60] and have been isolated in the solid state.[61] Acyl cations are stable in super acid solutions[60] (e.g. FSO_3H-SbF_5-SO_2) or in oleum[59] (concentrated sulfuric acid containing SO_3). Gas phase dissociation energies for CH_3COBr (151.1 kcal/mol) and t-BuBr (148.7 kcal/mol) indicate that the acetyl cation CH_3CO^+ is about as stable as the *t*-butyl cation.[62] Acyl cations are stabilized by charge delocalization, as depicted in Figure 18. In one canonical form, a triple bond exists between the oxygen and carbon with positive charge residing on the oxygen. However, in this linear intermediate, the other resonance form dominates and most of the positive charge resides on the carbon atom.[63]

Figure 18. Resonance stabilization in acylium ions

Studies of Solution-Phase Acyl Transfer

The mechanisms of acyl transfer reactions in solution have been extensively investigated and reviewed.[64,65] The solution phase experimental work up to 1960 was satisfactorily interpreted in terms of

a carbonyl addition-elimination mechanism proceeding through a covalently-bound tetrahedral intermediate.[64] More recently, Williams et al.[66-69] and Jencks et al.[70,71] have found evidence for a concerted pathway for acyl transfer between substituted phenolate nucleophiles and nitrophenyl acetate and formate substrates. In these reactions, bond making and bond breaking appear to be equivalent (or nearly so) in the transition state. Concertedness has also been suggested to occur in the solvolysis of acyl chlorides in aqueous media[72-74] and in alcoholic media.[75,76] Further variations, covering the entire S_N2-S_N1 mechanistic spectrum of acyl transfer reactions have been reported.[77]

Previous Gas-Phase Studies of Acyl Transfer

In addition to the solution phase debate, there has been considerable controversy concerning the mechanistic details of acyl group transfer in the gas phase as well. Early gas phase studies by Bowie and Williams[78] suggested that acyl transfer proceeded along a potential energy surface containing a single minimum which was believed to be the stable, covalently-bound tetrahedral intermediate observed in solution. In this work involving fluorinated formate nucleophiles and anhydride substrates, detection of a loose adduct ($CF_3CO_2^-\cdot(CF_3CO)_2O$) led to the assignment of the intermediate's structure. Further work by Riveros and coworkers suggested that these intermediates were formed via bonding between the nucleophilic oxygen of the formate and of the formyl group of the anhydride.[79,80]

However, in examining the reaction between methyl formate and nucleophilic hydroxide ions, Riveros found that the observed tetrahedral adduct ($HC(OMe)\cdot OH^-$) was more likely a local transition state than a

stable intermediate.[81,82] Furthermore, kinetic studies by Brauman et al.[83] of acyl transfer (figure 19) indicated slower reaction rates than the corresponding predicted collision rates. This implied that the potential energy surface for these reaction contains at least two minima separated by a barrier, which was estimated to be ca. 7 kcal/mol (from RRKM calculations).

Figure 19. Gas phase acyl transfer reactions examined by Brauman

In contrast, other gas phase studies suggest that acyl transfer occurs via an acylium ion intermediate (elimination-addition (S_N1)). For example, Caserio et al.[84] have examined acyl transfer reactions between protonated substrates ($AcOH_2^+$) and several oxygen and sulfur nucleophiles. They concluded that for these electron-deficient systems, acyl transfer occurs via the formation of acyl cation complexes rather than tetrahedral intermediates.

In addition, a number of theoretical studies have been conducted examining the mechanistic pathway(s) for acyl transfer reactions. These studies support the work of Brauman in suggesting a potential energy surface which contains two minima separated by a central barrier. However, while these studies largely agree on the general reaction model, they disagree on the nature of the intermediate state. One study by Blake and Jorgenson suggests the presence of a true tetrahedral

intermediate[85] which would support a pathway involving addition-elimination. Still another study by Yamabe and Minato[86] supports the participation of an unstable activated complex which would suggest that acyl transfer occurs via direct displacement (S_N2). Finally, theoretical work done by Park et al.[87] suggests a pathway where there is rate-limiting breakdown of the anionic intermediate.

Experimental studies have also failed to ascertain the nature of the intermediate state and whether it is a true intermediate. For instance, Brauman and co-workers[88] observed an unsymmetrical ion-molecule adduct for the reaction between Cl^- and CH_3OCOCl, but could not determine whether this adduct represented a true tetrahedral intermediate or an activated complex (transition state). Another study of carbanion additions to esters in the gas phase suggested the occurrence of addition-elimination-deprotonation as in solution Claisen condensation reactions.[89,90]

Gas Phase Acyl Transfer Reactions between Electron-Deficient Species

Most gas phase studies to date, and nearly all those discussed above, have examined acyl transfer reactions between neutral substrates and anionic nucleophiles. However, only a few studies have attempted to ascertain mechanistic details for acyl transfer in electron deficient systems. In general, these reactions are quite different energetically from their electron-rich counterparts and need to be further examined. In previous gas phase[91,92] and theoretical work[93-95], the mechanism of nucleophilic substitution was studied at saturated carbon atoms using charged pyridinium substrates of type $R\text{-}Py^+$. Such species have neutral leaving groups which allow both S_N1 and S_N2 reactions to proceed in low

dielectric constant media.[96-99] Furthermore, utilizing Fourier transform ion cyclotron resonance mass spectrometry (FTICR MS), N-substituted alkyl and arylpyridinium cations were isolated in the gas phase and subjected to CID (collisionally-induced dissociation) conditions in order to determine bond threshold energies.[91,100] Through these measurements, information was obtained regarding the energies required for bond breaking in aliphatic nucleophilic substitution reactions. In addition, attempts were made to generate gas phase nucleophilic substitution reactions with these pyridinium ions. This work will be discussed in the following chapter.

In this project, CID studies were conducted (as with the N-alkylpyridinium cations mentioned above) for a series of *N*-acylpyridinium cations in the gas phase in order to determine the bond (C(acyl)-N(pyridinium)) threshold energies. In addition, initial attempts to generate gas phase acyl transfer provided no definitive evidence for the process; however, a prior knowledge of these fragmentation energies should prove useful in future studies. Finally, future work may ascertain whether there is any correlation between these threshold energies and the observed mechanistic pathway for acyl transfer.

Experimental

Mass Spectrometry Techniques

All experiments were performed on a Bruker Apex 7e 4.7 tesla Fourier transform ion cyclotron resonance (FTICR) mass spectrometer

equipped with an external ion source. The ions were introduced from an Analytica electrospray ionization source as discussed in chapter 2. The acylpyridinium salts were sprayed from dry acetonitrile (0.1 mM concentration) at a flow rate of 60 µl/hr. The electrospray needle potential was maintained at +3500 V while the capillary was effectively kept at ground. The capillary was heated to 120 °C in order to desolvate the ions as they entered the Bruker external ion source. The pressure in the external source was maintained at $1x10^{-6}$ Torr via pumping by an 800 L/s cryopump. After entering the external ion source, the ions were guided to the analyzer region of the instrument via a series of electrostatic ion optics which were optimized for efficient ion transfer. Pressure in the analyzer region was maintained at $2x10^{-9}$ Torr via pumping by two 400 L/s cryopumps. Immediately before entering the analyzer cell, the ions were given a "sidekick" to prevent any z-axis loss.[58] Once in the cell, the ions were trapped using trapping potentials of +1.0 and +1.4 V on the two trapping plates.

Inside the FTICR analyzer cell, the acylpyridinium parent ion was isolated using an RF notch ejection. Following a 3 second cooling delay to allow for thermalization of the ions, argon was introduced via a piezoelectric pulsed valve (50ms pulse) for collisionally-induced dissociation (cell pressure = $1x10^{-7}$ Torr) of the parent ions. A 100 µs RF activation pulse was used to translationally excite the ions which were then allowed to fragment during a subsequent 0.25 sec reaction delay. The resulting reactant and product ions were detected via frequency-chirp excitation.

Broadband detection was utilized in these experiments, covering a mass range of 50 to 2500 amu. During detection, 20 spectra (8k data

sets) were acquired and averaged for excellent signal to noise (S/N 500/1).

Determination of Appearance Energies

The appearance energies for the formation of the acylium ions and protonated DMAP (depending on the fragmentation pathway) were determined as discussed previously.[100] In these calculations, at least 20 data points were utilized between 0 and 40% fragmentation of the acylpyridinium ion. In order to calculate the translational energy imparted to the parent ion, the infinite parallel plate capacitor approximation was utilized:

$$E_{ion} = q^2v^2t^2/8md^2 \qquad \text{(Eq 2)}$$

where q represents the ionic charge, V is the amplitude of the RF activation pulse, t is the RF activation pulse width, m represents the ionic mass of the parent ion, and d (0.06 m) is the distance between the excitation plates of the analyzer cell. Determination of the threshold energy was effected using the method of Chantry[101] which takes into account the spread in both ion and neutral translational energies. The percentage of fragmentation was plotted vs. nominal ion center of mass energy with the straight line portion of these plots being extrapolated to zero fragmentation.

It is possible that multiple collisions between translationally excited ions and argon neutrals may occur during the 250 ms reaction delay time. Despite this fact, ions are no longer undergoing excitation by this time, and therefore the maximum amount of energy available for conversion to internal energy of the ion may not exceed the CM energy of the initial translational activation of the parent ion. In fact,

further collisions of ions with neutrals may result in some cooling of the ions. The threshold energy for fragmentation corresponds to those collisions where all of the relative kinetic energy has been converted in the ion/molecule collision complex into internal energy in the ion. Over the reaction delay period, there is a finite probability that this internal energy will be localized in the normal mode which corresponds to cleavage of the weakest bond in the parent acylpyridinium cation. Finally, in these calculations, no attempts have been made to integrate the vibrational energies of the individual acylpyridiniums because of the strong structural similarities in all of the compounds studied. Thus, while the absolute values of the determined appearance energies may have some degree of error (± 5 kcal/mol), trends in the data provide extremely useful information as to the relative stability of various acylpyridiniums. In addition, much insight may be gained regarding the effect of various functional groups upon acylium ion stability.

Preparation of compounds

Three of the compounds studied (**1a, 1f, 3** (Figure 20)) were made by literature methods,[102] and characterized by ^{1}H and ^{13}C NMR spectroscopy and electrospray FTICR MS. All of the other N-acyl-4-(dimethylamino)-pyridinium salts (**1b-e, 8, 12** (Figure 20)) and N-(p-toluenesulfonyl)-4-(dimethylamino)pyridinium salts (**6**) were prepared in solution by mixing the 4-dimethylaminopyridine (DMAP) and the corresponding acyl chloride in acetonitrile at room temperature for 15 min. The resulting acetonitrile solutions were directly used in the CID

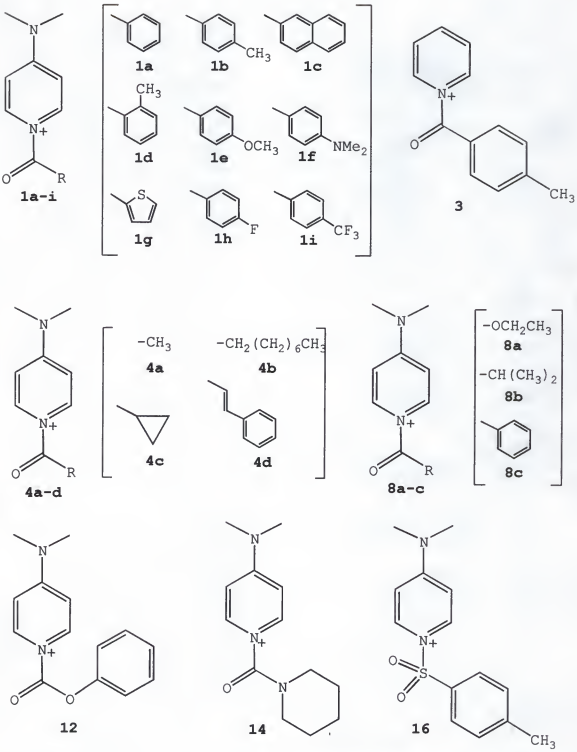

Figure 20. Acylpyridinium cations utilized in these CID studies

experiments without isolation and purification. The cation structures were all characterized by electrospray FTICR MS.

General Procedure for the Synthesis of N-Acyl-4-(dimethylamino)-pyridinium Tetraphenylborate Salts[102] (**1a,f,3** (Figure 20))

An anhydrous CH_3CN (5 mL) solution of DMAP (2 mmol) was added dropwise into a stirred, cooled (0-4 °C) solution of an appropriate acid chloride (2 mmol) and sodium tetraphenylborate (2 mmol) in CH_3CN (10 mL) under a nitrogen atmosphere. The reaction mixture was stirred for 30 min., after which the amine addition was complete. Then the white precipitate (NaCl) was allowed to settle and to pack at the bottom of the reaction flask. The supernatant was transferred by decanting and evaporated to produce a solid, which was recrystallized to give the pure product.

N-Benzoyl-4-(dimethylamino)pyridinium tetraphenylborate (**1a** (Figure 20))

This compound formed as yellow crystals, 90% yield, mp 179-180 °C (CH_2Cl_2-ether) 179-181 °C]; HRMS (FT-ICR for the cation) $C_{14}H_{15}N_2O$ requires 227.1184; found 227.117.

N-[4-(Dimethylamino)benzoyl]-4-(dimethylamino)pyridinium tetraphenylborate (**1f** (Figure 20))

yellow solid, 73% yield, mp 161-164°C (CH_2Cl_2-ether); ^1H NMR (300 MHz/DMSO-d_6) δ 8.48 (2H, d, *J* 8.0 Hz), 7.64 (2H, d, *J* 9.1 Hz), 7.17 - 7.22 (8H, m), 7.08 (2H, d, *J* 8.0 Hz), 6.91 - 6.96 (8H, m), 6.86 (2H, d, *J* 9.3 Hz), 6.77 - 6.82 (4H, m), 3.31 (6H, s), 3.10 (6H, s); ^{13}C NMR (75 MHz/DMSO-d_6) δ 166.7, 163.3 (q, *J* 49.3 Hz, ^{11}BC), 157.6, 154.4, 139.2, 135.5, 133.7, 125.2 (q, *J* 2.7 Hz, ^{11}BC), 121.4, 111.2, 106.7, 40.4, 39.6.

N-Carbopiperidinyl-4-(dimethylamino)pyridinium tetraphenylborate (**3**)

white solid, 82% yield, mp 183-186°C (CH_2Cl_2-hexane); ^1H NMR (300 MHz/acetone-d_6) δ 8.08 (2H, d, *J* 8.0 Hz), 7.33 - 7.39 (8H, m), 6.91 - 6.96 (8H, m), 6.77 - 6.83 (6H, m), 3.40 - 3.48 (4H, m), 3.18 (6H, s), 1.62 - 1.68 (6H, m); ^{13}C NMR (75 MHz/acetone-d_6) δ 164.8 (q, *J* 49.4 Hz, ^{11}BC), 158.4, 152.4, 139.6, 136.9, 126.0 (q, *J* 2.7 Hz, ^{11}BC), 122.3, 108.0, 48.45, 48.4, 40.8, 26.0, 24.4.

Results and Discussion

Fragmentation of N-(aracyl)-4-(dimethylamino)pyridinium cations

N-Benzoyl-4-(dimethylamino)pyridinium cation (**1a**) was subjected to CID experiments utilizing electrospray FTICR MS as discussed in the experimental section. It was first introduced and then isolated in the FTICR analyzer cell, where the intact parent ion was detected (m/z 227). Following the CID reaction delay period, two major ions were detected: the parent ion (**1a**) at m/z 227 and the daughter ion phenylacyl cation **2a** at m/z 105 (Figure 21 and 22). The observed appearance potential energy

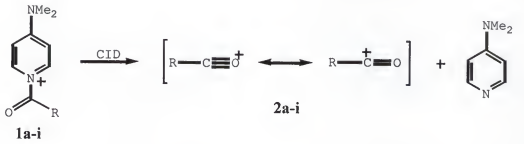

Figure 21. Collisionally-induced dissociation of N-(aracyl)-4-(dimethylamino)pyridinium cations

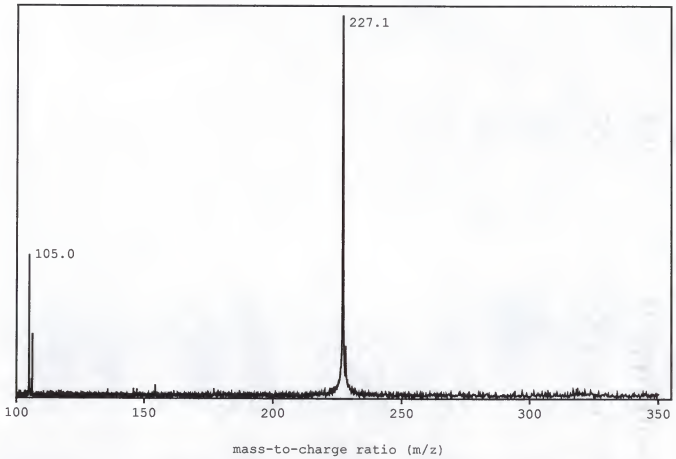

Figure 22. Fragmentation of N-Benzoyl-4-(dimethylamino)pyridinium cation

(E_{obs}) for the acylium ion **2a** was estimated as described in previous work (see experimental section).[100] The nominal center-of-mass energy (E_{cm}) was plotted vs the percent fragmentation observed (I / I_o), and the straight line portion of this plot was extrapolated to zero fragmentation. The x-intercept represents the observed appearance potential energy as depicted in Figures 23.

Five other N-aracyl-4-(dimethylamino)pyridinium cations (**1b-f**) were fragmented using the same CID conditions. A similar fragmentation pathway was observed for each of these acylpyridiniums in forming acylium ions **2b-f** (Figure 21). The Fragmentation energies (E_{obs}) were estimated as shown in Figures 23 and 24, and these results are summarized in Table 2.

The fragmentation of N-(2-Thienoyl)-4-(dimethylamino)pyridinium cation (**1g**) was also investigated. It was observed to follow the same fragmentation pattern as compounds **1a-f**. However, this compound underwent spontaneous fragmentation; thus its appearance potential energy could not be determined. Furthermore, attempts to isolate the parent ion only resulted in its further fragmentation. This result may be interpreted in two ways. Either the thienyl group destabilizes the C-N bond relative to the aforementioned acylpyridinium compounds (which require CID energy for fragmentation) or it further stabilizes the product acylium ion.

From Table 2, the E_{obs} for this series of N-(aracyl)-4-(dimethylamino)pyridinium cations (**1a-f**) increases as follows: **1f** < **1e** < **1d** < **1c** < **1b** < **1a**. This trend follows the order of electron donating capability for the R-groups used. Furthermore, the acylpyridiniums containing strong electron groups exhibited lower fragmentation energies

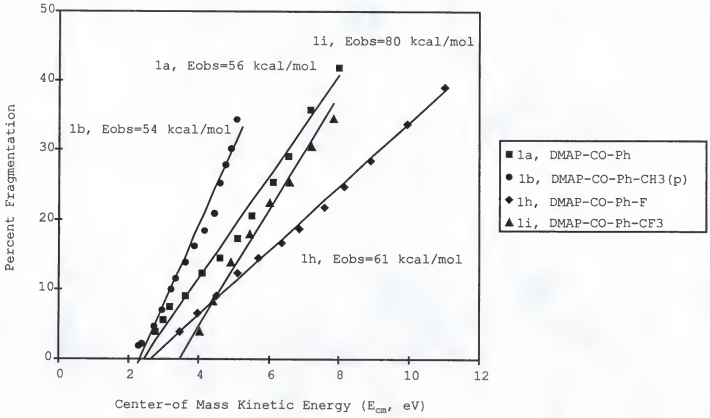

Figure 23. Plot of percent fragmentation vs.E_{cm}

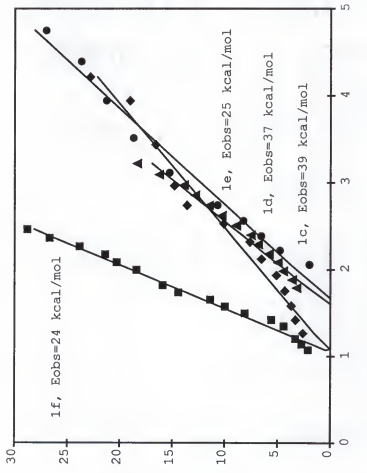

Figure 24. Plot of percent fragmentation vs. E_{cm}

Table 2. The E_{obs} (kcal/mol) of the fragmentation of N-aracyl-4 (dimethylamino)pyridinium cations to acylium ions

cmp 1-	R Group	m/z parent (**1a-g**)	m/z product (**2a-g**)	E_{obs} (kcal/mol)
a	Ph	227	105	56
b	p-MeC_6H_5	241	119	54
c	naphthalenyl	279	157	39
d	o-MeC_6H_4	241	119	37
e	p-$MeOC_6H_5$	257	135	25
f	p-$Me_2NC_6H_5$	270	148	24
g	2-thienyl	233	111	< 20
h	p-F-C_6H_5	245	123	61
i	p-CF_3-C_6H_5	295	173	80

than those containing groups of weaker donating ability. For instance, the strong electron-donating ability of the p-methoxyphenyl and p-dimethylaminophenyl R-groups lowered the E_{obs} of acylium ions **2e** and **2f** (25 and 24 kcal/mol) relative to the E_{obs} found for the benzoyl (**2a**, 56 kcal/mol) ion. In addition, the naphthalenyl substituted cation **2c**, which has a larger conjugated π system, was observed to have a fragmentation energy (39 kcal/mol) which was higher than the p-methoxyphenyl (**2e**) and p-dimethylaminophenyl (**2f**) ions, but considerably less than that observed for the benzoyl ion (**2a**).

In addition to the aforementioned electronic effect, a steric effect is observed when comparing the E_{obs} for the p-methylphenyl (**2b**) and o-methylphenyl (**2d**) cations. Both product ions are stabilized by the electron donating effect from the methyl substituent; however, in

the case of o-methyl substituted cation **2d**, the fragmentation energy is lower (37 kcal/mol). This lower energy probably results from greater steric hindrance and corresponding instability in the parent ion (**1d**). The higher E_{obs} for the para isomer (54 kcal/mol) may be attributed to less steric hindrance between the methyl group and the pyridyl moiety. Finally, for this series of acylpyridinium fragmentations, the observed electronic effect appears to be more important for the product ions, while the steric effect seems to involve the parent ions. Both of these effects will be discussed in greater detail in the conclusions section of this chapter.

N-(p-fluorophenyl)-4-(dimethylamino)pyridinium (**1h**) and N-(p-trifluoromethylphenyl)-4-(dimethylamino)pyridinium (**1i**) cations were chosen in order to study the effect of electron-withdrawing groups upon the observed fragmentation energies. These compounds were also subjected to CID (Figure 23) and the E_{obs} values for the acylium ions (**2h** and **2i**) were calculated to be 61 kcal/mol and 80 kcal/mol, respectively. These fragmentation energies are considerably higher than those observed for the corresponding benzoyl (**2a**) and p-methylphenyl (**2b**). This is not surprising based on the trend observed for the acylpyridiniums containing electron donating groups. Thus, electron withdrawing groups can be expected to destabilize the acylium ions relative to the parent ions and therefore more energy will be required to break the C-N bond. Furthermore, the effect of the p-trifluoromethylphenyl group was found to be much stronger than that observed for the p-fluorophenyl, which would be expected based on the stronger electron withdrawing capability of the former.

When N-(p-methylbenzoyl)pyridinium cation (**3**) was subjected to CID conditions, the product ion (p-methylphenylacyl cation (**2b**)), was observed (Figure 25). This fragmentation pattern was similar to that seen for cation **1b** however; no CID energy was required to dissociate cation **3** to acyl cation **2b**. Thus, the fragmentation energy may only be estimated to be less than 20 kcal/mol (as in the case of the thienyl cation). These results suggest that the p-dimethylamino electron-donating group serves to strengthen the carbon-nitrogen (acyl) bond of cation **1b** relative to compound **3**.

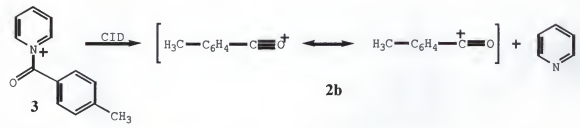

Figure 25. Fragmentation of N-(p-methylbenzoyl)pyridinium cation

Fragmentation of N-(alkylacyl)pyridinium cations

Four N-(alkylcarbonyl)pyridinium cations (**4a-d**, Figure 26) were investigated by the same method as described above. A novel fragmentation pathway was observed in these studies. After the parent ion, N-acetyl-4-(dimethylamino)pyridinium cation (**4a**), was isolated and energized in the analyzer cell, only protonated DMAP (**7**) was observed (other than the unreacted parent ion), as shown in Figure 26. The expected acetyl cation **5** was not detected. In addition, the E_{obs} for the protonated DMAP was estimated to be 39 kcal/mol. When N-octanoyl-4-(dimethylamino) pyridinium cation (**4b**) was used as the substrate, a

similar result was obtained in that protonated DMAP (**7**) was the only observed product ion. However, the appearance potential energy could not be determined since the reaction required no CID energy for dissociation of the parent cation. When N-(cyclopropanecarbonyl)-4-(dimethylamino)-pyridinium cation (**4c**) was subjected to CID conditions, again, the only observed product was protonated DMAP. In this case, the fragmentation energy was estimated to be 30 kcal/mol. Similarly, the estimated E_{obs} for N-cinnamoyl-4-(dimethylamino)pyridinium cation (**4d**) fragmentation was 24 kcal/mol. The center-of-mass kinetic energy is plotted vs. the observed percent fragmentation observed as shown in Figure 27.

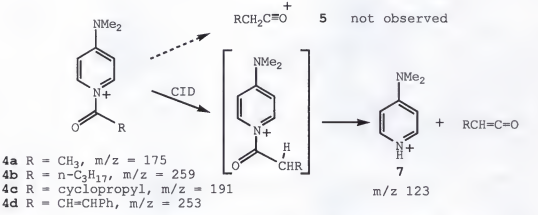

Figure 26. Fragmentation pathway for N-(alkylacyl)pyridinium cations

In previous work,[103,104] it was demonstrated that ion-molecular pair complexes[105,106] are involved in fragmentation pathways of N-alkylpyridinium cations. Such an ion-molecular pair is probably present (as an intermediate) in the fragmentation of the aforementioned N-(alkylacyl)pyridinium cations (**4a-d**). From this species, protonated

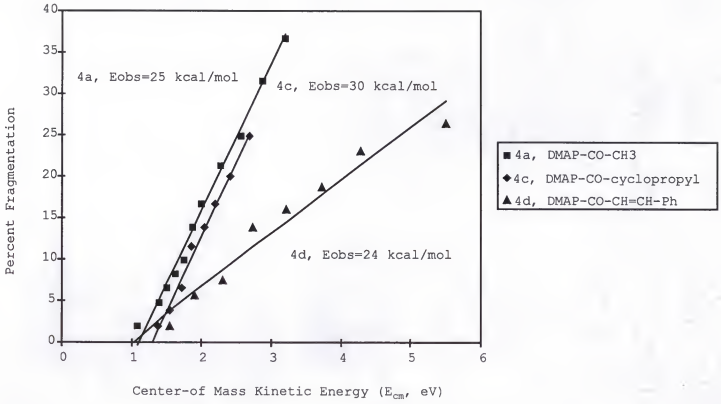

Figure 27. Plot of percent fragmentation vs. E_{cm}

DMAP (**7**) may form via β-elimination. Presumably, the β-elimination also produces a neutral ketene (Figure 26).

Fragmentation of N-(alkoxyacyl)pyridinium cations

N-(Ethoxyacyl)-pyridinium cation **8a** was also studied under the same CID experimental conditions. The fragment ions observed were N-carbohydroxy-4-(dimethylamino)pyridinium cation (**9**) at m/z 167 and protonated DMAP (**7**) at m/z 123 (Figure 28). Cation **9** was formed without introducing any CID energy, while additional energy was required for the formation of cation **7**. When the ion at m/z 167 was continuously ejected from the cell (during the reaction delay period), the ion at m/z 123 was no longer observed. This indicates that the ion at m/z 123 was formed from the ion at m/z 167 (via loss of carbon dioxide) and not directly from the parent ion **8a**. Additionally, when the ion at m/z 167 was isolated in the cell and further subjected to CID, as expected, the ion at m/z 123 was formed. Similarly, only cations **9** and **7** were formed when N-(isobutoxyacyl)pyridinium cation (**8b**) was fragmented under the same CID conditions.

When N-(benzyloxycarbonyl)-4-(dimethylamino)-pyridinium cation (**8c**) was isolated and then energized in the analyzer cell, immediate elimination of CO_2 took place and the only product observed was that of fragment **11**. A possible pathway for the formation of **9** and **11** is shown in Figure 28. In the fragmentation of cations **8a** and **8b**, a β-H elimination may have occurred (via a concerted mechanism) in the formation of intermediate **9** with concurrent generation of a neutral alkene. This intermediate (**9**) is relatively unstable and it can easily lose CO_2 when RF energy is applied. Interestingly, when sufficiently

high energy was transferred to cation **8b**, a second fragmentation pathway was observed. As in the case of cations **1a-f**, an acylium ion was

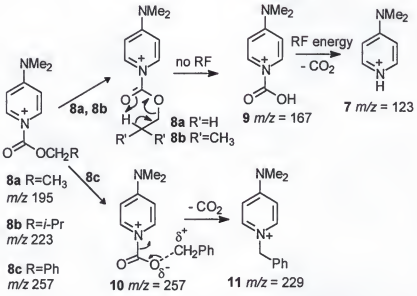

Figure 28. Fragmentation pathway for N-(alkoxyacyl)pyridinium cations

observed in addition to the protonated DMAP. This acylium ion must form via a higher energy pathway since it is not observed with lower activation energy.

When a β-H was not available, as in the case of ion **8c**, an ion-molecule complex **10** may have formed (same m/z as the starting pyridinium cation) via a bond breakage of C-O rather than C-N. Elimination of carbon dioxide was directly observed as a result of an intramolecular rearrangement in the ion-molecule complex **10** (Figure 28).

N-(Phenoxyacyl)-4-(dimethylamino)pyridinium cation (**12**) was observed to be quite stable under CID conditions. Only the parent ion was observed until very high RF energy was applied. Even with higher applied energies, no intermediate (**9**) at m/z 167 was detected and

protonated DMAP (**7**) was the only product ion observed (Figure 28). Furthermore, the measured E_{obs} was very high (72 kcal/mol). This may be explained by the fact that there are no available aliphatic β-hydrogens in cation **12**, unlike the pyridinium cations **8a,b**. Thus, the fragmentation pathway observed for **8a,b** is unavailable for cation **12**. Therefore, a phenyl hydrogen must be transferred in order to form the protonated DMAP. Such a transfer would require more energy and would result in the formation of neutral benzyne (**7**). As a result of the high activation energy used, the neutrals carbon dioxide and benzyne (Figure 29) are most likely lost simultaneously, forming ion **7**.

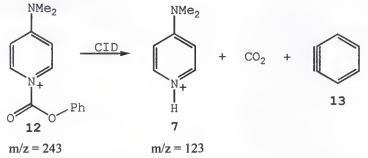

Figure 29. Fragmentation pathway for N-(phenoxyacyl)-4-(dimethylamino)-pyridinium cation

N-(Piperidinylacyl)-4-(dimethylamino)pyridinium cation (**14**) was also examined under the same CID conditions. Although it is structurally different from cations **1a-f**, cation **14** behaved similarly. The piperidinylacyl cation **15** was the only fragment ion observed during the CID experiment (Figure 30). The appearance potential energy was measured to be 67 kcal/mol.

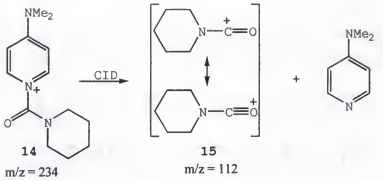

Figure 30. Fragmentation pathway of N-(piperidinylacyl)-4-(dimethylamino)pyridinium cation

N-(p-Toluenesufonyl)-4-(dimethylamino)pyridinium cation (**16**) was also studied under the above mentioned CID conditions. The parent ion was isolated in the analyzer cell, and following CID, two product ions were observed (Figures 31 and 32) at m/z 155 (p-toluenesulfonyl cation **17**) and at m/z 91 (tropylium ion and/or benzyl cation).[107,108] In order to verify the dissociation path for this reaction, cation **17** was continuously ejected from the cell, and as a result, the product ion at m/z 91 was no longer observed. This confirms that the starting cation **16** dissociates to p-toluenesulfonyl cation **17**, which can dissociate

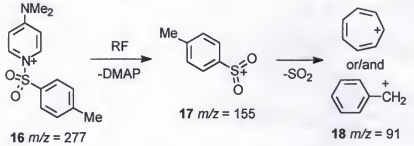

Figure 31. Fragmentation pathway of N-(p-toluenesulfonyl)-4-(dimethylamino)pyridinium cation

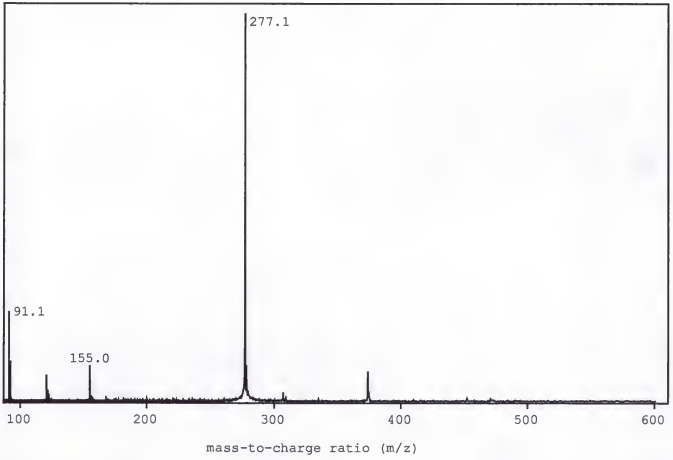

Figure 32. Fragmentation of N-(p-toluenesulfonyl)-4-(dimethylamino)pyridinium cation

further to the tropylium ion and/or benzyl cation as shown in Figure 31. The E_{obs} for this fragmentation was measured to be 38 kcal/mol. Compared to the 54 kcal/mol observed for the benzoyl cation **1b**, the significantly lower E_{obs} for N-sulfonyl cation **16** suggests that the nitrogen-carbon (acyl) bond is stronger than the nitrogen-sulfur bond in these pyridinium cations.

Gas Phase Bimolecular Reactions of Acylpyridinium Cations

As mentioned in the introduction, it was the eventual goal of this project to generate acyl transfer reactions within electron deficient systems in the gas phase. Initial attempts were made in this area with several of the species examined above. For these attempts, piperidine, n-hexanol, and 1-methylimidazole were utilized as the potential nucleophiles. Furthermore, compounds **1a** (E_{obs} = 56 kcal/mol), **1f** (E_{obs} = 24 kcal/mol), and **14** (E_{obs} = 67 kcal/mol) were employed as substrates because of the wide range of fragmentation energy observed between the them.

The same reaction conditions were used in this study as mentioned previously for the CID work. Of course, the neutral nucleophile was introduced in place of argon through the precision leak valve. When 1-methylimidazole was used as the nucleophile, no reaction products were observed in the absence of RF excitation heating. However, when sufficiently high energy was introduced, all three substrates were observed to fragment, forming the corresponding acylium ions mentioned earlier. Following fragmentation, each of the acylium ions was observed to undergo addition to with the 1-methylimidazole via elimination-

addition (Figure 33). Furthermore, there was no evidence of any addition-elimination or S_N2 (direct displacement) reaction chemistry. When piperidine was used as the nucleophile, a stable intermediate (m/z 312) was observed following reaction with compound **1a**. It could not be ascertained whether this species represented an ion-induced dipole complex or a covalently-bound intermediate (Figure 34). However, when excited by RF heating, this species underwent fragmentation to form

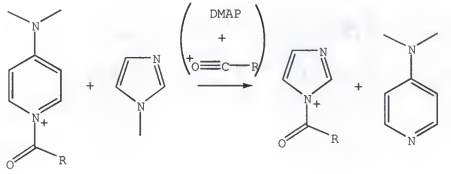

Figure 33. Reaction between acylpyridinium cations and 1-methylimidazole via an S_N1 pathway

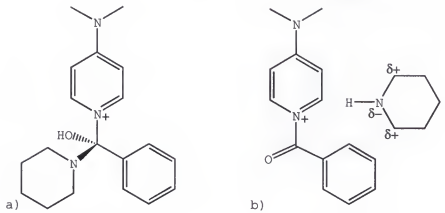

Figure 34. Reaction between compound **1a** and piperidine results in the formation of either a covalently-bound intermediate (a) or an ion-induced dipole complex (b).

the aforementioned acylium ion. Next, this acylium ion was observed to undergo addition with the piperidine via S_N1 chemistry as observed with 1-methylimidazole. In the case of the other two substrates, no intermediate species were observed with piperidine; however, both were found to undergo S_N1 chemistry with sufficiently high RF excitation. Finally, attempts were made to generate an S_N2 reaction between the aforementioned substrates and n-hexanol. In this case, RF-excitation resulted in the formation of protonated DMAP for all three substrates. This product may actually be formed as the result of an S_N2 reaction (see chapter 4); however, this could not be ascertained from these particular experiments.

Conclusions

The fragmentation study of the aforementioned series of N-acylpyridinium cations (**1a-i,3,4a-d,8a-c,12,14,16**) has provided a great deal of information regarding both the nature of fragmentation as well as the energies involved. As discussed in the preceding pages, these compounds fragment via several different pathways depending on the structure of the R-group present.

In one pathway, fragmentation resulted in the formation of an acylium ion and a neutral pyridine leaving group. The energies associated with this type of fragmentation ranged from less than 20 kcal/mol to 80 kcal/mol. In addition, trends were observed involving both electronic and steric effects. First, it was observed that compounds which contained R-groups which were more electron donating required less energy for fragmentation. Also, in examining fragmentation of the para and ortho isomers of N-(methylphenyl)-4-

(dimethylamino)pyridinium, it was determined that steric effects play an important role. Furthermore, for the ortho isomer, the parent ion is less stable due to steric hindrance between the methyl substituent and the pyridinium ring. This results in a lower energy of activation relative to the para isomer.

In the other major pathway observed, fragmentation lead to the formation of protonated DMAP via an intermediate complex. This type of complex has been observed previously in pyridinium systems and will be discussed further in chapter 4. The energies associated with this fragmentation pattern ranged from 24 kcal/mol to 72 kcal/mol. Also, it was observed that compounds containing R-groups with β-hydrogens underwent this type of fragmentation exclusively.

Finally, initial attempts were made to generate an S_N2 reaction between substrates **1a**, **1f**, **14**, and three potential nucleophiles: piperidine, 1-methylimidazole, and n-hexanol. Unfortunately, no direct evidence was observed for such chemistry among these species. Nevertheless, future attempts using some of the other acylpyridinium analogs might result in the desired chemistry.

CHAPTER 4

GAS PHASE NUCLEOPHILIC SUBSTITUTION (S_N2) REACTIONS AT SP^3-CARBON ATOMS

Introduction

In the whole of organic chemistry there is no reaction more important than the replacement by a nucleophile (Nu) of a leaving group (X) attached to an aliphatic carbon atom (R): Nu + RX → NuR + X. There are four main charge-type classes of such reactions: the substrate (RX) can be neutral or positively charged whereas the nucleophile (Nu) can be neutral or negatively charged.[109] Ingold recognized the fundamental distinction between a one-step bimolecular S_N2 reaction of Nu with RX and a two-step process with an initial unimolecular S_N1 scission of RX into R and X followed by combination of R with Nu.[110]

Most of the classical nucleophilic substitution mechanistic work in solution has been carried out with neutral substrates. For these, an S_N1 process RX → R^+ + X^- involves the creation of charge in the transition state, a process which is effectively inhibited in all but strongly polar solvents. Such solvents can also behave as nucleophiles and it is often difficult to disentangle whether such a solvent is simply a medium of dielectric constant sufficiently high to allow charge creation, or whether the solvent is behaving as a nucleophile. Such difficulties of interpretation are far fewer for cationic substrates because charge is then spread in an S_N1 transition state, rather than

created: $R^+X \rightarrow R^+ + X$. Thus S_N1-type reactions of cationic substrates are expected to, and do, occur in non-nucleophilic solvents of low dielectric constant. Extensive studies (over the period of 1978 - 1990)[109,111-113] have been conducted concerning the behavior of N-alkylpyridinium cations as substrates in nucleophilic substitution reactions, shed much light on their corresponding mechanisms, successfully demonstrating four distinct mechanisms (i) classical S_N1, (ii) Winstein S_N1,[114] (iii) classical S_N2, and (iv) Sneen[115] S_N2 routes. It was shown that these four mechanisms all remain distinct at borderlines with no merging.

Previous Work in the Gas Phase

As with solution studies, most of the published gas-phase work on nucleophilic substitution reactions has been carried out with neutral substrates, quite often involving halide anions displacing a halide leaving group from alkyl halides. On the basis of both experimental and theoretical work, Brauman and co-workers[116-119] demonstrated that such gas phase S_N2 reactions proceed over a potential energy surface with double-minima separated by a barrier (Figure 7, Ch. 1), and that the energy of the reactants is higher than that of this transition state. The two minima correspond to ion-dipole complexes that form as stable intermediates on either side of the transition state -- for example, $Cl^-(CH_3Br)$ and $(ClCH_3)Br^-$ in the case of the Cl^- / CH_3Br reaction. The formation and isolation of stable intermediates in gas-phase substitution reactions, and the activation of those intermediates to form products,[120-122] strongly supports this proposition. Most of the other S_N2 reactions so far reported have also involved anionic

nucleophiles with neutral substrates.[123-125] Clearly, S_N1 reactions of neutral substrates cannot normally be studied by mass spectral techniques.

Previous studies of S_N2 reactions between a neutral nucleophile and a cationic substrate are quite limited. In one study, a gas phase nucleophilic substitution reaction was observed involving an allylic substrate (oxygen-protonated but-1-en-3-ol and trans-but-2-en-1-ol) with loss of methanol via a concerted S_N2' mechanism in competition with the classical S_N2 mechanism.[126] In another study, attack of glycine on a dimethylchlorinium cation was shown by quadrupole mass spectrometry to result in methyl cation transfer.[127,128] However, the reaction was carried out in an external source prior to detection thus, no direct evidence was presented for an S_N2 pathway.

Some years ago, several studies reported on the collisionally induced dissociation of N-alkylpyridinium cations in the gas phase.[129,130] In this work, processes (Py^+-R $\rightarrow$ Py---R^+ $\rightarrow$ product) of two main types were observed: (i) to give as products Py and R^+ in which rearrangement of the carbocation R^+ frequently occurred within the intermediate ion-molecule complex and (ii) to give as products PyH^+ and the corresponding olefin formed by proton abstraction from R^+ in the ion-molecule complex. However, no evidence was presented for the occurrence of S_N2 reactions. This project represented an extension of that work with further attempts to generate gas phase S_N2 processes in electron deficient systems (reactions involving a neutral nucleophile and a cationic substrate).

Experimental

Laser Desorption Experiments

These experiments were performed using a Finnigan FTMS (formerly Nicolet) FTICR mass spectrometer equipped with an IonSpec data station utilizing a 3T superconducting magnet, and a heated inlet system equipped with dual precision leak valves. The vacuum chamber was pumped by a 300 Ls^{-1} oil diffusion pump maintaining the background pressure of the system below 1-2 x 10^{-8} Torr when the solids probe was inserted into the vacuum chamber. Ions formed by laser desorption were trapped in a 2.54 inch cubic cell with a trap voltage of 2V.

For laser desorption experiments, a quench pulse was applied to the trap plates to eject all ions from the cell. Next, a focused CO_2 laser pulse desorbed N-benzylpyridinium cations from a dried sample of ca. 1 mm thickness on a stainless steel solids probe tip. The ions formed were stored in the FTICR analyzer cell for 750 ms or more in the presence of 5 x 10^{-7} Torr of argon and at least partially thermalized by ion/neutral collisions. Next, a series of ejection sweeps was applied to isolate the molecular ion of interest. Then a variable delay time allowed the ion/molecule reactions to take place. The ions were excited by the standard frequency chirp excitation method and 64k time-domain points were acquired during broadband detection (20-400 amu). For each reaction delay time, 10 scans were averaged to enhance the signal to noise ratio.

Reagent gases were leaked into the chamber up to a pressure of 1-3 x 10^{-6} Torr via a variable leak valve. A Lumonics TE 860 pulsed carbon dioxide laser, operating in the static gas mode, was used to desorb the

ions. The laser was focused through a 7.63 cm focal length, 1.27 cm diameter ZeSe lens onto the end of a solids probe tip. The area of laser irradiation was 0.8 mm^2. The laser was fired with an average energy of 1.0 J/pulse, as measured at the laser exit window. Ten laser pulses were fired at the solids probe tip in its initial position and then it was rotated manually to provide a fresh surface for the next set of pulses. All the samples were used after multiple freeze-pump-thaw cycles.

Electrospray Ionization Experiments

All experiments were performed using a Bruker BioApex™ 7e external source FTICR spectrometer (Spectrospin AG, Fallanden, Switzerland) equipped with a horizontal room-temperature, 15 cm inner diameter, 7 T superconducting magnet, an external source, and a 170 mm^3 cylindrical RF-shimmed Infinity™ analyzer cell.[131] The standard external source FTICR instrument was described in chapter 1 thus, only relevant details are discussed here. Numerous problems associated with the installation of this nominal 7 T magnet resulted in operating the magnet at 4.7 T during this study. The FTMS external source design has two stages of differential pumping which achieves a pressure differential of up to 10^5 Torr between the external source and analyzer regions. The high and ultra-high vacuum regions were maintained using cryopumps (Edwards High Vacuum Co., Woburn, MA). An 800 l/s cryopump (N_2) was used to pump the high gas load region of the external source vacuum compartment where ions exiting the ESI source were accelerated toward the mass analyzer using a series of electrostatic optics. A 400 l/s cryopump evacuated the region between the first and second

conductance limits that contained the electrostatic ion transfer optics. An additional 400 l/s cryopump was used to maintain the ultra-high vacuum in the analyzer cell region.

After exiting the high pressure ESI source and entering the electrostatic ion optics, ions were accelerated to 2.5 kV and tightly focused through the two conductance limits before being accumulated and trapped in the FTMS analyzer cell. Ions were continuously produced by the ESI source and a set of x-, y-deflection plates were pulsed during the ion accumulation period for 50 to 200 ms to allow time for ions to accumulate in the analyzer cell. The trapped ions were resonantly excited using a broadband swept frequency RF "chirp". Ions were detected using the broadband detection mode covering a mass range from 50 to 2500 amu. Typically, 25 individual transients were co-added prior to Fourier transformation.

ESI Source

A dual stage ESI source equipped with a hexapole ion-guide was used for this work. The source was modified by replacing the normal glass capillary (0.5 mm ID. x 150 mm) used with nitrogen counter-current drying gas with a heated stainless steel capillary of similar dimensions. The stainless steel capillary was housed in a brass support with a 200 W cartridge heater and a 100 ohm platinum resistor. The heater maintained the capillary at 115 °C using a RTD temperature controller that regulated the heater power supply. In this configuration the source was operated without a counter-current drying gas.

Ions were electrosprayed from a needle maintained at a potential of 4.2 kV (capillary was kept at ground with respect to the needle). The pressure between the capillary exit and the first skimmer (1.0 mm diameter) was maintained at 1 mbar with a 500 L/min mechanical pump (Edwards, Model EM32). The pressure between the first skimmer and conductance limit near the center of the hexapole ion guide was maintained at ca. 1×10^{-3} mbar (as measured using a Pirani gauge TPR 010, Balzers AG, Liechtenstein) with a turbo molecular drag pump (Edwards, Model EXT 250H/180). The pressure after the ESI hexapole guide in the normal FTICR external source housing was ca. 1.0×10^{-6} mbar as pumped by the 800 L/s cryopump.

The samples were dissolved in 50/50 water/methanol solution at a concentration of 0.1 mg/ml and were introduced into the ESI source at a flow rate of 1 ml/min.

Collisionally-Induced Dissociation

The experimental procedure for collisionally-induced dissociation (CID) first involved a 100 ms quench pulse to remove any ions remaining in the cell from a previous experiment. After the quench pulse, an ion accumulation period of 5000 ms followed. During the ion accumulation, the electrostatic optics were pulsed to allow accumulation of ions in the analyzer cell. The precursor pyridinium cation was isolated using swept-frequency ejection pulses of 200 ms duration to eject all other ions. Argon was introduced via a leak valve to a background pressure of 2×10^{-7} Torr. The precursor ions were excited using a variable amplitude on-resonance excitation pulse of 10 ms duration. A 6.5 to 19 volt range of RF amplitudes was used to study the energy dependence of

the CID process. Following excitation of the precursor ion, a 1 sec delay was introduced to allow for collisions to occur, resulting in fragmentation of the ion. Calculation of the threshold energies and has been described in chapter 3.[129]

Deuterium Labeling Experiments.

The hydroxy deuteriated analog **15** (Figure 44) of salt **7** (Figure 40) was formed by dissolving 0.5 mg of salt **7** in 2.5 ml D_2O with stirring for 2 h. Following the deuterium transfer, the compound was immediately electrosprayed from this solution in order to minimize deuterium scrambling. Mass spectrometric analysis showed that 73% of the parent contained the deuterium label. The parent ion **15** was isolated using swept frequency ejection pulses; however, to minimize inadvertent RF-heating of the labeled compound, the protic impurity was not ejected prior to the reaction delay. A slight increase in the protic impurity of the product (33%) may be attributed either to deuterium scrambling during the reaction delay or to uneven RF excitation during the detection process.

Preparation and Characterization of Pyridinium Salts

The preparation and characterization of most of the compounds used in this study has been published previously.[132] Other new pyridinium salts were made by literature methods.[133] N,N-diethyl-1,4-butadiamine and N,N-dibutyl-1,4-butadiamine were prepared employing a reported method.[134]

Results and Discussion

The general strategy of this project was to study gas phase S_N2 reactions involving a neutral nucleophile and a cationic substrate (containing a neutral leaving group). Also, attempts were made to understand the mechanistic details involved in these processes and to make a comparison to past gas phase studies involving anionic nucleophiles with neutral substrates. Considerable effort has been directed toward generating the S_N2 reaction via both intramolecular and intermolecular pathways.

Ion / Molecule Reactions between N-Benzylpyridinium and Pyridine

This study was initiated with the expectation that a benzyl ion would be transferred in bimolecular reactions from N-benzylpyridinium **1a** (Py^+Bz) and *N*-benzyl-4-dimethylaminopyridinium **1b** ($4\text{-}Me_2NPy^+Bz$) cations to various neutrals such as pyridine (Py), 4-ethylpyridine (4-EtPy), 4-dimethylaminopyridine ($4\text{-}Me_2NPy$), and quinoline (Q) (Figure 35). Laser desorption of $Py^+Bz \cdot ClO_4^-$ and $4\text{-}Me_2NPy^+Bz \cdot ClO_4^-$ resulted in intact molecular ions Py^+Bz (**1a**) and $4\text{-}Me_2NPy^+Bz$ (**1b**) at m/z 170 and 213, respectively, and also in the fragment ion, benzyl cation **2** (Bz^+) at m/z 91. No ions resulting from fragmentation of the pyridine ring were observed.

The N-benzylpyridinium cations were formed by laser desorption, as described in the experimental section, and introduced either Py, 4-EtPy, $4\text{-}Me_2NPy$, or Q directly into the analyzer region using a precision leak valve until the pressure reached a value of 3×10^{-6} Torr (argon + neutral gas pressure). Next, a variable reaction delay was introduced. Ion intensities of both parent ion and product ion(s) were plotted for each

of the aforementioned nucleophiles as a function of time. The kinetic behavior seen is consistent with very rapid dissociation of the Py^+Bz (m/z 170) to form benzyl ion **2** (m/z 91), followed by somewhat slower addition of the benzyl cations to 4-EtPy to form the $4\text{-}EtPy^+Bz$ ion (**3b**) at m/z 198.

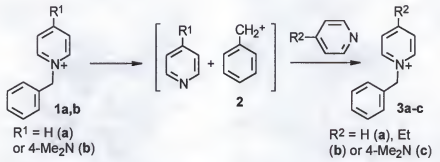

Figure 35. Benzyl cation transfer via nucleophilic substitution (S_N1)

When benzyl ions were continually ejected from the analyzer cell during the reaction period, no reaction products were seen. Attempts to enhance what is evidently, at best, a very slow bimolecular benzyl-transfer reaction by adding kinetic energy to reactant Py^+Bz did result in product ion formation. However, ejection of m/z 91 benzyl ions during this reaction process again resulted in no product formation. Thus, we conclude that "heating" the parent ions by adding kinetic energy only served to further fragment them via the CID process, forming benzyl ions, which then reacted as previously documented[135] to form product ions. When parent Py^+Bz was completely ejected from the analyzer cell immediately following laser desorption/ionization no reaction was observed). However, subsequent studies, described below, indicated that this lack of reactivity was due to the fact that after

ejection no parent ions were available to form the benzyl cations via dissociation.

Thus, no direct bimolecular (S_N2) reactions were observed between Py^+Bz (**1a**) and 4-Me_2NPy^+Bz (**1b**) cations and Py, 4-EtPy and Q neutrals (Figure 35). In each case, fragmentation of the parent cation gave benzyl cation **2** (m/z 91), which then added to the neutrals to give Py^+Bz **3a** (m/z 170), 4-$EtPy^+Bz$ **3b** (m/z 198), 4-Me_2NPy^+Bz **3c** (m/z 213), and Q^+Bz (m/z 220) cations. Transfer of benzyl cation from Py^+Bz to 4-Me_2NPy should be exoergic (ΔH = -16 kcal/mol - the heats of dissociation, $\Delta\Delta H_f$, of the Py^+Bz and 4-Me_2NPy^+Bz are 41 and 57 kcal/mol[129] [Note: calculated in the same way as for Py^+Bz by AM1], respectively), since 4-Me_2NPy is more basic than Py. These results suggest the presence of a barrier to ion / molecule reactions between 4-Me_2NPy^+Bz and Py, 4-EtPy and Q in order to explain the low abundance of product ions.

Intramolecular Gas Phase S_N2-Like Reactions

N-Substituted pyridinium salts have been shown to be useful synthetic intermediates in solution,[136,137] in addition to their effective use in mechanistic studies of nucleophilic substitution reactions at sp^3-hybridized carbon.[109,111-113]

For example, reactions of N-[ω-amino-(or ω-hydroxy-)alkyl]-pyridinium salts in the solution phase have been found to cyclize to form ethers or rearrange to aldehydes upon heating.[132] Particularly interesting results came from the pyridinium salt made from 5-aminopentanol. It was found to undergo cyclization to give tetrahydropyran via intramolecular nucleophilic attack by the oxygen. Moreover, derivatives from N-(ω-aminoalkyl)-pyridinium salts are known

to cyclize upon heating to give heterocyclic compounds. These results provided motivation to reinvestigate these reactions in the gas phase, with the intent of generating an intramolecular S_N2 reaction.

A series of these N-[ω-amino-(or ω-hydroxy-)alkyl]-pyridinium substrates were therefore selected for the investigation of gas phase intramolecular S_N2 reactions. Finally, previous work had demonstrated that these pyridinium compounds could be examined very effectively using FTICR mass spectrometry.[129-130,138]

Fragmentation Pathways

Two distinct fragmentation pathways were observed in these studies. The first one involved scission of the C-N bond thus, producing a charged heterocyclic compound and, presumably, a neutral substituted pyridine (Figure 36). The second one (which will be discussed later in this chapter) also involved the same C-N bond cleavage, but produced a protonated pyridinium cation and neutral acridine (Figure 39).

When N-(2-piperidinylethyl)-2,4,6-triphenylpyridinium cation (**4a**) was trapped in the FT-ICR analyzer cell, two ions were detected after a 3 second reaction delay period: the parent ion **4a** (m/z 419) was observed as well as a product ion at m/z 112, which was formed via the fragmentation of ion **4a** from non-thermalized ions with a 10% yield (Figure 36 and 37). The structure of the product ion (m/z 112) is assumed to be the cyclic compound **5a**, which is the most thermodynamically stable product. When the isolated precusor ion was excited translationally with a 10 μs RF pulse, the reaction proceeded 100% to the product ion. The internal energy of the unenergized parent

ions was estimated to be less than 23 kcal/mol (1.0 ev; trapping voltage utilized) based on previously reported results.[130] Similarly, when the CID experiment was performed on N-(2-diethylamino)-ethyl-2,4,6-trimethylpyridinium cation **4b**, the fragmentation resulted in the formation of cation **5b** (m/z 100). Again, the appearance potential energy was extremely low and could only be estimated to be less than 23 kcal/mol. It is very likely that the three-membered, charged,

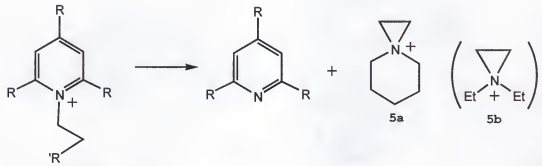

4a R = Ph, R' = piperidinyl
4b R = Me, R' = NMe2

Figure 36. Gas phase intramolecular S_N2 reaction

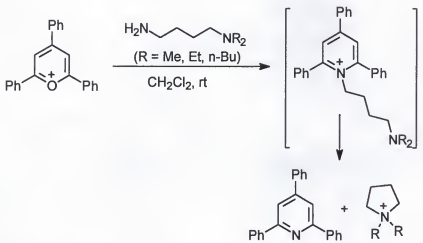

Figure 37. Sythesis of N-(4-dialkylamino)butyl-2,4,6-triphenyl pyridinium tetrafluoroborate resulting in a direct intramolecular (S_N2) reaction

heterocyclic products (**5a,b**) are produced from an intramolocular nucleophilic displacement via attack of the terminal nitrogen upon the aliphatic side chain α-carbon.

Attempts were made to prepare N-(4-dialkylamino)butyl-2,4,6-triphenylpyridinium tetrafluoroborate, which should also undergo an S_N2 intramolecular reaction in the gas phase as observed with compounds **4a,b**. However, this compound could not be isolated. Instead, the final products formed in the solution-phase reaction of triphenylpyrylium salt and the N,N-dialkyl-1,4-butanediamines were 2,4,6-triphenylpyridine and dialkylcyclobutyleneammonium salt. These products probably form as a result of a spontaneous intramolecular S_N2 reaction in the solution phase via the target pyridinium cation.

The unimolecular gas phase reaction of the N-(3-dimethylamino) propyl-2,4,6-triphenylpyridinium cation was also examined. However, a different fragmentation pathway was observed. After the parent ion at m/z 393 was isolated and energized, a product ion at m/z 348 was observed as the only product following the reaction delay (Figure 38). The structure of this product was determined to be the N-cyclopropyl-2,4,6-triphenylpyridinium cation. The apparent reaction mechanism is depicted in figure 38. In this case, cyclization via intramolecular S_N2 attack would result in the formation of an unstable, cationic, 4-membered ring. Furthermore, the observed product ion was probably formed via an initial [1,4] hydrogen shift followed by a more favorable cyclization resulting in the formation of a cyclopropyl ring substituent and a concurrent loss of dimethylamine. This hydrogen shift could occur through a favorable 5-membered transition state.

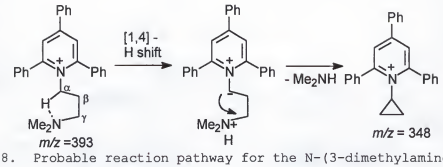

Figure 38. Probable reaction pathway for the N-(3-dimethylamino)-2,4,6-triphenylpyridinium cation

Three N-(ω-aminoalkyl)-5,6,8,9-tetrahydro-7-phenyldibenzo-[c,h]acridinium salts **6a-c**, and *N*-(5-hydroxypentyl)-5,6,8,9-tetrahydro-7-phenyldibenzo[c,h]acridinium salt **7** were each subjected to the same reaction conditions as discussed above. In each case, only the protonated acridinium cation **8** (m/z = 360) and remaining unreacted parent ion were detected in the analyzer cell following the reaction delay (Figure 39). The observed product (**8**) could be formed by two possible routes. The first involves the dissociation of N-alkylacridinium cation to acridinium cation and neutral olefins as reported in a previous study[130] (Figure 39, route a). Another more probable path involves an intramolecular nucleophilic attack of the exocyclic nitrogen or oxygen on the side chain α-carbon thus, affording an ion-molecule pair of the corresponding cation **11** and acridine **10** (Figure 39, route b). Subsequent fast proton transfer from cation **11** to substituted acridine would result in the formation of the protonated acridinium cation **8** and the corresponding neutral cyclic structure. While cation **11** was never detected at any time, this ion-molecule pair (**10**·**11**) would have the same m/z as the corresponding parent ion (**6** or **7**) and, it is reasonable to assume that proton transfer within the complex could preclude dissociation in forming the observed product(s). N-(ω-

Aminoalkyl)-2,4,6-triphenylpyridinium salts **13a,b** were also examined via the aforementioned reaction conditions and were found to behave similarly with the corresponding formation of protonated

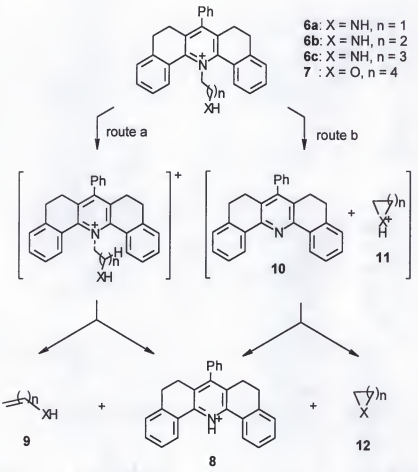

Figure 39. Possible gas phase fragmentation routes for N-substituted acridinium cations

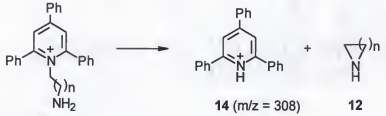

Figure 40. Fragmentation pathway for N-substituted alkylpyridinium cations

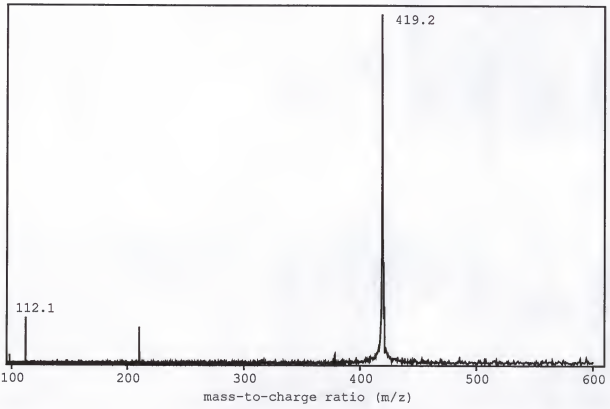

Figure 41. Intramolecular gas phase S_N2 reaction involving N-(2-piperidinylethyl 2,4,6-triphenylpyridinium cation

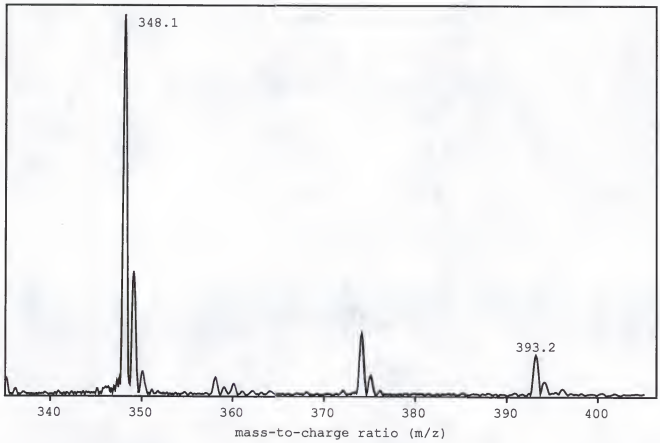

Figure 42. Intramolecular cyclization of N-(3-dimethylamino)-2,4,6-triphenyl pyridinium cation with concurrent loss of dimethylamine

triphenylpyridinium cation. Attempts to measure the exact appearance potential energies for these products were unsuccessful as the required activation energy is minimal. Therefore, their appearance potential energies may only be estimated (for each of these cases) to be less than 23 kcal/mol (Table 3).

Table 3. Estimated appearance energies of gas phase intramolecular reaction products

compounds	4	6a	6b	6c	7	13a	13b
appearance energy (kcal/mol)	<23	<23	<23	<23	<23	<23	<23

Control Experiments

In order to ascertain the pathway for fragmentation of the N-alkylacridinium cations, two control experiments were performed. In the first experiment, deuterium labeling was utilized in order to determine the source of proton transfer for these reactions. Thus, the hydroxy deuteriated analog (**15**) of salt **7** was submitted to the experimental conditions described above (Figure 43). If the reaction were occurring

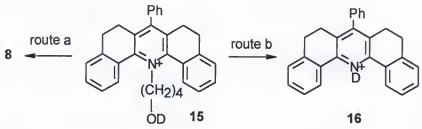

Figure 43. Deuterium labeling experiment to determine the source of proton transfer in the fragmentation of N-butylacridinium cation

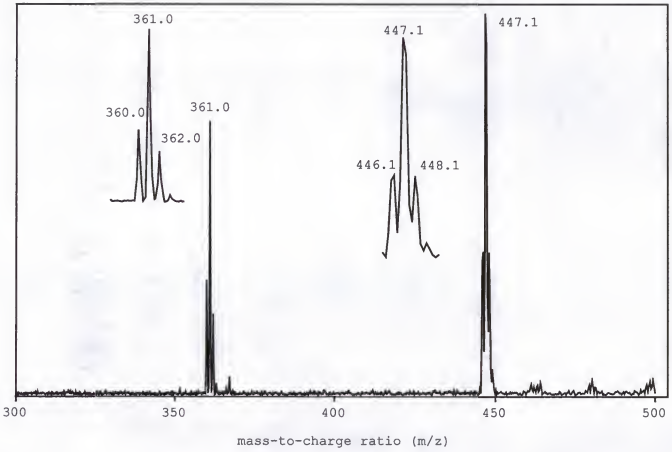

Figure 44. Deuterium labelling control experiment

via route a, a proton should be transferred from the β-CH_2 group to give **8**,[130] however, if the reaction is proceeding by route b, a deuterium would be transferred from the deuteroxy group of the starting acridinium salt **15** to give **16**. The parent ion **15** (containing 27% protic impurity) was allowed to react in the analyzer cell during a 1 second reaction delay. Following detection, it was observed that the reaction afforded product **16** with a 40% yield (figure 44). The slight increase in protic impurity in going from reactant to product (6% increase) could be attributed to deuterium scrambling. The product forms from non-thermalized ions since no translational heating via RF excitation was used to drive the reaction. Furthermore, no further product formation was detected when longer reaction delays were used.

The second control experiment was conducted in order to determine the appearance potential energy for the fragmentation of an N-butylacridinium cation containing no nucleophilic moiety. To that end, N-Butyl-5,6,8,9-tetrahydro-7-phenyldibenzo[c,h]acridinium salt **17** was fragmented via CID to produce the protonated acridinium cation and a neutral alkyl fragment. This same fragmentation product was observed with cations **6a-c**; however, the appearance potential energy for 18 was measured to be 41 kcal/mol (Figure 46). This value is very much in agreement with the appearance potentials (36 to 58 kcal/mol) previously reported[130] for N-alkyl substituted pyridinium salts (Table 4), but, significantly different from the energies observed for the ω-amino- or hydroxy-alkyl substituted pyridinium or acridinium salts. Finally, the results of these control experiments indicate that the pyridinium and acridinium salts **6a-c, 7, 13a,b** are following route a (Figure 39) and thus, undergo intramolecular (S_N2) nucleophilic substitution.

Table 4. Energy (kcal/mol) of fragmentation for several 1-substituted pyridinium cations (**17** and **19b-e**) to protonated pyridine and olefin

compounds	17	19b	19c	19d	19e
appearance energy (kcal/mol)	41.4	62[a]	47[a]	45[a]	38[a]

[a] Results from Ref. 130

17

Figure 45. CID fragmentation of n-butylacridinium cation

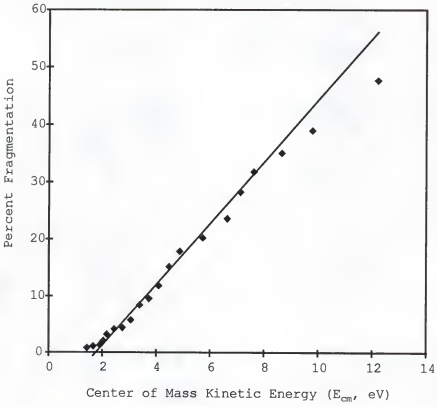

Figure 46. Plot of percent fragmentation for n-butylpyridinium cation

Intermolecular Gas Phase S_N2 Reactions

In addition to the aforementioned intramolecular S_N2 reactions, additional attempts were made to generate an intermolecular reaction. Furthermore, various N-methyl cations were submitted to gas phase study via electrospray FT-ICR mass spectrometry and were allowed to react in the presence of neutral nucleophiles as summarized in Table 5. Unfortunately, no evidence for gas phase S_N2 reactions was found for the chemical systems studied. In one example, 1-methylpyridinium cation was found to undergo aromatic nucleophilic substitution with 4-dimethylaminopyridine (DMAP) as the nucleophile to give N-(4-pyridyl)-4-dimethylaminopyridinium cation with concurrent loss of methane. This is of interest since this chemical system has been observed to undergo S_N2 chemistry in solution.

Another 1-methylpyridinium (N-methyl-5,6,8,9-tetrahydro-7-phenyldibenzo[c,h] acridinium) cation is known to undergo S_N2 chemistry in solution;[114] however, this reaction was not observed in the gas phase when DMAP, 1-methylimidazole, tetramethylthiourea, or triphenylphosphine were used as nucleophiles. Two other substrates examined were the methylviologen dication and 1-methylpyrazinium cation. In the presence of 1-methylimidazole and tetramethylthiourea, no S_N2 reactions were observed for the latter. Furthermore, no S_N2 reactions were observed for the dimethylviologen dication when DMAP and 1-methylimidazole were used as nucleophiles.

An ion-induced dipole complex was observed in high yield in the reaction between trimethylsulfoxonium cation with tetramethylthiourea. This is certainly of interest in that it demonstrates some interaction

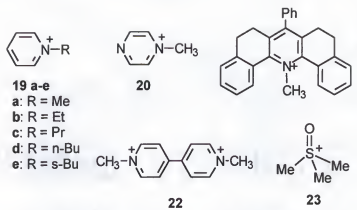

Figure 47. Various substrates used in attempts to generate an intermolecular gas phase S_N2 reaction

Table 5. Intermolecular reactions in the gas phase using FTICR MS

Substrate[a]/ Nucleophile	Dimethyl-amino-pyridine	1-Methyl-imidazole	Tetramethyl-thiourea	Piperidine	Triphenyl-phosphine
19a (m/z 94)	nucleophilic aromatic substitution (m/z 123, 200)	protonation of nucleophile (m/z 83)	protonation of nucleophile (m/z 133)	-	no reaction
20 (m/z 95)	-	no reaction	no reaction	-	-
21 (m/z 374)	no reaction	no reaction	no reaction	-	no reaction
22 m/z 93 (z = 2)	protonation of nucleophile (m/z 123, 185)	protonation of nucleophile (m/z 83)	-	-	-
23 (m/z 93)	-	-	ion-induced dipole complex (m/z 225)	-	-

[a]The structures of compounds **19 - 23** are shown in Figure 47

between the nucleophile and the substrate. Unfortunately, the ion-dipole complex could not be driven to the substitution products using RF excitation. The presence of a barrier on the potential energy surface probably prevents the S_N2 reaction and any excitation simply results in the conversion of complex back to reactants.

Gas Phase Nucleophilic Aromatic Substitution

In addition to the aforementioned attempts to generate S_N2 reactions with electron deficient aliphatic species, several potential reactions involving aromatic substitution were examined. This type of reaction (involving nucleophilic aromatic substitution) proceeds along a different pathway than observed for aliphatic systems in that it occurs at an aromatic sp^2 hybridized carbon (as opposed to sp^3). Nevertheless, this reaction also may proceed via a number of different mechanisms involving varying degrees of bond making and breaking in the transition state.[37]

First, 2,4-dinitrobenzyl-1-pyridinium (**24**, m/z 246) and 2,4-dinitrobenzyl-1-(4-imidazolyl)pyridinium (**25**, m/z 311) were utilized as the substrate in the presence of DMAP, which was used as the nucleophile. No reaction was observed to occur spontaneously between these species, so RF heating was used to drive these reactions. Unfortunately, the reaction products observed exhibited only a loss of NO_2 groups from the parent. For example, compound **25** (m/z 311) fragmented to give products at m/z 265 (-1 NO_2) and m/z 219 (-2 NO_2) as depicted in figure 48.

In addition to these electron poor substrates (**24** and **25**), more electron rich substrates were also utilized in attempts to generate aromatic nucleophilic substitution. In one case, 2-pyridyl-1-pyridinium cation (**26**) was employed as the substrate, while morpholine was used as the potential nucleophile (Figure 49). This reaction resulted in the formation of protonated morpholine with no RF heating being necessary. This is not terribly surprising since most good nucleophiles, such as morpholine, are also known to be good bases. In addition, this type of

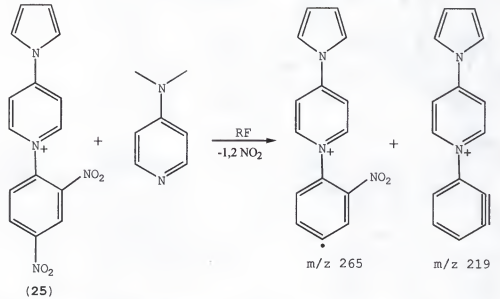

(25)

Figure 48. Reaction between compound **25** and DMAP results in simple CID of **25** with a loss of one or two NO_2 groups

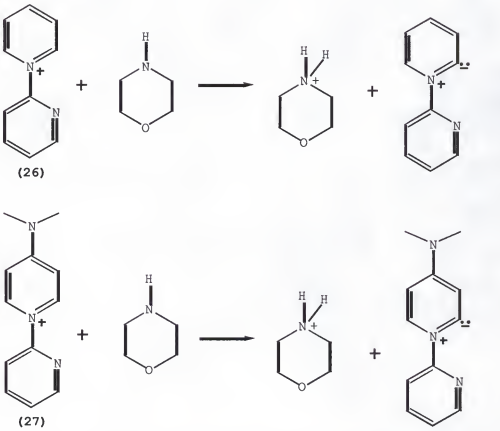

(26)

(27)

Figure 49. Proton transfer reactions involving pyridylpyridiniums

reaction was also observed when 2-pyridyl-1-(4-dimethylamino)pyridinium cation (**27**) was utilized as the substrate in the presence of both DMAP or morpholine (Figure 49).

Finally, an attempt was made to generate an S_N2 reaction using 1-methylpyridinium cation (**28**) as the substrate and DMAP as the nucleophile. In this case, proton transfer was again observed, analogous to that discussed above for the pyridylpyridinium cations; however, besides protonated DMAP (m/z 123), a proton-bridged dimer of DMAP (m/z 245) was also seen (Figure 50). Furthermore, upon RF heating of the substrate, a third product ion was observed at m/z 200 (**29**). This ion is likely the result of a substitution reaction where neutral methane is lost. Ejection of both of the product ions (m/z 123, 245) during the reaction delay had no effect on the intensity of **29**. Therefore, it may be assumed that neither of these ions serve as intermediates in the formation of **29**.

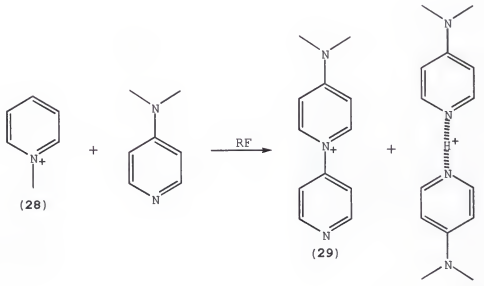

Figure 50. Reaction between 1-methylpyridinium cation and DMAP resulting in nucleophilic aromatic substitution

Also, no addition intermediate (m/z 216) was observed and RF irradiation at this m/z frequency had no effect on formation of **29**. All of this suggests that the substitution reaction is proceeding by a concerted (S_N2) process; however, it is difficult to determine whether the substitution is occurring at the 2 or 4 position on the pyridine ring. Nevertheless, this does appear to be an example of a gas phase aromatic S_N2 process.

Conclusions

Attempts to generate a gas phase intramolecular S_N2 reaction (in an electron deficient system) were successful. Furthermore, two different mechanistic pathways were observed which apparently lead to substitution products. In the first pathway, direct nucleophilic attack by the terminal nitrogen or oxygen resulted in the formation of a heterocyclic cation and a neutral pyridine (or acridine). In the second pathway observed, cyclization results in the formation of a transient ion-molecule complex which quickly undergoes internal proton transfer to give a protonated pyridine (or acridine) and presumably, a cyclic heterocycle. While this second mechanistic appraisal cannot be proven, control experiments support this conclusion.

In contrast, intermolecular S_N2 chemistry involving these same types of sytems was not observed. Since many of the reactions studied are known to be exothermic, the lack of reactivity must be explained by the presence of a large transition state barrier. There is however one other possible explanation, and this will be discussed in chapter 6.

In addition to the aliphatic systems examined, several attempts were made to generate a gas phase aromatic substitution reaction

(preferably S_N2). All of the pyridyl substrates examined underwent proton transfer reactions spontaneously (no RF heating was needed); however, 1-methyl pyridinium also appeared to undergo competing aromatic nucleophilic substitution with RF heating. The nature of this substitution was studied using RF ejection of the various products. From these ejection studies, it seems evident that substitution is occurring via a concerted process (S_N2). Further study of this particular reaction seems warranted and will be discussed in chapter 6.

CHAPTER 5
DETERMINATION OF PROTON AFFINITIES OF COMMON MALDI MOLECULES

Introduction

Since its introduction by Karas and co-workers in 1987, matrix-assisted laser desorption ionization (MALDI) has rapidly become a vital tool in the study of large molecules.[139-148] The mechanism of ionization during MALDI is still poorly understood, and no adequate quantitative model for the complete process exists. The MALDI technique involves both laser ablation and ionization of the matrix/analyte mixture. Spectra are dominated by matrix photoproducts, protonated molecular ions, and adduct ions. Several groups have developed models for the ablation process.[144-146,149] However, full models of MALDI await more detailed knowledge of ionization mechanisms, kinetics, and thermodynamics of the species involved.

Ablation models are the best developed aspect of MALDI theory. The majority of the energy absorbed by the matrix relaxes by rapid internal conversion from electronic states to vibrationally excited ground states and contributes to rapid heating. Ehring and Sundquist[150] studied the luminescence of two common MALDI matrices and found that the luminescence quantum yields are very low (0.2), which indicates that most of the energy is converted into matrix heating following photoexcitation. Models proposed to describe the laser ablation of the matrix include quasi-thermal evaporation, layer-by-layer expansion, and

pressure pulse expansion. In all three models, analyte molecules are assumed to be entrained within the flux of matrix molecules ejected from the surface, but these models do not address the formation of ions.

Evidence exists that analyte ionization occurs both in the surface and in the expanding plume. A small proportion of the analyte ionization occurs in the surface layers as proposed by Johnson.[149,151,152] At the threshold fluence, the ion yield increases rapidly until a fixed layer depth is ejected,[153] but the ionization is heavily quenched when the ejection yields are large.[154] This model is supported by a recent report from the Russell group which reported two thresholds for analyte ion formation in MALDI.[155] At low laser fluences of 2 mJ/cm^2, Vitamin B 12 gives an $(M+H)^+$ and a $(M-CN+H)^+$ ion in α-cyano-4-hydroxycinnamic acid. These ions are observed from the first laser shot on a spot and only the first shot. At three times higher laser fluences, the $(M+H)^+$ ion disappears. Russell proposed that a surface component is desorbed and ionized in the first shot at the lower ionization threshold. At the higher laser fluence, a component from the bulk material is desorbed.

There also appears to be an important component of ionization originating from analyte molecules entrained in the expanding plume. Mowry and Johnson,[156] studying the relative amounts of ions and neutrals desorbed from various matrices, found that the ratio of neutrals-to-ions ejected was on the order of 10,000 or greater at threshold irradiances. The ratio decreases with increasing irradiance of the desorption laser. These authors favor a collisional mechanism for analyte ion formation. Temporal profile analysis of MALDI analyte ions by Kinsel, Edmondson, and Russell[157] indicates that there are two regimes of ionization. A prompt ionization that occurs within ten to fifteen nanoseconds after

the laser pulse gives rise to a sharp component of the ion profile and comes from surface ionization of the analyte followed by emission. A broad, mass dependent component is attributed to entrained neutral material which is accelerated to a constant velocity and subsequently ionized in the gas phase.

Examination of the molecular ion region in the mass spectrum of MALDI matrices usually shows the presence of both molecular radical ions and $(M+H)^+$ ions. With some matrices the intensity of the $(M+H)^+$ ion is greater than that of the molecular radical ion, e.g. 2,5-dihydroxybenzoic acid. Protonated molecular ions of analytes in MALDI are frequently the most intense ions observed, especially when the concentration of alkali cations is low. Ehring, Karas and Hillenkamp[158] observed a dramatic increase in the $(M+H)^+$ ion intensity for cytochrome c in indole-2-carboxylic acid when the laser wavelength was shifted from 266 to 337 nm. A corresponding increase was also observed for the $(M+H)^+$ ion of the matrix. A logical source for these protonated analyte ions is proton donation from the $(M+H)^+$ ion of the matrix. Beavis, Chaudhary, and Chait[159] suggested that the low intensity of matrix ions observed in α-cyano-4-hydroxycinnamic acid (4-HCCA) might involve production of protonated matrix ions followed by exhaustive reaction with analyte or other species. Their supposition is supported by the observation that the protonated peptide signals from 4-HCCA matrices are substantially higher than from other cinnamic acid derivatives used as matrices. Karas and Hillenkamp[160] and Spengler et al.[161] proposed that proton transfer occurs from the matrix ions to the analyte.

A knowledge of the proton affinities of the common MALDI matrices should play a critical role in understanding why some matrices favor

proton transfer and are "hotter" than others, leading to more post source decay, as well as prompt decay. Jorgensen, Vulpius and Bojesen[162] used the "kinetic method" to determine the relative gas-phase proton affinities of five MALDI matrices generated by fast atom bombardment. In this work, efforts are presented to establish some of the thermodynamic parameters, namely the proton affinities, of eight common MALDI matrices using the gas phase proton transfer bracketing approach with Fourier transform ion cyclotron resonance (FTICR) mass spectrometry.

Experimental

Materials

All of the proton transfer reagents used as reference compounds in these experiments were obtained from commercial sources and used without additional purification. Benzene, n-butanol, cyclohexane, and dimethyl sulfoxide were obtained from Fisher Scientific (Pittsburgh, PA). Nitroethane and morpholine were obtained from Aldrich Chemical Co. (Milwaukee, WI). Pyrrole and 1-methylnaphthalene were obtained from Eastman Chemical Co. (Rochester, NY). The 4-ethylpyridine was obtained from J.T. Baker, Inc. (Phillipsburg, NJ). The MALDI compounds were all obtained from Aldrich Chemical Co. (Milwaukee, WI) and used as received: nicotinic acid, 2,5-dihydroxybenzoic acid, 3,5-dimethoxy-4-hydroxycinnamic acid, trans-3-indoleacrylic acid, α-cyano-4-hydroxycinnamic acid, 2-(4-hydroxyphenylazo)-benzoic acid, trans-4-hydroxy-3-methoxycinnamic acid, and 1,8,9-anthracenetriol (dithranol).

Mass Spectrometry

All analyses were conducted using a Bruker 4.7 Tesla FTICR mass spectrometer equipped with an external ion source. Each MALDI matrix molecule was introduced first into the external source using a solids probe heated to 150^0 C (Figure 51). Methane chemical ionization (CI) was employed to form the corresponding protonated MALDI molecule with the pressure in the CI source being adjusted to approximately 1 torr of methane. Following ionization, the methane cation radical is known to form two primary reactive species which may act as proton donors. For this study, $C_2H_5^+$ (m/z 29, Figure 52) was detected as the chemical ionizing agent (Figure 53) prior to addition of the MALDI analyte. While CH_5^+ may act as a proton donor in methane CI, this species was never detected. As mentioned above, the MALDI molecules were introduced via a heated solids probe (Figure 51) and subsequent proton transfer from the $C_2H_5^+$ resulted in the formation of the protonated MALDI adducts. The protonated molecules then exited the CI source into the instrument's external source housing, maintained at 1 x 10^{-5} torr.

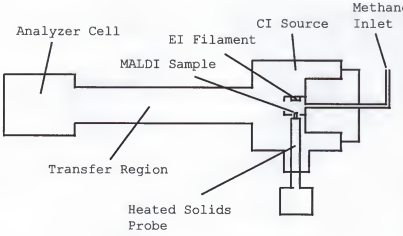

Figure 51. Bruker CI source used in MALDI molecule ionization

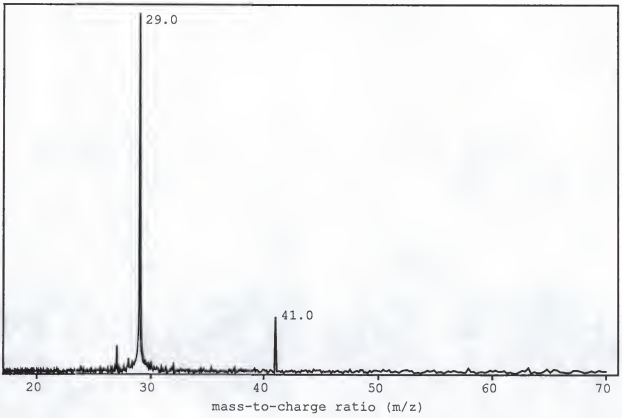

Figure 52. Spectrum of CI proton transfer adducts formed in the absence of analyte

Figure 53. Ionization of neutral MALDI molecules

Ions were subsequently transferred via electrostatic optics to an RF-shimmed analyzer cell.[163] The ions were trapped in the analyzer cell at a +1.0 V potential. Following introduction of the protonated MALDI molecules, a 5 second delay was utilized to allow for collisional and radiative cooling. Coarse isolation of the protonated molecules was accomplished using a frequency-swept notch ejection.[164] Any remaining ions (near the m/z of the ion of interest) were ejected using a series of single frequency ejections. The proton transfer reagents were introduced via a precision leak valve to a background pressure of 2 x 10^{-7} torr in the analyzer cell. The reactions were carried out until less than ten percent of the reactant ions remained to ensure that the proton transfer reactions were occurring from ground state ions which had been completely relaxed rather than from a small population of excited ions. Product ions were excited and subsequently detected via a standard frequency-chirp excitation with the detection window covering a mass range of 50 to 2500 amu. For all experiments, 16 time domain transient response data packets (32k data sets) were obtained and co-added prior to Fourier transformation to obtain a signal-to-noise ratio greater than 500 to 1.

Results and Discussion

Table 6 shows the results of the bracketing experiments for the eight MALDI matrices studied and the reference compounds used. Figure 54 presents the results of proton transfer between an isolated protonated matrix molecule $(M+H)^+$ (nicotinic acid in this case) and the reference compound used (morpholine). Table 7 presents the measured ground state proton affinities (PA) for eight common MALDI matrices, which ranged from 183 kcal/mole to 215 kcal/mole. Values reported for each compound in Table 7 are the averages of the upper and lower bracketing compounds presented in Table 6.

While proton transfer was observed for most of the systems examined, several of the compounds underwent different chemistry. For example, electron transfer was found to occur for several of the MALDI molecules. In some cases, the electron transfer occurred in competition with the desired proton transfer while, at other times, it was observed to be dominant. Also, several chemical reactions resulted with several of the compounds studied. For example, DHB was found to lose water (with all of the reference compounds) in forming a product at m/z 137. In addition, some dimerization was seen for DHB-H^+ and of the aforementioned ions observed at m/z 137. These reaction products are also observed when DHB is used as a matrix in MALDI.

Comparison to Other Results

The results obtained using this thermodynamic approach agree for nicotinic acid but differ for several of the matrices tested with those obtained by Jorgensen et al.[162] using the "kinetic approach." The order these authors obtained was nicotinic acid > sinapinic acid > ferulic

Table 6. Results from bracketing experiments

MALDI Compound	Cyclo-hexane 169.0 kcal/mol	Benzene 181.3 kcal/mol	Nitro-ethane 184.8 kcal/mol	Butanol 191.1 kcal/mol	1-methyl naphthalene 200.7 kcal/mol	pyrrole 207.6 kcal/mol	DMSO 211.3 kcal/mol	morpholine 219.4 kcal/mol	4-ethyl-pyridine 224.6 kcal/mol
DHB	no	no	----	no	no	yes	yes	yes	----
SA	----	no	----	no	no	yes	yes	----	----
DTL	no	no	no	no	no	no	yes	yes	----
α-CNCA	no	no	yes	yes	----	----	----	----	----
HABA	no	no	yes	yes	----	----	----	----	----
t3-IAA	----	----	no	----	no	----	no	yes	yes
FER	no	no	yes	----	yes	yes	yes	----	----
NA	no	no	----	no	no	no	no	yes	yes

DHB : 2,5-dihydroxybenzoic acid
SA : 3,5-dimethoxy-4-hydroxycinnamic acid
DTL : 1,8,9-anthracenetriol (dithranol)
α-CNCA : a-cyano-4-hydroxycinnamic acid
HABA : 2-(4-hydroxyphenylazo)-benzoic acid
t3-IAA : trans-3-indoleacrylic acid
FER : trans-4-hydroxy-3-methoxy-cinnamic acid (ferulic acid)
NA: nicotinic acid

"no" : no proton transfer was observed from the MALDI compound to the reference compound

"yes": proton transfer was observed

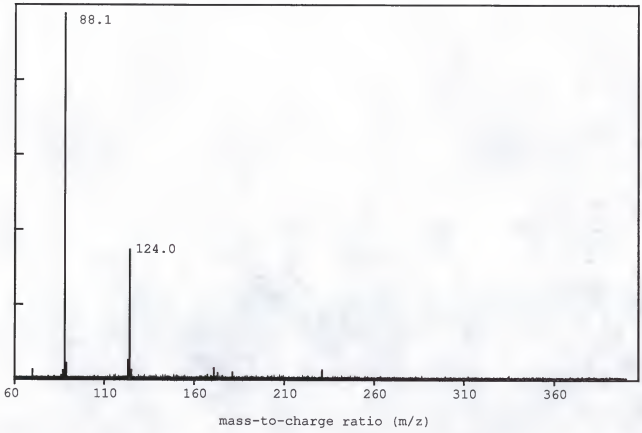

Figure 54. Mass spectrum showing proton transfer from nicotinic acid (m/z 124) to morpholine (m/z 88)

acid > 2,5-dihydroxybenzoic acid > α-cyano-4-hydroxycinnamic acid. In the present study 2,5-dihydroxybenzoic acid and ferulic acid are reversed. The differences in the measured proton affinities may reflect differences in methodology. The kinetic method employs high energy collision induced dissociation of proton bound dimers formed by fast atom bombardment ionization, and thus can involve internally excited molecules. On the other hand, the thermodynamic approach used here involved a 5 sec cooling step prior to introduction of the reference compound. This cooling step was used to insure that ground state proton affinities were being measured. Nelson, et al.[165] reported a proton affinity for 2,5-dihydroxybenzoic acid of 202.9 kcal/mole, which is in agreement with the results reported here.

Mechanistic Implications

For proton transfer to occur, the proton affinity of the acceptor must be greater than the proton affinity of the donor. For proteins and peptides, the presence of the amide bond with its high proton affinity suggests a ready route for formation of the protonated peptide by proton transfer from the ground state $(Matrix+H)^+$ ion, e.g. Locke and Mclver[166] reported a proton affinity for glycine of 213 kcal/mole. Wu and Fenselau[167] obtained proton affinities for polyglycines which ranged from 211.6 kcal/mol for glycine to 244.0 kcal/mole for decaglycine. These results also suggest that for some matrix/analyte combinations proton transfer does not occur from the ground state, protonated matrix since the matrix proton affinities are too high for this mechanism to be operable, e.g. trans-3-indole acrylic acid and nicotinic acid have PA = 215 kcal/mole (Table 7). For some synthetic polymers, the dominant form

Table 7. Proton affinities of 8 common MALDI molecules

MALDI Compound	Proton Affinity (kcal/mol)
nicotinic acid	215 ± 4.0
trans-3-indoleacrylic acid	215 ± 4.0
1,8,9-anthracenetriol	209 ± 1.9
2,5-dihydroxybenzoic acid	204 ± 3.5
3,5-dimethoxy-4-hydroxycinnamic acid	204 ± 3.5
α-cyano-4-hydroxycinnamic acid	183 ± 1.8
ferulic acid	183 ± 1.8
2-(4-hydroxyphenylazo)benzoic acid	183 ± 1.8

Table 8. Comparison of present results to past work

*Results from Bracketing Experiments (FTICR MS)	†Results from Kinetics Experiments (FAB MS)
(Highest Proton Affinities)	
nicotinic acid	nicotinic acid
trans-3-indoleacrylic acid	sinapinic acid
1,8,9-anthracenetriol	ferulic acid
2,5-dihydroxybenzoic acid	2,5-dihydroxybenzoic acid
sinapinic acid	α-cyano-4-hydroxy- cinnamic acid
α-cyano-4-hydroxycinnamic acid	
ferulic acid	
2-(4-hydroxyphenylazo)benzoic acid	
(Lowest Proton Affinities)	

*Results obtained from our present studies
†Results reported by Thomas J.D. Jorgensen, Tore Vulpius, and Gustav Bojesen at the 13th International Mass Spectrometry Conference in Budapest, 1994

of ionization is through alkali ion attachment. This may reflect the low proton affinity of some of the synthetic polymers which would not enable proton transfer from the ground state $(Matrix+H)^+$ ion of matrices such as dihydroxybenzoic acid (PA=204 kcal/mole) and 2-(4-hydroxyphenylazo)-benzoic acid (PA= 183 kcal/mole). For example, polyethers such as polyethylene glycol should have relatively low proton affinities by analogy to the measured proton affinities of cyclic ethers, dimethyl ether, methylethyl ether, and some short aliphatic primary alcohols which have proton affinities in the range of 188 to 205 kcal/mole.[168] These results are consistent with suggestions of some authors that proton transfer occurs from excited states of the matrix molecules.[169,170]

The relatively low proton affinities of several of the matrices measured (PA = 183 kcal/mole) indicates that for some analytes proton transfer could occur from the ground state $(Matrix+H)^+$ ion. The possibility exists that both mechanisms may be operable dependent upon matrix and analyte combinations. The high proton affinities of some matrices could also lend credence to the common practice of adding cationization reagents such as Na^+, K^+, or Ag^+ salts to MALDI matrices for polymers to increase the signal from these difficult to protonate species. The low proton affinities of some matrices could also lead to the observation that some of these matrices are considered "hot" matrices in that they lead to more extensive post source decay. For example, Karas, et al.[171] observed extensive metastable fragmentation for analysis of sperm whale apomyoglobin using α-cyano-4-hydroxycinnamic acid (PA=182 kcal/mole) as the matrix in a reflectron-TOF instrument; whereas and little metastable fragmentation was observed with a matrix

mixture of 2,5-dihydroxybenzoic acid (PA=204 kcal/mole) with 10 percent 2-hydroxy-5-methoxybenzoic acid (s-DHB).

Conclusions

As discussed above, the proton affinities of eight commonly used MALDI molecules were determined via bracketing studies. The proton affinities ranged from 183 to 215 kcal/mol for these compounds. From this work, it appears that proton transfer in MALDI experiments may occur from both the ground state and/or the excited state of the matrices. The mechanism probably depends on the nature of the analyte as well as the sample preparation used for a given experiment. Nevertheless, determination of these proton affinities should prove valuable in explaining the corresponding reactivity of these MALDI molecules. As mentioned, the low proton affinities observed for several of the compounds studied may explain the high degree of post-source decay often resulting with their use. Furthermore, proton transfer from these MALDI compounds should occur with greater exothermicity (especially with an analyte possessing high proton affinity).

While this study was conducted with the notion that ionization in MALDI is generated via proton transfer, certainly other pathways to ionization are available depending on the system. As discussed above, electron transfer was observed several times between the reference compound and the protonated MALDI molecule. At times, it appeared that both processes were occurring in direct competition while, some combinations produced either one process or the other.

Finally, while some MALDI ionization may occur via the excited state of the matrix used, these results should still prove useful.

Furthermore, the ordering of these ground state proton affinities probably parallels those exhibited by the excited state analogs despite the quantitative differences.

CHAPTER 6
FINAL CONCLUSIONS AND FUTURE WORK

In this work, various examples of ion-molecule interactions have been examined via Fourier transform ion cyclotron resonance mass spectrometry (FTICR). From unimolecular to bimolecular systems, various mechanistic pathways have been unraveled through the use of time-resolved detection, which results from the aforementioned multiplex advantage. Furthermore, as demonstrated repeatedly in these four projects, reaction precursors, products, and even intermediates may be effectively isolated and excited using various RF excitation protocols (e.g. shaped pulses, sweep ejections, single frequency shots, etc.). This also aids in the determination of reaction mechanisms, as demonstrated in chapter 3 and 4.

In addition, FTICR has again proven to be a reliable method for examining the energetics involved in these processes. Using controlled, energy-resolved RF excitation, fragmentation energies have been measured in attempts to better understand the dynamics of these gas phase reaction processes. Finally, through electrospray ionization (in conjunction with FTICR) solvated species can now be generated systematically, and subsequently trapped for several seconds. This capability should lead to a great deal of interesting work involving microsolvent effects. Furthermore, chemical reactivity as well as photophysical parameters of these species may be examined as a function of solvation.

Specific Solvation of Ruthenium Ammine Complexes

As discussed in chapter 2, a methodology has been developed which will allow for the controlled production of organometallic solvates. In this work, solvates of $BpyRu(NH_3)_4^{2+}$ and $IsnRu(NH_3)_5^{2+}$ were formed with acetonitrile, acetone, and butyronitrile. These solvates were isolated in the FTICR analyzer cell for several seconds prior to decomposition. Because of this instability, the solvent bonding energy could not be determined; however, it is certainly less than 23 kcal/mol (maximum internal energy that may be imparted to species when a 1 V trapping potential is utilized). In future work, this trapping voltage may be reduced up to 70%, which should facilitate lower excitation of the trapped solvates. If so, the solvent binding energy may be determined via methods discussed in chapter 3.

Initial attempts to induce photofragmentation of these ruthenium ammine solvates failed to produce the desired result. In these efforts, laser irradiation from 525 nm to 640 nm was employed with the intention of exciting metal-to-ligand (MLCT) charge transfer bands. This electronic excitation should be followed by some degree of internal conversion to vibrational energy, which may result in fragmentation of the parent solvate and the corresponding formation of desolvated products. By following this fragmentation as a function of photoirradiation, it should be possible to map the MLCT spectrum for these species as a function of microsolvation.

In going from solution to the gas phase, it is likely that the aforementioned ruthenium solvates will exhibit a blue shift in the MLCT band. It is possible that this shift may be more profound than anticipated. Furthermore, irradiation at shorter wavelengths (<500 nm)

may be necessary in order to generate the intended MLCT and thus, the corresponding photofragmentation. Finally, a large pressure burst was observed in these experiments shortly after the laser was fired. It is possible that the laser beam was insufficiently collimated to pass through the cell. Thus, irradiation of the cell walls may result in an unwanted high pressure burst of neutral gas.

In addition to the photophysical studies discussed above, it would be interesting to examine the chemical reactivity of these solvates via ligand exchange reactions. Again, this study could be conducted as a function of solvation, with individual solvates being isolated prior to the reaction period.

Collisionally Activated Dissociation of N-Acylpyridinium Cations

In this study, a number of N-acylpyridinium cations were fragmented via collisionally induced dissociation. By following this fragmentation as a function of RF excitation, the appearance energies of product formation were determined. Two major fragmentation pathways were observed for this series of compounds. In the first, excitation resulted in the formation of an acylium cation as well as a neutral adduct which was lost. The appearance energies for this fragmentation mechanism ranged from <23 kcal/mol to 80 kcal/mol. The second major fragmentation pathway observed resulted in the formation of a neutral ketene and a protonated adduct. Energies for this type of dissociation ranged from 24 kcal/mol to 72 kcal/mol. In addition, as discussed in chapter 3, this process appears to be favored in acylpyridinium compounds containing β-hydrogens, which suggests the presence of a five-membered transition state involving a [1,4] hydrogen shift.

Furthermore, compounds containing aromatic β-hydrogens were found to undergo this pathway, but with much higher energies of dissociation (as would be expected).

Initial attempts to generate an S_N2 acyl group transfer resulted in no direct evidence for this process. As mentioned previously, protonated DMAP was observed for some of the systems studied which could indicate an S_N2 reaction followed by proton transfer within an ion-induced dipole complex. However, this type of pathway cannot be substantiated at this time.

Future work in this area should be directed toward attempts at generating acyl transfer reactions with these acylpyridinium compounds. Knowledge of the mechanistic aspects of these reactions coupled with the energies of fragmentation determined in this work should provide an excellent understanding of gas phase acyl transfer reactions. Finally, this type of comparative study would provide a means for predicting the mechanistic nature of other acyl transfer reactions, both in the gas phase and in solution.

Gas Phase Nucleophilic Substitution (S_N2) Reactions at sp^3-Carbon Atoms

In this work, numerous attempts were made to generate an S_N2 reaction in the gas phase utilizing systems which were electron deficient. Many gas phase studies have been conducted with the generation of S_N2 reactions involving a neutral substrate and an anionic nucleophile; however, little work has been done using a neutral nucleophile with a cationic substrate. It was thus our motivation to generate this type of S_N2 reaction in the gas phase and in so doing, to study the corresponding mechanistic details.

Initial difficulties associated with generating a gas phase intermolecular S_N2 reaction resulted in attempts to generate an analogous intramolecular process. In doing so, two probable intramolecular S_N2 reaction pathways were observed. In the first, direct attack (S_N2) by a terminal amino group (Figure 36, chapter 4) upon the α-carbon of N-(2-piperidinylethyl)-2,4,6-triphenylpyridinium cation (**4a**) resulted in immediate cyclization with a loss of neutral 2,4,6-triphenylpyridine. This mechanism was also found to occur with N-(2-diethylamino)ethyl-2,4,6-trimethylpyridinium cation. Attempts to measure the appearance energies for these processes were unsuccessful since the reactions occur in a spontaneous fashion. However, the energy may be assumed to be less than 23 kcal/mol (1 eV), which is the trapping potential used in the analyzer cell.

In the other type of intramolecular process observed, apparent internal cyclization of the heteroatomic sidechain in several N-amino (or hydroxy)alkyl-1-substituted acridinium cations resulted in the formation of protonated acridine and presumably a corresponding neutral heterocycle. Since no intermediate structure(s) can be ascertained (they would probably have the same m/z as the precursor), this reaction process has been tentatively assigned as an S_N2 cyclization. Furthermore, following cyclization, an ion-induced dipole complex may form with subsequent fast proton transfer to the acridine, which would result in the formation of the protonated acridine. While this explanation for the observed product ion(s) is far from certain, two control experiments were performed which support this conclusion.

First, the heterocyclic group on the aforementioned acridinium cation was deuterium-labelled (**15**) and subjected to the same reaction

conditions. Again, the same reaction process was observed (as seen for the protiated analog) resulting in the formation of a deuteriated acridinium cation. This indicates that proton (deuterium) transfer is coming exclusively from the heterocylic group. In the second control experiment, n-butylacridinium cation (**17**) was fragmented via CID and the appearance energy (E_{obs}) of the protonated acridinium cation was determined. The E_{obs} of 41 kcal/mol is considerably higher than the estimated energy of fragmentation observed for the corresponding heteroatomic analog (**6c**, E_{obs} < 23 kcal/mol). Therefore, a driving force must be present in the reaction of **6c** which is not present in the case of **17**. This evidence coupled with the results from the deuterium-labeling experiment leads to the conclusion that **6c** is undergoing cyclization via an internal S_N2 mechanism. This is the first time this type of reaction (intramolecular S_N2 cyclization) has been observed in the gas phase.

As mentioned previously, attempts to generate a gas phase intermolecular reaction for systems involving a cationic substrate with a neutral nucleophile were not so successful. Furthermore, numerous attempts to examine an aliphatic S_N2 reaction produced no real evidence for this process. Again, this is somewhat surprising since the corresponding chemistry involving anionic nucleophiles (with neutral substrates) has been examined in numerous gas phase studies. It seems evident that a large enthalpic barrier must be present, which prevents this type of chemistry. Brauman has certainly observed this barrier to be present for anionic systems.[101-103] However, the barrier to reaction must not be as great for anionic systems since they are observed to undergo S_N2 reactions. In fact, another possible explanation arises

when considering the aforementioned results involving intramolecular reactions.

While an enthalpic barrier to reaction is certainly present, it seems likely that entropy may also be a factor in the lack of intermolecular reactions observed. In gas phase reactions, the lack of a guiding influence (by solvent molecules) presents a different kind of barrier, where statistically few collisions (often inelastic) result in the proper orientation of the reactants for a necessary backside attack (in S_N2 reactions). In fact, ion-induced dipole interaction may provide some degree of guiding influence; however, this guiding influence may also prevent the necessary backside orientation of the nucleophile relative to the substrate. Furthermore, differences between anionic ion-induced dipoles and cationic dipoles are not well understood at this time and thus, no direct comparison can be drawn. However, it is evident that a comparative theoretical study should prove useful in providing a more detailed explanation.

Determination of Proton Affinities of Common MALDI Molecules

In this study, the proton affinities of 8 compounds, commonly used as MALDI matrices, were determined via bracketing experiments using reference compounds with known proton affinities. These proton affinities were found to range from 183 kcal/mol to 215 kcal/mol. Knowledge of these values should prove useful in elucidation of the MALDI mechanism for ionization. Furthermore, comparison of these proton affinities to the corresponding reactivity of the matrices has provided some understanding as to why certain matrices are known to produce greater post-source fragmentation of various analytes. For example, α-

hydroxycinnamic acid has been found to produce a great deal of fragmentation in certain analytes, while 2,5-dihydroxybenzoic acid does not. The proton affinity determined for the former (P.A. = 183 kcal/mol) is lower than that observed for the latter (P.A. = 204 kcal/mol) which may explain the aforementioned post-source fragmentation observed with α-hydroxycinnamic acid. Proton transfer from α-hydroxycinnamic acid should be more exothermic (and thus produce a greater likelihood for fragmentation) than for 2,5-dihydroxybenzoic acid, which has a higher proton affinity. Furthermore, the results of this study may explain similar phenomena which have been observed for other MALDI matrices.

This study does not delineate whether proton transfer occurs from the excited state of these MALDI molecules or from the ground state. However, the general trend for these proton affinities should remain relatively unchanged with the corresponding excited state values. Nevertheless, future work in determining the proton affinities for the excited state would be very useful in providing an improved understanding of the mechanism of MALDI ionization.

LIST OF REFERENCES

1. Beauchamp, J.L., Anders, L.R., Baldeschwieler, J.D. *J. Am. Chem. Soc.* **1967**, 89, 4569.

2. McIver, R.T., Jr.; *Rev. Sci. Inst.* **1970**, 41, 555.

3. McIver, R.T., Jr.; Dunbar, R.C. *Int. J. Mass Spectrom. Ion Phys.* **1971**, 7, 471.

4. Comisarow, M.B.; Marshall, A.G. *Chem. Phys. Lett.* **1974**, 25, 282.

5. Comisarow, M.B.; Marshall, A.G. *Chem. Phys. Lett.* **1974**, 26, 489.

6. Ijames, C.F.; Wilkins, C.L. *J. Am. Chem. Soc.* **1988**, 110, 2687.

7. Wanczek, K.P. *Int. J. Mass Spectrom. Ion Proc.* **1989**, 95, 1.

8. Lebrilla, C.B.; Wang, D.T.S.; Hunter, R.L.; McIver, R.T., Jr. *Anal. Chem.* **1990**, 62, 878.

9. Cody, R.B.; Freiser, B.S. *Int. J. Mass Spectrom. Ion Proc.* **1982**, 41, 199.

10. Marshall, A.G.; Verdun, F.R. *Fourier Transforms in NMR, Optical, and Mass Spectrometry: A User's Handbook* **1990**, Elsevier Science Publishers B.V., New York.

11. Asamoto, B. (Ed.) *FT-ICR/MS: Analytical Applications of Fourier Transform Ion Cyclotron Resonance Mass Spectrometry* **1991**, VCH Publishers, Inc., New York.

12. Ghaderi, S.; Kulkarni, P.S.; Ledford, E.B., Jr.; Wilkins, G.L.; Gross, M.L. *Anal. Chem.* **1981**, 53, 428.

13. Carlin, T.J.; Freiser, B.S. *Anal. Chem.* **1983**, 55, 571.

14. McCrery, D.A.; Ledford, E.G.; Gross, M.L. *Anal. Chem.* **1982**, 54, 1435.

15. Hunt, D.F.; Shabanowitz, J.; Yates, J.R. III; Zhu, N.Z.; Russell, D.H.; Castro, M.E. *Proc. Natl. Acad. Sci. USA* **1987**, 84, 620.

16. Castro, M.E.; Russell, D.H. *Anal. Chem.* **1984**, 56, 578.

17. Castro, M.E.; Russell, D.H. **1985**, 57, 2290.

18. Amster, I.J.; Loo, J.A.; Furlong, J.P.; McLafferty, F.W. *Anal. Chem.* **1987**, 59, 313.

19. Amster, I.J.; McLafferty, F.W.; Castro, M.E.; Russell, D.H.; Cody, R.B.; Ghaderi, S. *Anal. Chem.* **1986**, 58, 483.

20. Kellerhals, H.; Alleman, M. U.S. Patent 4,563,579 **1986**.

21. Weller, R.R.; Viswanadham, S.K.; Sheetz, M.A.; Giam, C.S.; Hercules, D.M. Paper presented at the 34th Annual Conference on Mass Spectrometry and Allied Topics, Cincinnati, OH, June 8-13, **1986**.

22. Loo, J.A.; Williams, E.R.; Amster, I.J.; Furlong, J.P.; Wang, B.H.; McLafferty, F.W. *Anal. Chem.* **1987**, 59, 1880.

23. Loo, J.A.; Williams, E.R.; Furlong, J.P.; Wang, B.H.; McLafferty, F.W.; Chait, B.T.; Field, F.H. *Int. J. Mass Spectrom. Ion Proc.* **1987**, 78, 305.

24. Viswanadham, S.K.; Hercules, D.M.; Weller, R.R.; Giam, C.S. *Biomed. Environ. Mass Spectrom.* **1987**, 14, 43.

25. Irion, M.P.; Bowers, W.D.; Hunter, R.L.; Rowland, F.S.; McIver, R.T., Jr. *Chem. Phys. Lett.* **1982**, 93, 357.

26. Sack, T.M.; McCrery, D.A.; Gross, M.L. *Anal. Chem.* **1985**, 57, 1290.

27. Henry, K.D.; Williams, E.R.; Wang, B.H.; McLafferty, F.W.; Shabanowitz, J.; Hunt, D.F. *Proc. Natl. Acad. Sci. USA* **1987**, 84, 620.

28. Wilkins, C.L.; Weil, D.A.; Yang, C.L.C.; Ijames, C.F. *Anal. Chem.* **1985**, 57, 520.

29. Wilkins, C.L.; Yang, C.L.C. *Int. J. Mass Spectrom. Ion Proc.* **1986**, 72, 195.

30. Yao, J.; Dey, M.; Salvador, J.P.; Wilkins, C.L. *Anal. Chem.* **1995**, 67, 3638.

31. Bruce, J.E.; Cheng, X.; Bakhtiar, R.; Wu, Q.; Hofstadler, S.A.; Anderson, G.A.; Smith, R.D. *J. Am. Chem. Soc.* **1994**, 116, 7839.

32. Yamashita, M.; Fenn, J.B. *J. Phys. Chem.* **1984**, 88, 4451.

33. Marshall, A.G.; Wang, T.C.; Ricca, T.L. *J. Am. Chem. Soc.* **1985**, 107, 7893.

34. Gauthier, J.W.; Trautman, T.R.; Jacobson, D.B. *Anal. Chim. Acta* **1991**, 246, 211.

35. Savard, G.; Becker, S.; Bollen, G.; Kluge, H.J.; Moore, R.B.; Schweikhard, L.; Stolzenberg, H.; Wiess, U. *Phys. Lett. A* **1991**, 158, 247.

36. Cody, R.B.; Freiser, B.S. *Int. J. Mass Spectrom. Ion Proc.* **1982**, 41, 199.

37. Isaacs, N.S. *Physical Organic Chemistry* **1987**, Wiley, New York.

38. Carey, F.; Sundberg, R. *Advanced Organic Chemistry Part A: Structure and Mechanisms* **1990**, Plenum Press, New York.

39. Brauman, J.I.; Pellerite, M.J. *J. Am. Chem. Soc.* **1983**, 105, 2672.

40. Brauman, J.I.; Pellerite, M.J. *J. Am. Chem. Soc.* **1980**, 5993.

41. Kebarle, P.; Tang, L. *Anal. Chem.* **1993**, 65, 972.

42. Burns, T.D.; Spence, T.G.; Mooney, M.A.; Posey, L.A. *Chem. Phys. Lett.* **1996**, 258, 669.

43. Ramanathan, R. PhD Dissertation, University of Florida, **1994**.

44. Dole, M.; Mack, L.L.; Hines, R.L.; Mobley, R.C.; Ferguson, L.D.; Alice, M.B. *J. Chem. Phys.* **1968**, 49, 2240.

45. Iribarne, J.V.; Thomson, B.A. *J. Chem. Phys.* **1976**, 64, 2287.

46. (A) Balt, S.; Gamelkoorn, H.J. *J. Chem. Soc.* **1985**, 659-661. (B) Balt, S.; Gamelkoorn, H.J.; Renkema, W.E. *J. Chem. Soc.* **1983**, 2415-2418. (C) Burgess, J. *J. Chem. Soc.* **1973**, 825-828. (D) Dash, A.C.; Dash, N.; Pradhan, J. *Indian J. Chem.* **1992**, 31A, 824-831. (E) Grancicova, O.; Benko, J.; Vollarova, O; Holba, V. *Transition Met. Chem. (London)* **1993**, 18, 110-112. (F) Grancicova, O.; Holba, V. *Collect. Czech. Chem. Commun.* **1989**, 54, 3230-3237. (G) Grancicova, O.; Holba, V. *Transition Met. Chem. (Weinheim)* **1984**, 9, 322-325. (H) Grancicova, O.; Fabulova, I. *Transition Met. Chem. (London)* **1992**, 17, 190-195. (I) Holba, V.; Grancicova, O. *Transition Met. Chem. (London)* **1990**, 15, 27-30. (J) Hubinger, S.; Purcell, W.L. *Inorg. Chem.* **1991**, 30, 3707-3710. (K) Jackson, W.G.; Lawrence, G.A.; Lay, P.A.; Sargeson, A.M. *Aust. J. Chem.* **1982**, 35, 1561-1580. (L) Ohyoshi, A.; Shinohara, T.; Hosoyamada, Y.; Yamada, T.; Hiroshima, Y. *Bull. Chem. Soc. Jap.* **1973**, 46, 2133-2136. (M) Panasyuk, V.D.; Golub, V.A. *Zh. Neorg. Khim.* **1969**, 14, 457-461.

47. (A) Curtis, J.C.; Sullivan, B.P; Meyer, T.J. *Inorg. Chem.* **1983**, 22, 224-236. (B) Doorn, S.K.; Hupp, J.T. *J. Am. Chem. Soc.* **1989**, 111, 4704-4712. (C) Matsubara, T.; Efrima, S.; Metiu, H.I.; Ford, P.C. *J. Chem. Soc.* **1979**, 75, 390-400. (D) Saleh, A.A.; Crutchley, R.J. *Inorg. Chem.* **1990**, 29, 2132-2135.

48. (A) Brunschwig, B.S.; Ehrenson, S.; Sutin, N. *J. Phys. Chem.* **1986**, 90, 3657-3668. (B) Callahan, R.W.; Keene, F.R.; Meyer, T.J.; Salmon, D.J. *J. Am. Chem. Soc.* **1977**, 99, 1064-1073. (C) Chang, J.P.; Fung, E.Y.; Curtis, J.C. *Inorg. Chem.* **1986**, 25, 4233-4241. (D) Chou, M.H.; Creutz, C.; Sutin, N. *Inorg. Chem.* **1992**, 31, 2318-2327. (E) Curtis, J.C.; Blackbourn, R.L.; Ennix, K.S.; Hu, S.; Roberts, J.A.; Hupp, J.T. *Inorg. Chem.* **1989**, 28, 3791-3795. (F) Hupp, J.T.; Dong, Y.; Blackbourn, R.L.; Lu, H. *J. Phys. Chem.* **1993**, 97, 3278-3282. (G) Lau, K.W.: Hu, A.M.-H.; Yen, M.H.-J; Fung, E.Y.; Grzybicki, S.; Matamoros, R.; Curtis, J.C. *Inorg. Chim. Acta* **1994**, 226, 137-143. (H) Naklicki, M.L.; Crutchley, R.J. *Inorg. Chim. Acta* **1994**, 225, 123-127. (I) Naklicki, M.L.; Crutchley, R.J. *J. Am. Chem. Soc.* **1994**, 116, 6045-6046. (J) Powers, M.J.; Callahan, R.W.; Salmon, D.J.; Meyer, T.J. *Inorg. Chem.* **1976**, 15, 1457-1459.

49. (A) Bergkamp, M.A.; Watts, R.J.; Ford, P.C. *J. Am. Chem. Soc.* **1980**, 102, 2627-2631. (B) Bergkamp, M.A.; Watts, R.J.; Ford, P.C. *J. Chem. Soc.* **1979**, 623-624. (C) Endicott, J.F.; Ferraudi, G.J.;

Barber, J.R. *J. Am. Chem. Soc.* **1975,** 97, 219-220. (D) Gutierrez, A.R.; Adamson, A.W. *J. Phys. Chem.* **1978,** 82, 902-907. (E) Kane-Maguire, N.A.P.; Kerr, R.C.; Walters, J.R.; *Inorg. Chim. Acta* **1979,** 33, L163-L165. (F) Langford, C.H.; Kane-Maguire, N.A.P. *J. Chem. Soc. D.* **1971,** 895-896. (G) Langford, C.H.; Tipping, L. *Can. J. Chem.* **1972,** 50, 887-891. (H) Langford, C.H.; Lindsay, E. *Inorg. Chem.* **1990,** 29, 1450-1451. (I) Zinato, E.; Adamson, A.W.; Riccieri, P. *J. Phys. Chem.* **1985,** 89, 839-845.

50. (A) Ando, I.; Ishimura, D.; Ujimoto, K.; Kurihara, H. *Inorg. Chem.* **1994,** 33, 5010-5014. (B) Ando, I.; Ishimura, D.; Mitsumi, M.; Ujimoto, K.; Kurihara, H. *Polyhedron* **1992,** 11, 2335-2340. (C) Farmer, J.K.; Gennett, T.; Weaver, M.J. *J. Electroanal. Chem. Interfacial Electrochem.* **1985,** 191, 357-366. (D) Jaworski, J.S.; Kebede, Z.; Malik, M. *J. Electroanal. Chem.* **1992,** 333, 371-378. (E) Jaworski, J.S.; Kebede, Z. *J. Electroanal. Chem.* **1994,** 370, 259-267. (F) Sahami, S.; Weaver, M.J. *J. Electroanal. Chem. Interfacial Electrochem.* **1981,** 122, 171-181. (G) Sahami, S.; Weaver, M.J. *J. Electroanal. Chem. Interfacial Electrochem.* **1981,** 124, 35-51. (H) Todd, M.D.; Dong, Y.; Horney, J.; Yoon, D.I.; Hupp, J.T. *Inorg. Chem.* **1993,** 32, 2001-2004. (I) Weaver, M.J. *J. Phys. Chem.* **1979,** 83, 1748-1757. (J) Weaver, M.J.; Nettles, S.M. *Inorg. Chem.* **1980,** 19, 1641-1646. (K) Zhang, X.L.; Kankel, C.R.; Hupp, J.T. *Inorg. Chem.* **1994,** 33, 4738-4743.

51. Stavrev, K.K.; Zerner, M.C.; Meyer, T.J. *J. Am. Chem. Soc.* **1995,** 117, 8684.

52. Gutmann, V. *Coord. Chem. Rev.* **1976,** 18, 225.

53. Drago, R.; Richardson, D.E.; George, J., submitted for publication.

54. Drago, R. *Electrostatic-Covalent Models in Chemistry*; Surfside Press, 1994.

55. (A) Smith, R.D.; Loo, J.A.; Ogorzalek, R.R.; Busman, M.; Udesth, H.R. *Mass Spectrom. Rev.* **1991,** 10, 359-452. (B) Smith, R.D.; Loo, J.A.; Edmonds, C.G.; Barinaga, C.J.; Udesth, H.R. *Anal. Chem.* **1990,** 62, 882-899. (C) Fenn, J.B.; Mann, M.; Meng, C.K.; Wong, S.F.; Whitehouse, C.M. *Mass Spectrom. Rev.* **1990,** 9, 37-70. (D) Loo, J.A. *Bioconjugate Chem.* **1995,** 6, 544-665.

56. (A) Marshall, A.G. *Acc. Chem. Res.* **1985,** 18, 316. (B) Gross, M.L.; Rempel, D.L. *Science* **1984,** 226, 261. (C) Eyler, J.R.; Baykut, G. *Trends Anal. Chem.* **1986,** 5, 44. (D) Sharpe, P.; Richardson, D.E. *Coord. Chem. Rev.* **1989,** 93, 59.

57. (A) Katta, V.; Chowdhury, S.K.; Chait, B.T. *J. Am. Chem. Soc.* **1990,** 112, 5348. (B) Blades, A.T.; Jayaweera, P.; Ikonomou, M.G.; Kebarle, P. *Int. J. Mass Spectrom. Ion Proc.* **1990,** 101, 325. (C) Blades, A.T.; Jayaweera, P.; Ikonomou, M.G.; Kebarle, P. *Int. J. Mass Spectrom. Ion Proc.* **1990,** 102, 251. (D) Jayaweera, P.; Blades, A.T.; Ikonomou, M.G.; Kebarle, P. *J. Am. Chem. Soc.* **1990,** 112, 2452-2454.

58. Caravatti, P., United States Patent no. 4,924089.

59. Deno, N.C.; Pittman, C.U., Jr.; Wisotsky, M.J. *J. Am. Chem. Soc.* **1964,** 86, 4370.

60. Olah, G.A.; Dunne, K.; Mo, Y.K.; Szilagyi, P. *J. Am. Chem. Soc.* **1972**, 94, 4200.

61 Olah, G.A.; Kuhn, S.J.; Tolgyesi, W.S.; Barker, E.B. *J. Am. Chem. Soc.* **1962**, 84, 2733.

62. Staley, R.H.; Wieting, R.D.; Beauchamp, J.L. *J. Am. Chem. Soc.* **1977**, 99, 5964.

63. Boer, F.P. *J. Am. Chem. Soc.* **1968**, 90, 6706.

64. Bender, M.L. *Chem. Rev.* **1960**, 60, 53.

65. Jencks, W.P. *Catalysis in Chemistry and Enzymology* **1969**, McGraw-Hill book Company, New York.

66. Williams, A.; Douglas, K.T. *Chem. Rev.* **1975**, 75, 627.

67. Ba-Saif, S.; Luthra, A.K.; Williams, A. *J. Am. Chem. Soc.* **1987**, 109, 6362.

68. Williams, A. *Acc. Chem. Res.* **1989**, 22, 387.

69. Williams, A. *Chem. Soc. Rev.* **1994**, 23, 93.

70. Jencks, W.P. *Chem. Soc. Rev.* **1981**, 10, 345.

71. Stefanidis, D.; Cho, S.; Dhe-Paganon, S.; Jencks, W.P. *J. Am. Chem. Soc.* **1993**, 115, 1650.

72. Bentley, T.W.; Carter, G.E.; Harris, C.H. *J. Chem. Soc. Chem. Commun.* **1984**, 387.

73. Bentley, T.W.; Carter, G.E.; Harris, C.H. *J. Chem. Soc. Perkin Trans. II* **1985**, 983.

74. Bentley, T.W.; Harris, H.C. *J. Chem. Soc. Perkin Trans. II* **1986**, 619.

75. Kevill, D.N.; Kim, C.B. *Bull. Soc. Chim. Fr.* **1988**, 383.

76. Kevill, D.N.; Kim, C.B. *J. Chem. Soc. Perkin Trans. II* **1988**, 1353.

77. Bentley, T.W.; Shim, C.S. *J. Chem. Soc. Perkin Trans. 2* **1993**, 1659.

78. Bowie, J.H.; Williams, B.D. *Aust. J. Chem.* **1974**, 27, 1923.

79. Isolani, P.C.; Riveros, J.M. *Chem. Phys. Lett.* **1975**, 33, 362.

80. Faigle, J.F.G.; Isolani, P.C.; Riveros, J.M. *J. Am. Chem. Soc.* **1976**, 98, 2049.

81. Takashima, K.; José, S.M.; do Amaral, A.T.; Riveros, J.M. *J. Chem. Soc. Chem. Commun.* **1983**, 1255.

82. Riveros, J.M.; José, S.M.; Takashima, K. *Advances in Physical Organic Chemistry* **1985**, Academic Press, London.

83. Asubiojo, O.I.; Brauman, J.I. *J. Am. Chem. Soc.* **1979**, 101, 3715.

84. Kim, J.K.; Caserio, M.C. *J. Am. Chem. Soc.* **1981**, 103, 2124.

85. Blake, J.F.; Jorgenson, W.L. *J. Am. Chem. Soc.* **1987**, 109, 3856.

86. Yamabe, S.; Minato, T. *J. Org. Chem.* **1983**, 48, 2972.

87. Park, Y.S.; Kim, C,K.; Lee, B.S.; Lee, I,; Lim, W.M.; Kim, W.K. *J. Phys. Org. Chem.* **1995**, 8, 325.

88. Wilbur, J.L.; Brauman, J.I. *J. Am. Chem. Soc.* **1994**, 116, 5839.

89. Bartmess, J.E.; Hays, R.L.; Caldwell, G. *J. Am. Chem. Soc.* **1981**, 103, 1388.

90. McDonald, R.N.; Chowdhury, A.K. *J. Am. Chem. Soc.* **1983**, 105, 7267.

91. Katritzky, A.R.; Watson, C.H.; Dega-Szafran, Z.; Eyler, J.R. *J. Am. Chem. Soc.* **1990**, 112, 2479.

92. Katritzky, A.R.; Malhotra, N.; Dega-Szafran, Z; Savage, G.P.; Eyler, J.R.; Watson, C.H. *Org. Mass. Spectrom.* **1992**, 27, 1317.

93. Katritzky, A.R.; Dega-Szafran, Z; Watson, C.H.; Eyler, J.R. *J. Chem. Soc. Perkin Trans. 2* **1990**, 1051.

94. Katritzky, A.R.; Malhotra, N.; Ford, G.P.; Anders, E.; Tropsch, J. G. *J. Org. Chem.* **1991**, 56, 5039.

95. Anders, E.; Koch, R.; Katritzky, A.R.; Malhotra, N.; Eyler, J.R.; Zimmerman, J.A. *Chem. Ber.* **1992**, 125, 177.

96. Katritzky, A.R.; Musumarra, G. *Chem. Soc. Rev.* **1984**, 13, 47.

97. Katritzky, A.R. and Sakizadeh, K. *Heterocycles* **1985**, 23, 1765.

98. Katritzky, A.R. and Brycki, B.E. *J. Phys. Org. Chem.* **1988**, 1, 1.

99. Katritzky, A.R.; Brycki, B.E. *Chem. Soc. Rev.* **1990**, 19, 83.

100. Katritzky, A.R.; Watson, C.H.; Dega-Szafran, Z.; Eyler, J.R. *J. Am. Chem. Soc.* **1990**, 112, 2471.

101. Chantry, P.J. *J. Chem. Phys.* **1971**, 55, 2746.

102. King, J.A., Jr.; Brayant, G.L., Jr. *J. Org. Chem.* **1992**, 57, 5136.

103. Watson, C.H.; Baykut, G.; Eyler, J.R. *Anal. Chem.* **1987**, 59, 113.

104. Watson, C.H.; Baykut, G.; Mowafy, Z.; Katritzky, A.R.; Eyler, J.R. *Anal. Instrum.* **1988**, 17, 155.

105. Moylan, C.R.; Brauman, J.I. *J. Am. Chem. Soc.* **1985**, 107, 761.

106. Bowen, R.D. *J. Chem. Soc. Perkin Trans. 2* **1982**, 409.

107. Lifshitz, C. *Acc. Chem. Res.* **1994**, 27, 138.

108. Katritzky, A.R.; Dega-Szafran, Z.; Ramanathan, R.; Eyler, J.R. *Org. Mass. Spectrom.* **1994**, 29, 96.

109. Katritzky, A.R.; Brycki, B.E. *Chem. Soc. Rev.* **1990**, 19, 83.

110. Ingold, C.K. *Structure and Mechanism in Organic Chemistry* **1969**, Cornell Univ. Press, New York.

111. Katritzky, A.R.; Brycki, B.E. *J. Phys. Org. Chem.* **1988**, 1, 1.

112. Katritzky, A.R.; Sakizadeh, K. *Heterocycles* **1985**, 23, 1765.

113. Katritzky, A.R.; Musumarra, G. *Chem. Soc. Rev.* **1984**, 13, 47.

114. Winstein, S.; Clippinger; Fainberg; Heck; Robinson *J. Am. Chem. Soc.* **1956**, 78, 328.

115. Weiner; Sneen *J. Am. Chem. Soc.* **1965**, 87, 292.

116. Olmstead, W.N.; Brauman, J.I. *J. Am. Chem. Soc.* **1977**, 99, 4219.

117. Han, C.C.; Dodd, J.A., Brauman, J.I. *J. Phys. Chem.* **1986**, 90, 471.

118. Dodd, J.A.; Brauman, J.I. *J. Phys. Chem.* **1986**, 90, 3559.

119. Brauman, J.I. *J. Mass Spectrom.* **1995**, 30, 1649.

120. Graul, S.T.; Bowers, M.T. *J. Am. Chem. Soc.* **1991**, 113, 9696.

121. Cyr, D.M.; Posey, L.A.; Bishea, G.A.; Han, C.C.; Johnson, M.A. *J. Am. Chem. Soc.* **1991**, 113, 9697.

122. Wilbur, J.L.; Brauman, J.I. *J. Am. Chem. Soc.* **1991**, 113, 9699.

123. Lum, R.C.; Grabowski, J.J. *J. Am. Chem. Soc.* **1993**, 115, 7823.

124. Viggiano, A.A.; Morris, R.A.; Su, T.; Wladkowski, B.D.; Craig, S. L.; Zhang, M.; Brauman, J.I. *J. Am. Chem. Soc.* **1994**, 116, 2213.

125. Wladkowski, B.D.; Wilbur, J.L.; Brauman, J.I. *J. Am. Chem. Soc.* **1994**, 116, 2471.

126. Dezi, E.; Lombardozzi, A.; Pizzabiocca, A.; Renzi, G.; Speranza, M. *J. Chem. Soc. Chem. Commun.* **1995**, 547.

127. O'Hair, R.A.J.; Freitas, M.A.; Gronert, S.; Schmidt, J.A.R.; Williams, T.D. *J. Org. Chem.* **1995**, 60, 1990.

128. O'Hair, R.A.J.; Freitas, M.A.; Williams, T.D. *J. Org. Chem.* **1996**, 61, 2374.

129. Katritzky, A.R.; Watson, C.H.; Dega-Szafran, Z.; Eyler, J.R. *J. Am. Chem. Soc.* **1990**, 112, 2471.

130. Katritzky, A.R.; Watson, C.H.; Dega-Szafran, Z.; Eyler, J.R. *J. Am. Chem. Soc.* **1990**, 112, 2479.

131. Caravatti, P.; Allemann, M. *J. Mass Spectrom.* **1991**, 26, 514.

132. Katritzky, A.R.; Langthorne, R.T.; Patel R.C.; Lhommet, G. *Tetrahedron*, **1981**, 37, 2383.

133. Katritzky, A.R.; Bapat, J.B.; Claramunt-Elquero, R.M.; Yates, F. S.; Dinculescu, A.; Balaban, A.T.; Chiraleu, F. *J. Chem. Res. (M)* **1978**, 4783.

134. Amundsen, L.H.; Sanderson, J.J. *Org. Synth. Coll. III* **1955**, 256.

135. Katritzky, A.R.; Dega-Szafran, Z.; Ramanathan, R.; Eyler, J.R. *Org. Mass Spectrom.* **1994**, 29, 96.

136. Katritzky, A.R. *Tetrahedron* **1980**, 36, 679.

137. Katritzky, A.R.; Marson, C.M. *Angew. Chem. Int. Ed. Engl.* **1984**, 23, 420.

138. Watson, C.H.; Baykut, G.; Mowafy, Z.; Katritzky, A.R.; Eyler, J. R. *Anal. Instrum.* **1988**, 17, 155.

139. Karas, M.; Bachmann, D.; Hillenkamp, F. *Anal. Chem.* **1985**, 57, 2935.

140. Karas, M.; Hillenkamp, F. *Anal. Chem.* **1987**, 60, 2299.

141. Karas, M.; Bachmann, D.; Bahr, U.; Hillenkamp, F. *Int. J. Mass Spectrom. Ion Proc.* **1987**, 78, 53.

142. Tanaka, K.; Waki, H.; Ido, Y.; Akita, S.; Yoshida, Y.; Yoshida, T. *Rapid Commun. Mass Spectrom.* **1988**, 2, 151.

143. Beavis, R.S.; Chait, B.T. *Rapid Commun. Mass Spectrom.* **1989**, 2, 233; *Rapid Commun. Mass Spectrom.* **1989**, 3, 432; *Anal. Chem.* **1990**, 1836.

144. Nelson, R.W.; Rainbow, M.J.; Lohr, D.E.; Williams, P. *Science* **1989**, 246, 1585.

145. Spengler, B.; Cotter, R.J. *Anal. Chem.* **1990**, 62, 793.

146. Hillenkamp, F.; Karas, M.; Beavis, R.C.; Chait, B.T. *Anal. Chem.* **1991**, 63, 1193A.

147. Karas, M.; Bahr, U.; Giessmann, U. *Mass Spectrom. Rev.* **1991**, 10, 335.

148. Spengler, B.; Kaufmann, R. *Analysis* **1992**, 20, 91.

149. Johnson, R.E. *Int. J. Mass Spectrom. Ion Proc.* **1994**, 139, 25.

150. Ehring, E.; Sundqvist, B.U.R. *J. Mass Spectrom.* **1995**, 30, 1303.

151. Johnson, R.E. *Ion Formation from Organic Solids V* **1989**, Wiley, New York.

152. Johnson, R.E.; Banerjee, S.; Hedin, A.; Fenyo, D.; Sundqvist, B.U.R. *Methods and Mechanisms for Producing Ions from Large Molecules* **1991**, Plenum Press, New York.

153. Beavis, R.C. *Org. Mass Spectrom.* **1992**, 27, 864.

154. Spengler, B.; Bahr, M.; Karas, M.; Hillenkamp, F. *Anal. Instrum.* **1988**, 17, 173.

155. Edmondson, R.D.; Campo, K.K.; Russell, D.H. *Proceedings of the 43rd ASMS Conference on Mass Spectrometry and Allied Topics* **1995**, 686.

156. Mowry, C.D.; Johnson, M.V. *Rapid Commun. Mass Spectrom.* **1993**, 7, 569.

157. Kinsel, G.R.; Edmondson, R.D.; Russell, D.H. *Proceedings of the 43rd ASMS Conference on Mass Spectrometry and Allied Topics* **1995**, 690.

158. Ehring, H.; Karas, M.; Hillenkamp, F. *Org. Mass Spectrom.* **1992**, 27, 472.

159. Beavis, R.C.; Chaudhary, T.; Chait, B.T. *Org. Mass Spectrom.* **1992**, 27, 156.

160. Karas, M.; Hillenkamp, F., presented at *Desorption '94* **1994**.

161. Spengler, B.; Kaufmann, R.; Bokelmann, V.; Huubert, M.; Kirsch, D., presented at *Desorption '94* **1994**.

162. Jorgensen, T.J.D.; Vulpius, T.; Bojesen, G. *Abstracts of the 13th International Mass Spectrometry Conference* **1994**, 175.

163. Caravatti, P.; Allemann, M. *Org. Mass Spectrom.* **1991**, 26, 514.

164. Noest, A.J.; Kort, C.F.W. *Comput. Chem.* **1983**, 7, 81.

165. Nelson, C.M.; Smith, L.M.; Crellin, K.C.; Berry, J.; Beauchamp, J.L., presented at the *44th ASMS Conference on Mass Spectrometry and Allied Topics* **1996**.

166. Locke, M.J.; McIver, R.T., Jr. *J. Am. Chem. Soc.* **1983**, 105, 4226.

167. Wu, Z.; Fenselau, C. *J. Am. Soc. Mass Spectrom.* **1992**, 3, 863.

168. Lias, S.G.; Liebman, J.F.; Levin, R.D. *J. Phys. Chem. Ref. Data* **1984**, 13, 695.

169. Preston-Schaffer, L.M.; Kinsel, G.R.; Russell, D.H. *J. Am. Soc. Mass Spectrom.* **1994**, 5, 800.

170. Chiarelli, M.P.; Sharkey, A.G., Jr.; Hercules, D.M. *Anal. Chem.* **1993**, 65, 307.

171. Karas, M.; Bahr, U.; Strupat, K.; Hillenkamp, F.; Tsarbopoulus, A.; Pramanik, D.N. *Anal. Chem.* **1995**, 67, 675.

BIOGRAPHICAL SKETCH

Richard D. Burton was born on April 8, 1967 in Kewannee, Illinois. He lived the first 12 years of his life in Buda, Illinois before moving to Princeton, Illinois. He graduated from Princeton High School in 1985. During the next 6 years, he attended Illinois State University where he received his B.S. degree in Chemistry in 1989 and his M.S. degree in Chemistry in 1992. He began his studies at the University of Florida in the fall of 1992 with his main research interests centered around gas phase physical organic chemistry.

I certify that I have read this study and that in my opinion it conforms to acceptable standards of scholarly presentation and is fully adequate, in scope and quality, as a dissertation for the degree of Doctor of Philosophy.

John R. Eyler

John R. Eyler, Chair
Professor of Chemistry

I certify that I have read this study and that in my opinion it conforms to acceptable standards of scholarly presentation and is fully adequate, in scope and quality, as a dissertation for the degree of Doctor of Philosophy.

Alan R. Katritzky
Kenan Professor of Chemistry

I certify that I have read this study and that in my opinion it conforms to acceptable standards of scholarly presentation and is fully adequate, in scope and quality, as a dissertation for the degree of Doctor of Philosophy.

K. S. Schanze

Kirk S. Schanze
Associate Professor of Chemistry

I certify that I have read this study and that in my opinion it conforms to acceptable standards of scholarly presentation and is fully adequate, in scope and quality, as a dissertation for the degree of Doctor of Philosophy.

John A. Zoltewicz
Professor of Chemistry

I certify that I have read this study and that in my opinion it conforms to acceptable standards of scholarly presentation and is fully adequate, in scope and quality, as a dissertation for the degree of Doctor of Philosophy.

James F. Klausner

James F. Klausner
Associate Professor of Mechanical Engineering

This dissertation was submitted to the Graduate Faculty of the Department of Chemistry in the College of Liberal Arts and Sciences and to the Graduate School and was accepted as partial fulfillment of the requirements for the degree of Doctor of Philosophy.

May 1997

Dean, Graduate School